

Jets, tidal disruption and lenses

Plan and reviews

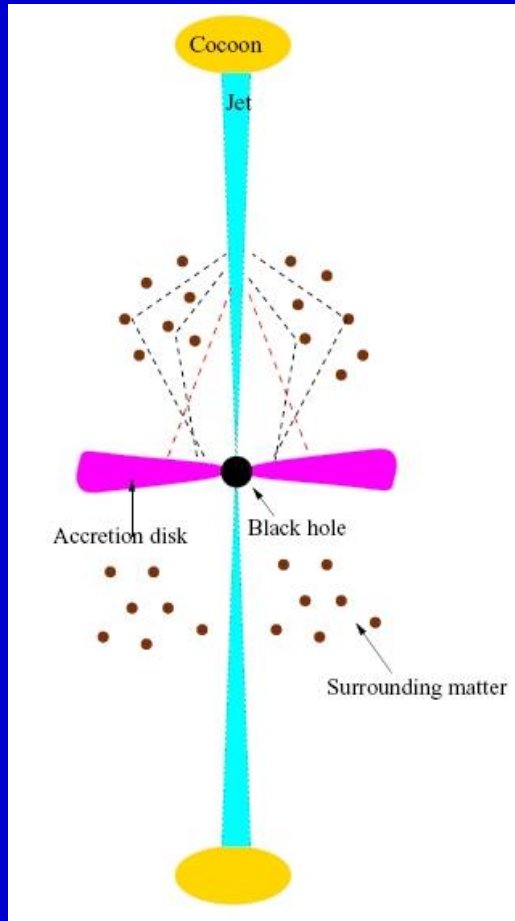
Plan

1. Jets: AGNs and close binary systems
2. Tidal disruption of stars by SMBHs
3. Spectral lines and lensing

Reviews

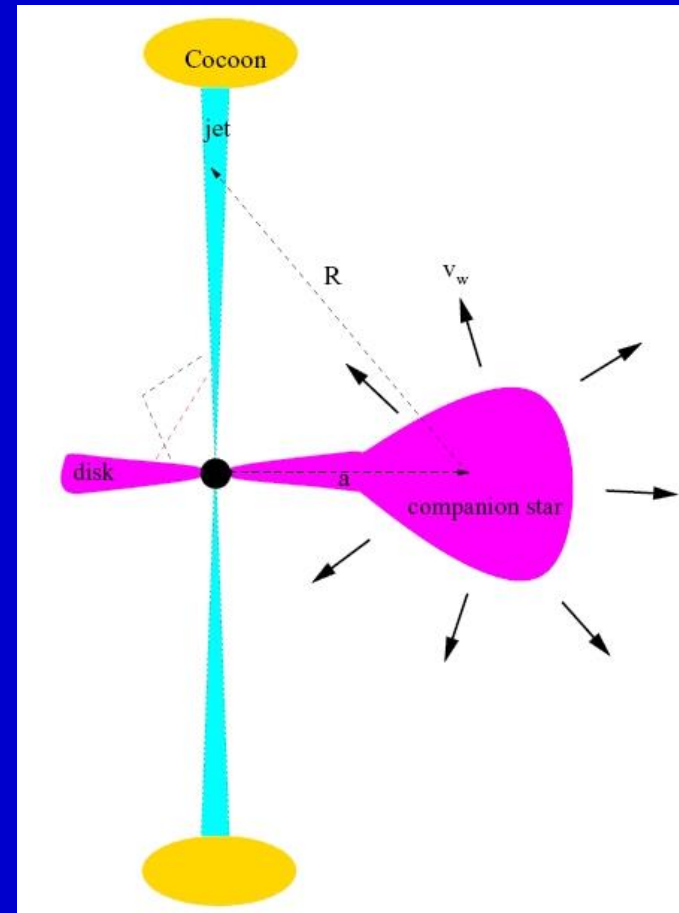
- [astro-ph/0611521](#) **High-Energy Aspects of Astrophysical Jets**
- [astro-ph/0306429](#) **Extreme blazars**
- [astro-ph/0312545](#) **AGN Unification: An Update**
- [astro-ph/0212065](#) **Fluorescent iron lines as a probe of astrophysical black hole systems**
- [arXiv: 1104.0006](#) **AGN jets**
- [astro-ph/0406319](#) **Astrophysical Jets and Outflows**
- [arXiv: 2003.06322](#) **Relativistic Jets of Blazars**
- [arXiv: 1707.07134](#) **AGNs of different types**
- [arXiv: 2101.08839](#) **Jets**
- [arXiv: 2104.14580](#) **TDEs**

Jets in AGNs and close binaries



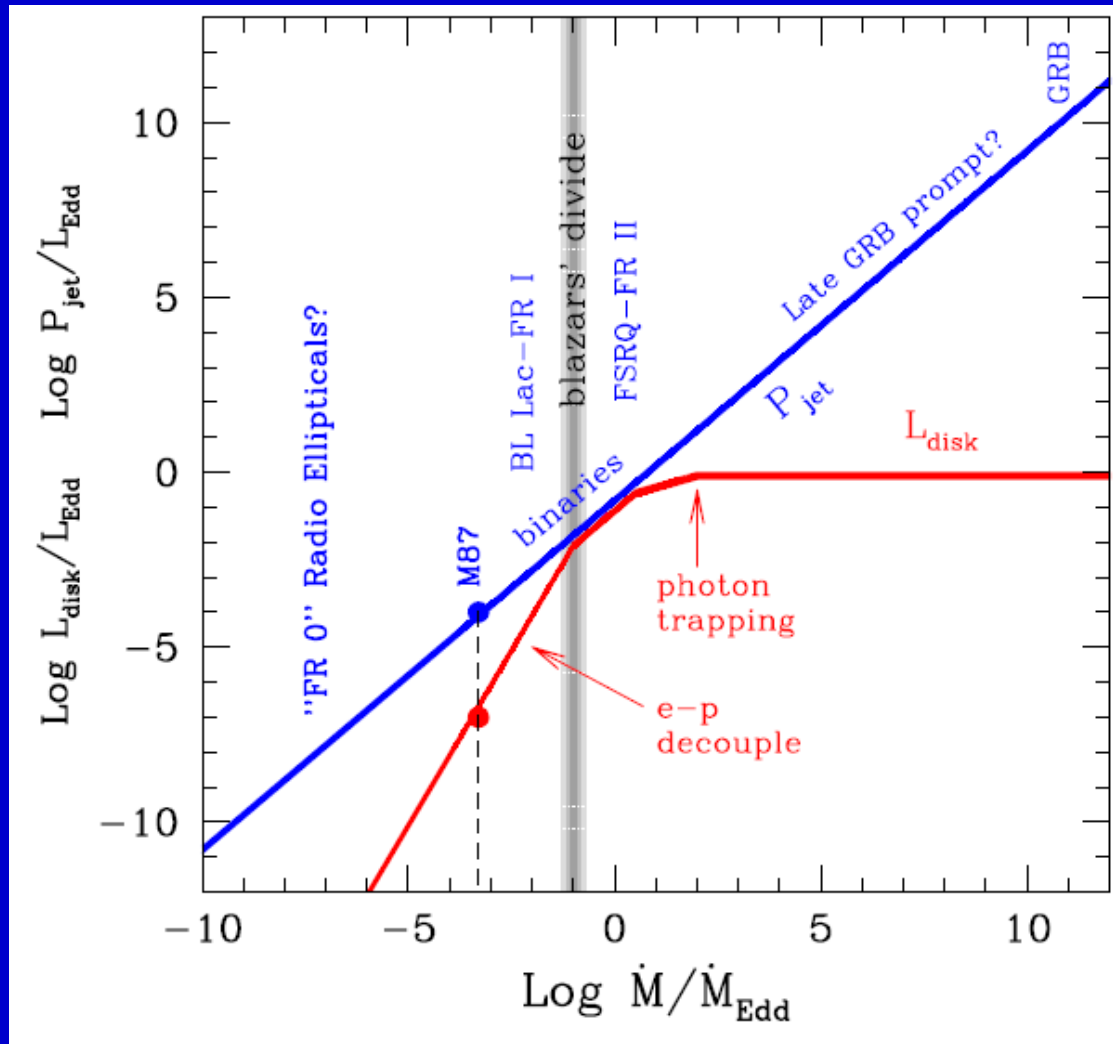
AGN: $M_{\text{BH}} = 10^8 - 10^9 M_{\odot}$
 $L < \sim L_{\text{Edd}} \sim 10^{42} - 10^{47} \text{ erg/s}$
 $< \text{few Mpc}$
 $\Gamma \sim 5 - 50$
 $\Delta t \sim \text{hours-years}$

CBS: $M_{\text{BH}} \sim 10 M_{\odot}$
 $L < \sim L_{\text{Edd}} \sim 10^{37} - 10^{40} \text{ erg/s}$
 $\sim \text{pc}$
 $\Gamma \sim 1 - 10$
 $\Delta t \sim \text{days}$



see astro-ph/0611521

All jets in one plot

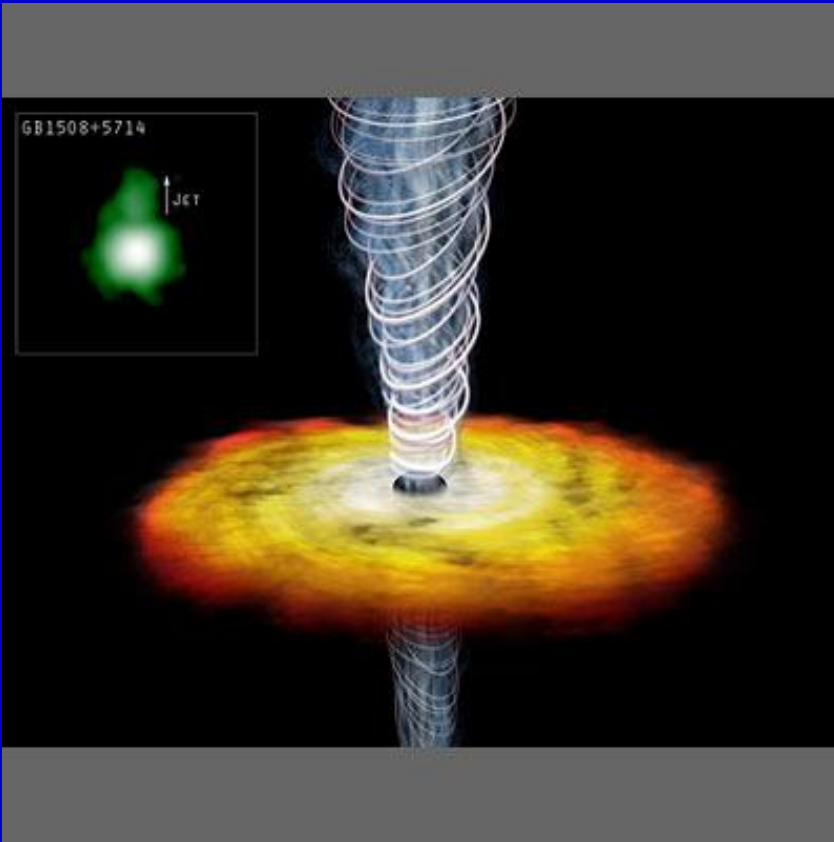


A schematic plot for different jets.

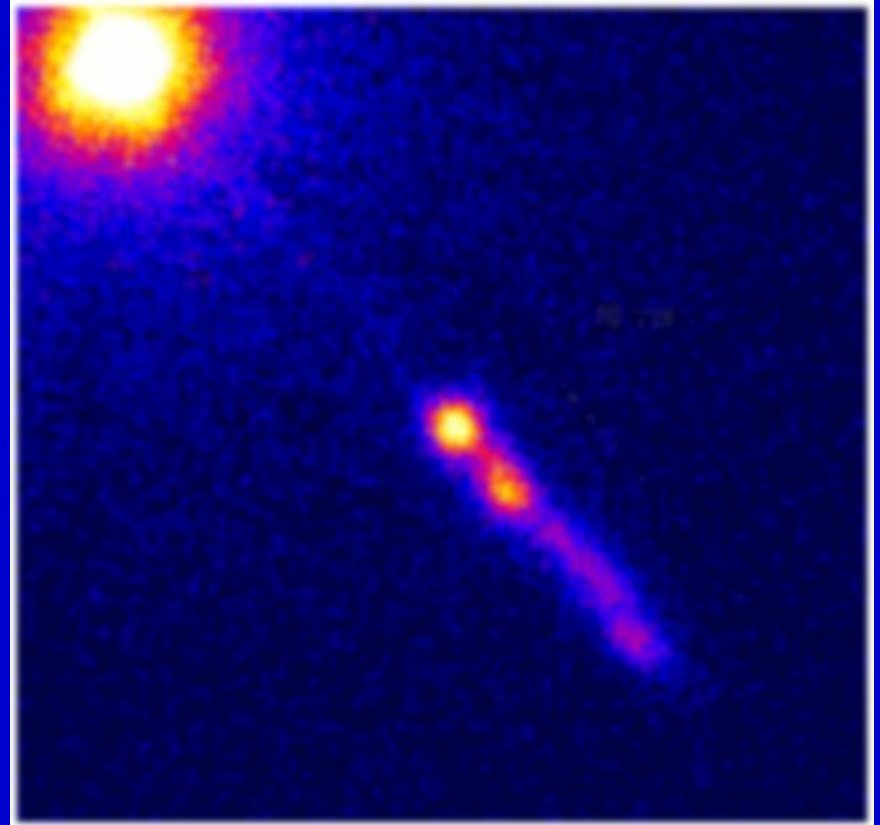
It is assumed that the jet power always scales linearly with \dot{M} , while accretion rates below a critical value produce radiatively efficient accretion disks.

Close-by and far-away jets

1% of SMBH are active. 10% out of them launch relativistic jets.
Jets are not magnetically dominated.



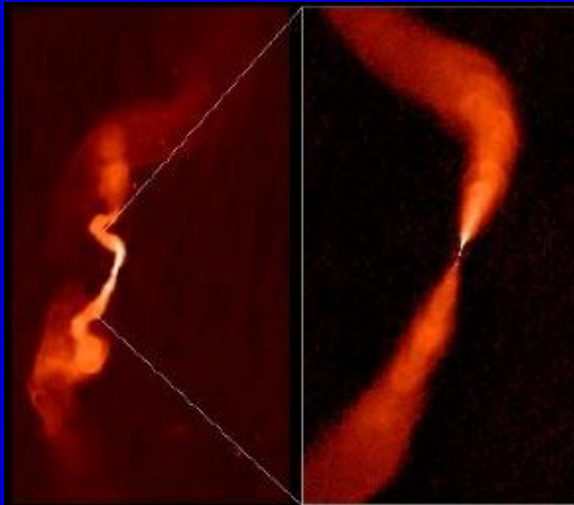
GB1508+5714 $z=4.30$



3C273

See a review in 1104.0006

Classification of AGN radio jets



FR Class I source: radio galaxy 3C31

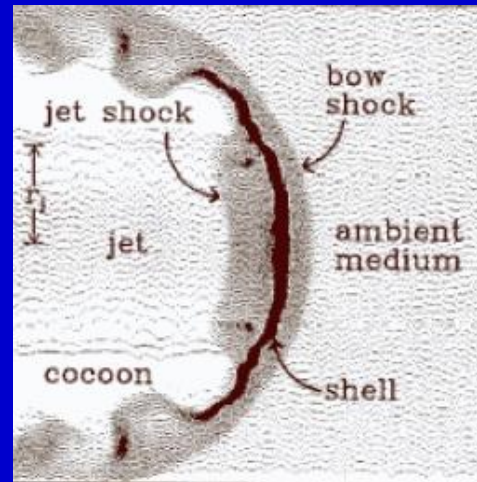


FR Class II source: quasar 3C175

FR I. Two-sided jets.

Jets dominate in the emission.

Usually are found in rich clusters.



FR II. One-sided jets.

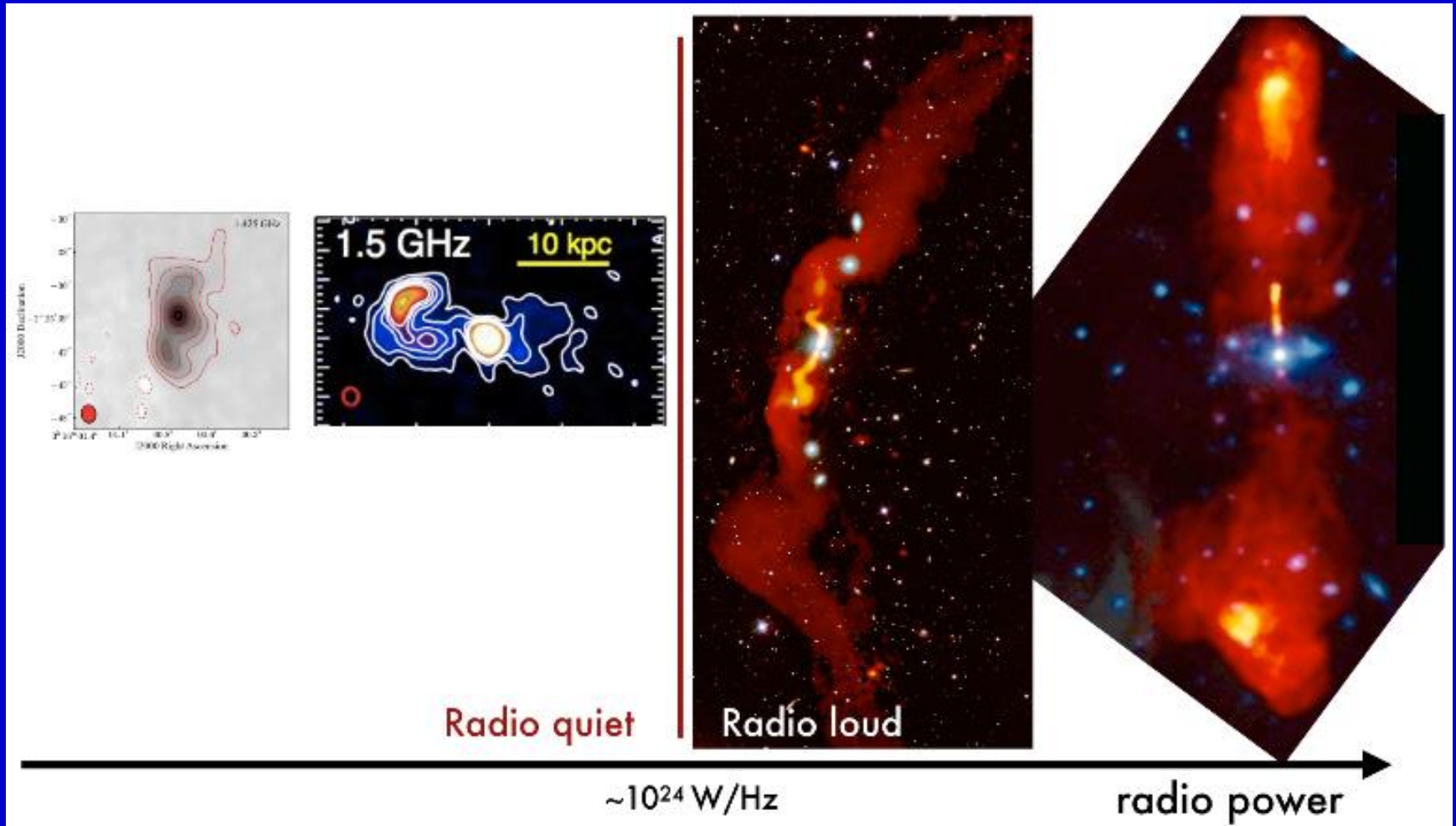
Radio lobes dominate over jets.

Mostly isolated galaxies
or poor groups.

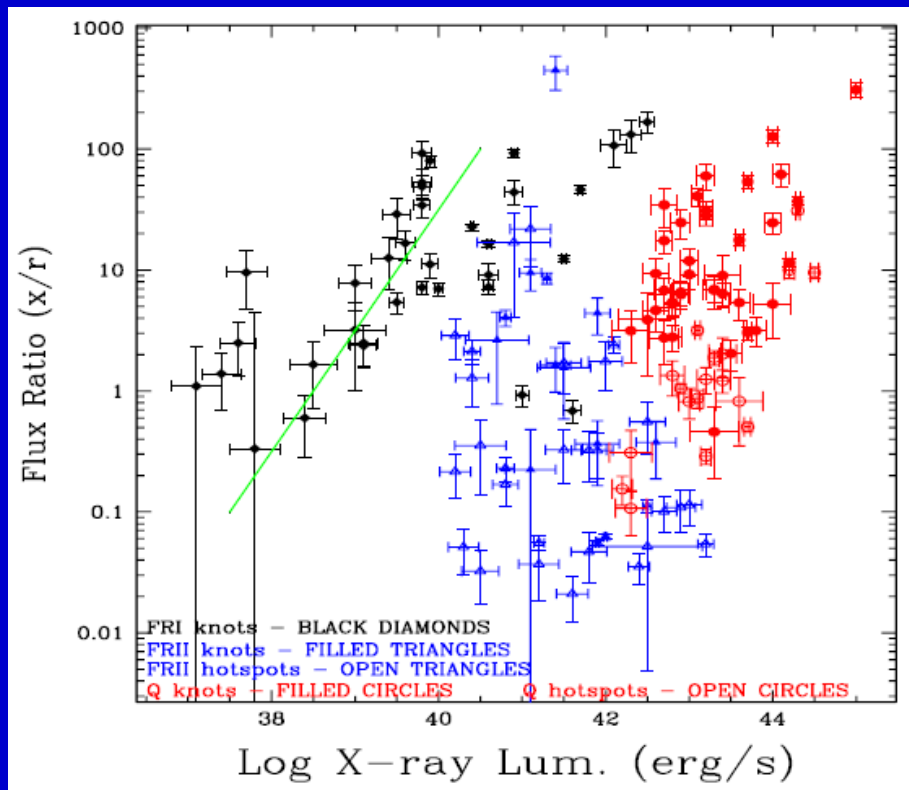
astro-ph/0406319

See a review on radio galaxies in arXiv: 1101.0837

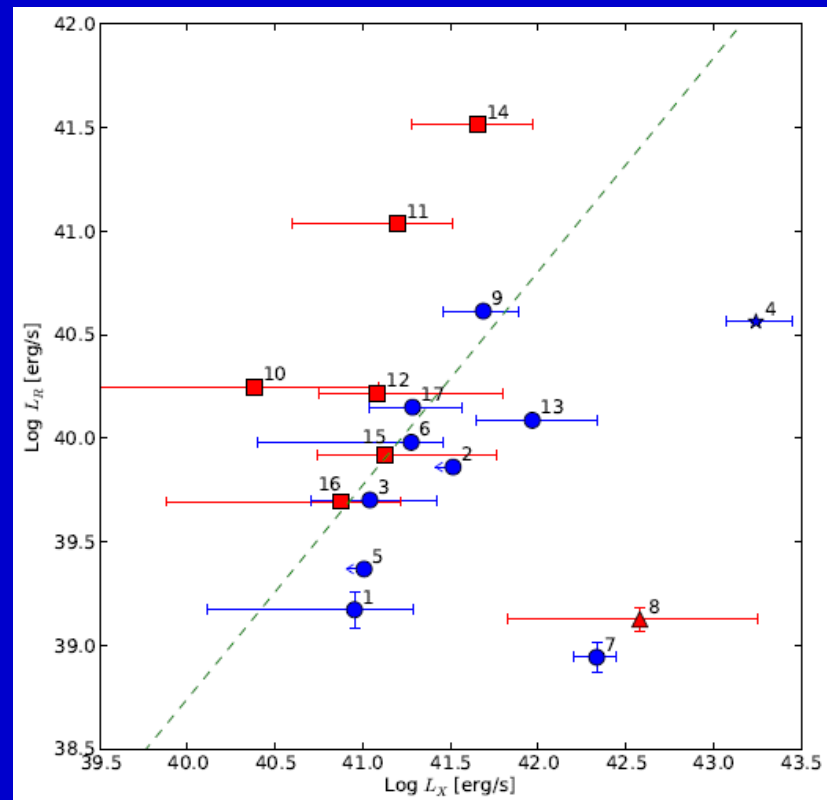
Diversity of radio jets



X-ray and radio properties



1003.0976



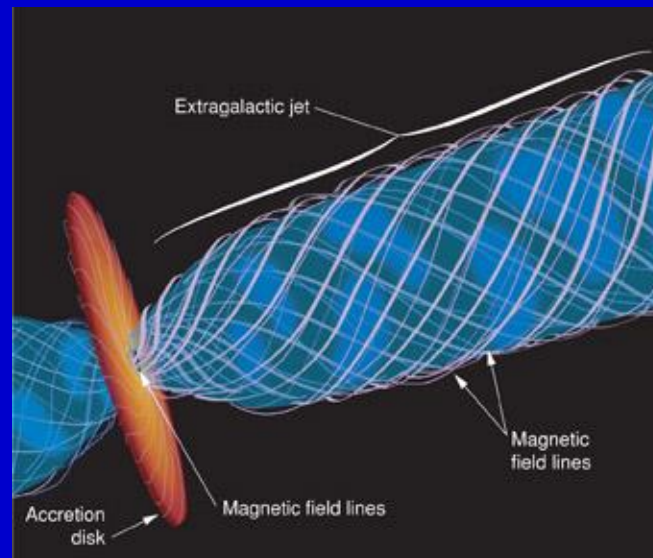
1104.3575

Magnetic field in a jet



Observations of M87 tell us that the magnetic field in the jet is mostly parallel to the jet axis, but in the emission regions (“knots”) it becomes perpendicular (see [astro-ph/0406319](https://arxiv.org/abs/astro-ph/0406319)).

The same structure is observed in several jets with radio lobes.

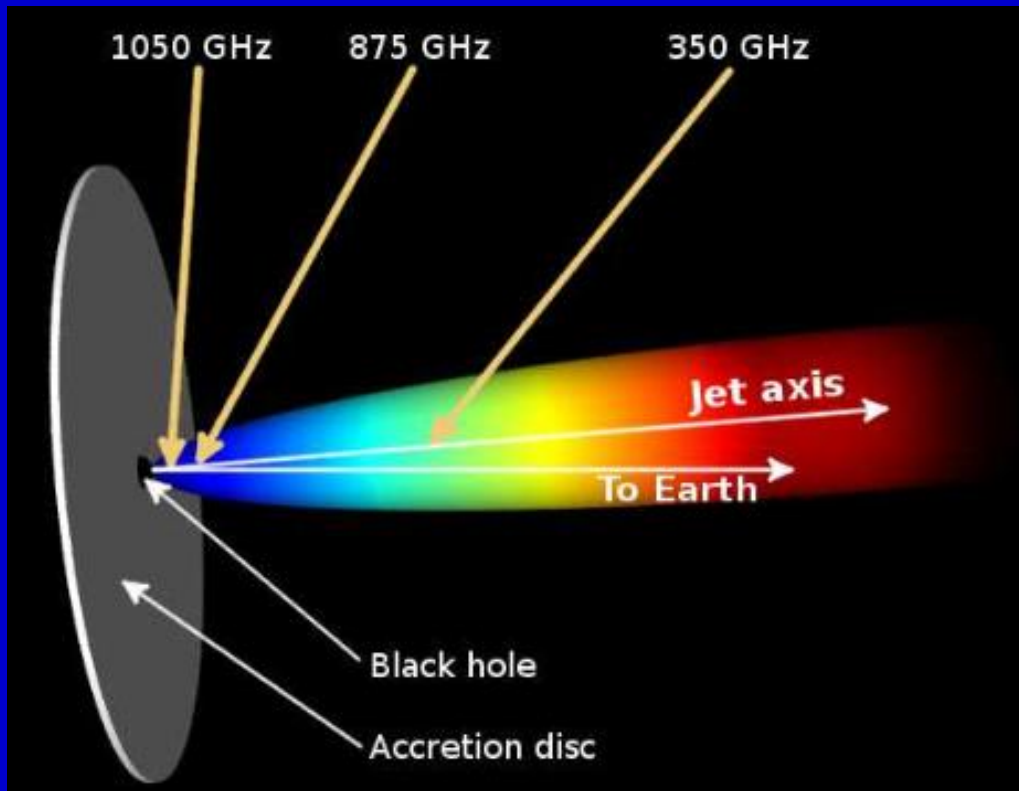


New RadioAstron data give some new insights.

Magnetic field in the jet

Due to modern high resolution observations new important results on the magnetic field in jets are obtained.

ALMA 0.01 pc scale

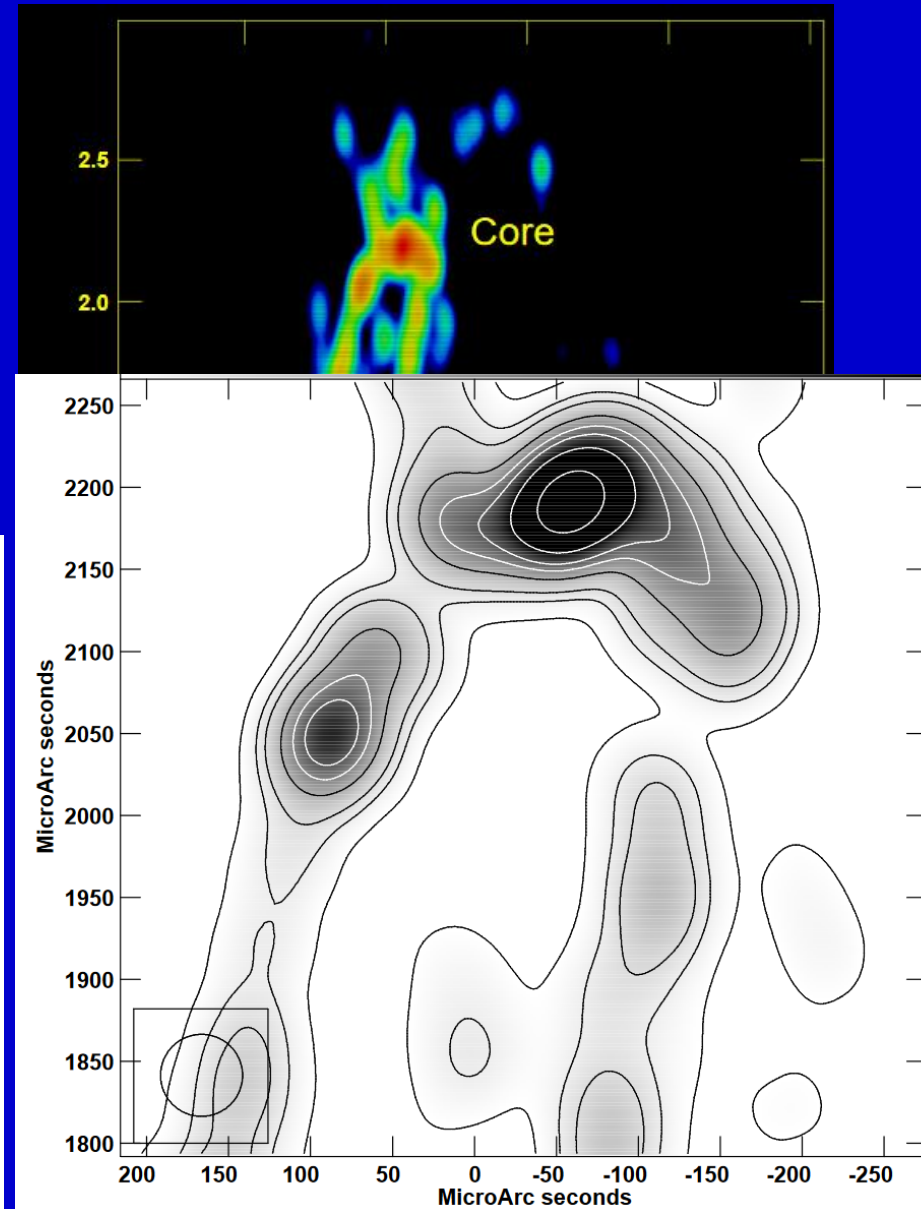
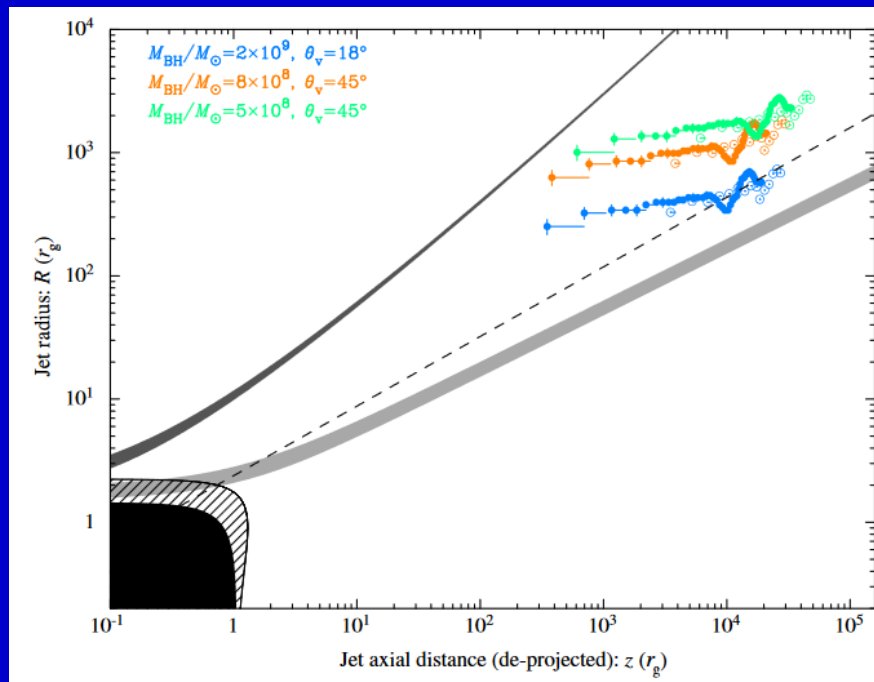


Magnetic fields of at least tens of Gauss (and possibly considerably higher) on scales of the order of light days (0.01 pc) from the black hole.

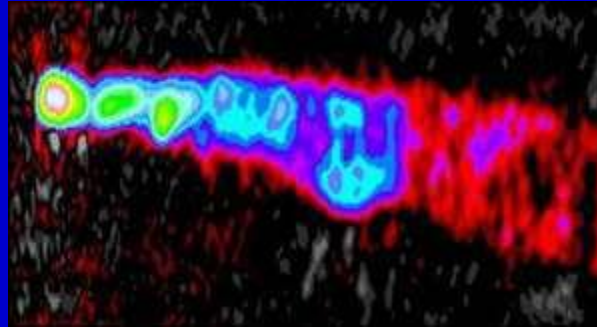
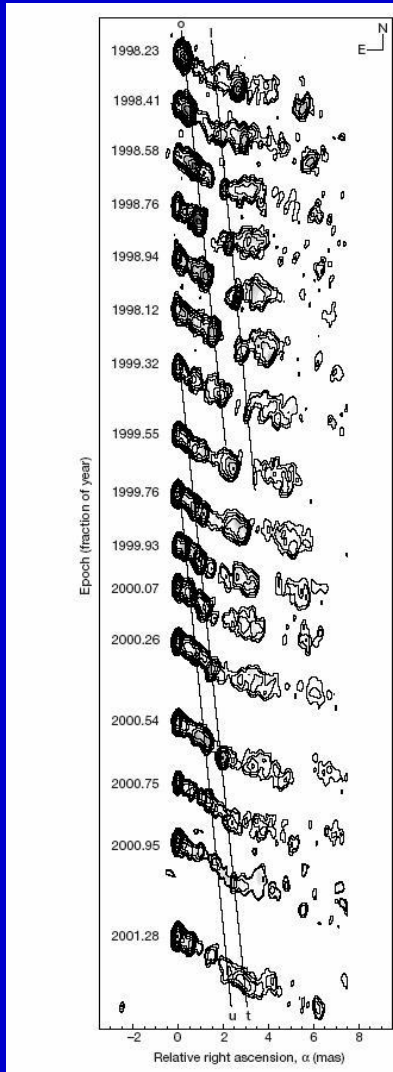
3C84 jet

Jet followed down to $>\sim 100 R_{\text{sh}}$
BH mass $\sim 2 \cdot 10^9$

Jet is already cylindrical at few $100 R_{\text{sh}}$
Jet from the disc, not from ergosphere?



Blobs in jets

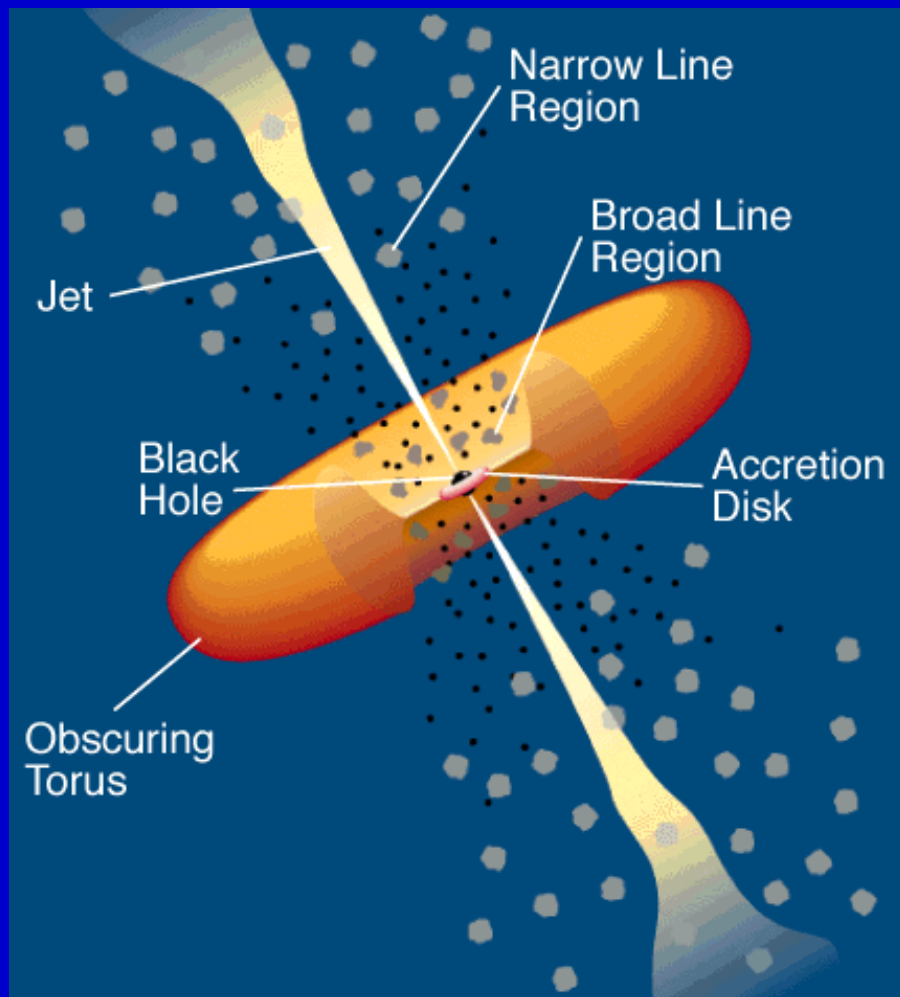


It is believed that bright features in AGN jets can be results of the Kelvin-Helmholtz instability. This instability leads to a spiral structure formation in a jet. (see, for example, astro-ph/0103379).

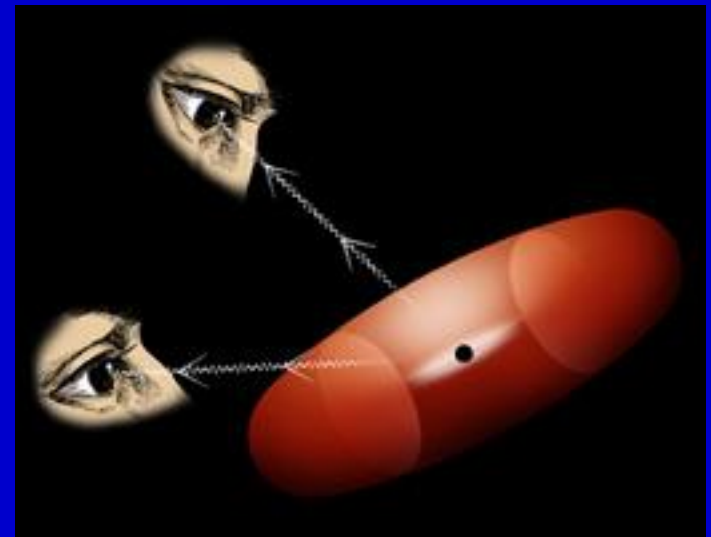
3C 120

However, in the case of 3C 120 the blobs appearance is due to processes in the disc. Dips in X-rays (related to the disc) appear before blobs ejection (Marscher et al. 2002).

Blazars



If a jet is pointing towards us, then we see a *blazar*.



Blazars at very high energies

Blazars are powerful gamma-ray sources. The most powerful of them have equivalent isotropic luminosity 10^{49} erg/s.

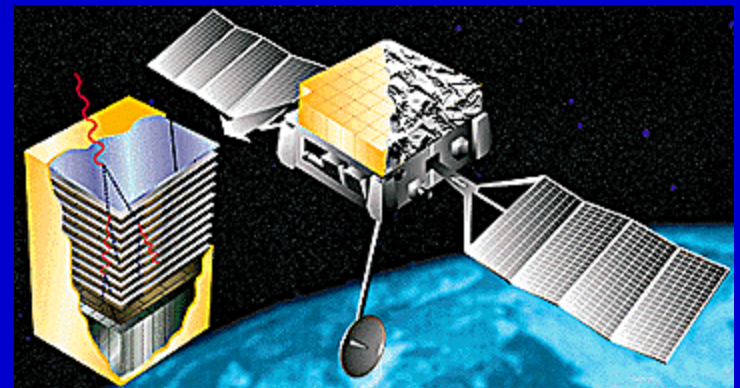
Collimation $\theta^2/2 \sim 10^{-2} - 10^{-3}$. θ – jet opening angle.

EGRET detected 66 (+27) sources of this type.

More results have been obtained after the launch of GLAST.

Many sources have been detected in the TeV range by ground-based gamma-ray telescopes. All of them, except M87, are BL Lacs at $z < 0.2$ (more precisely, to high-frequency-peaked BL Lac – HBL).

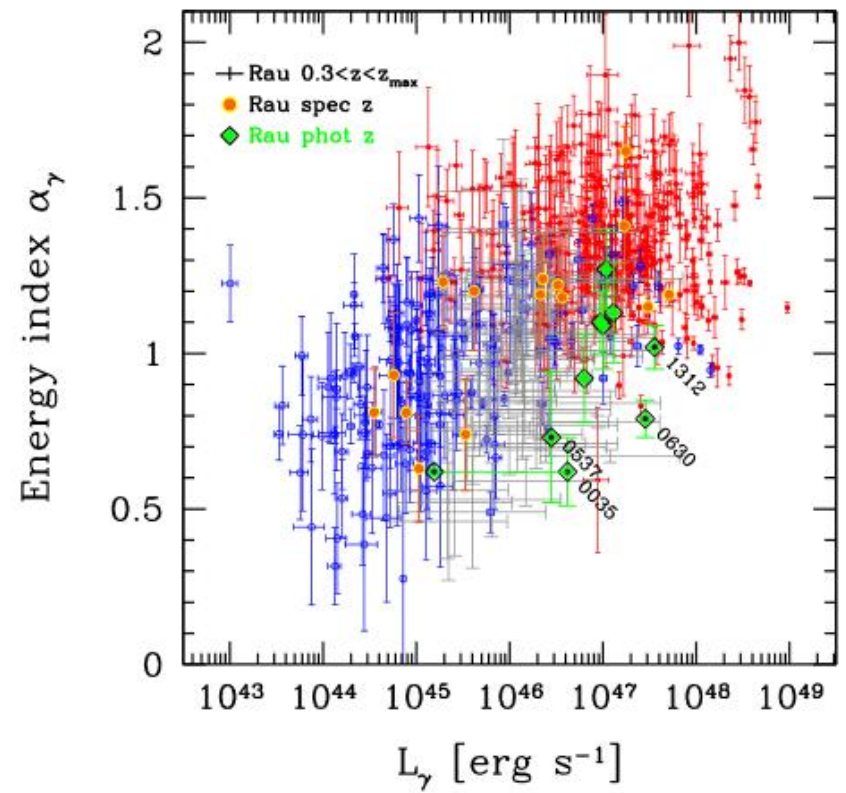
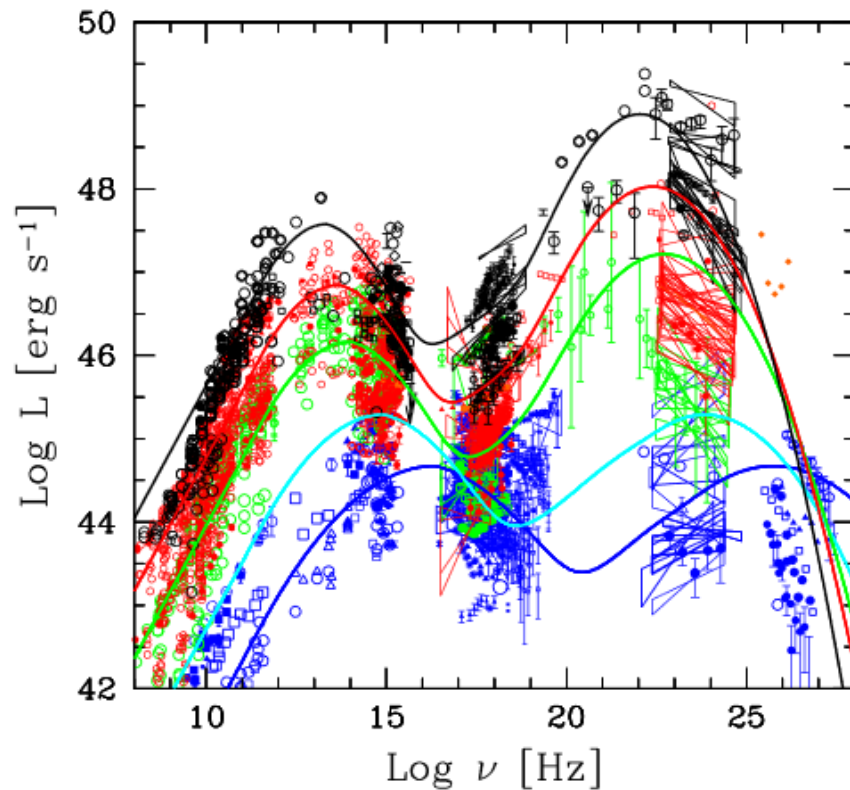
Observations show that often (but not always) after a gamma-ray bursts few weeks or months later a burst happens also in the radio band.



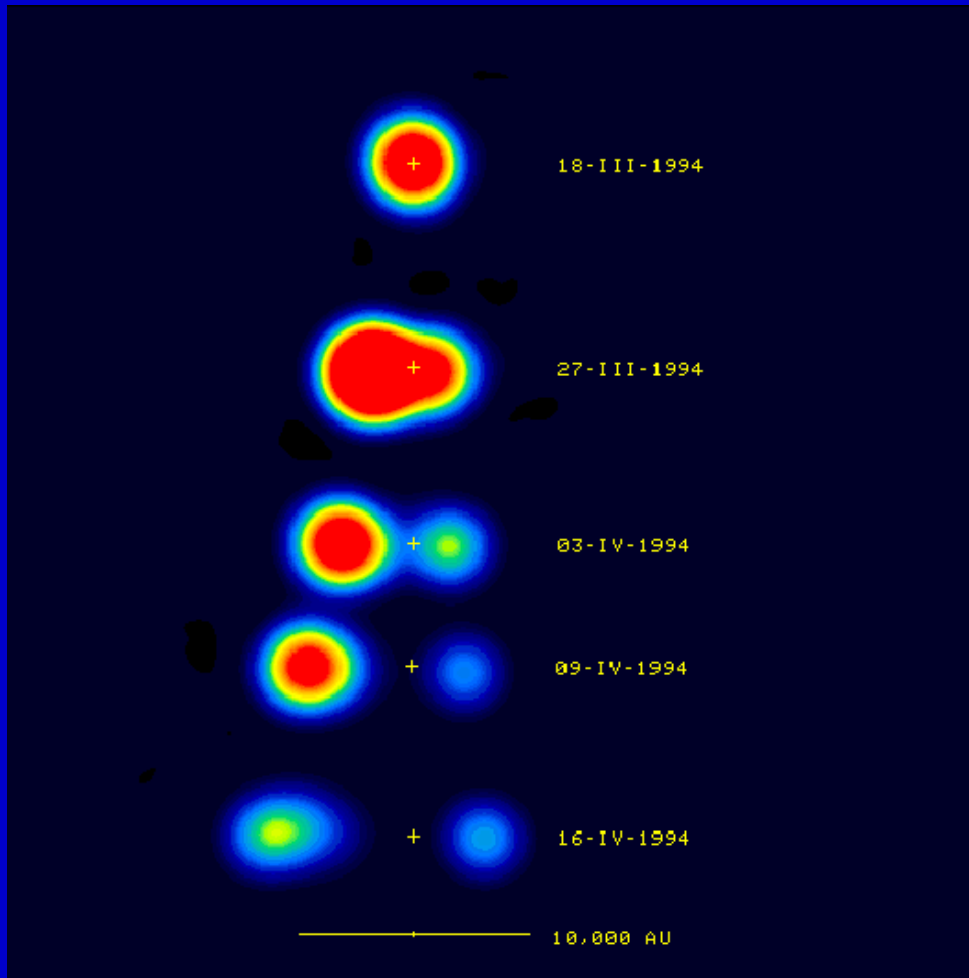
Fermi

see astro-ph/0611521, but notice rapid progress

Blazar spectra



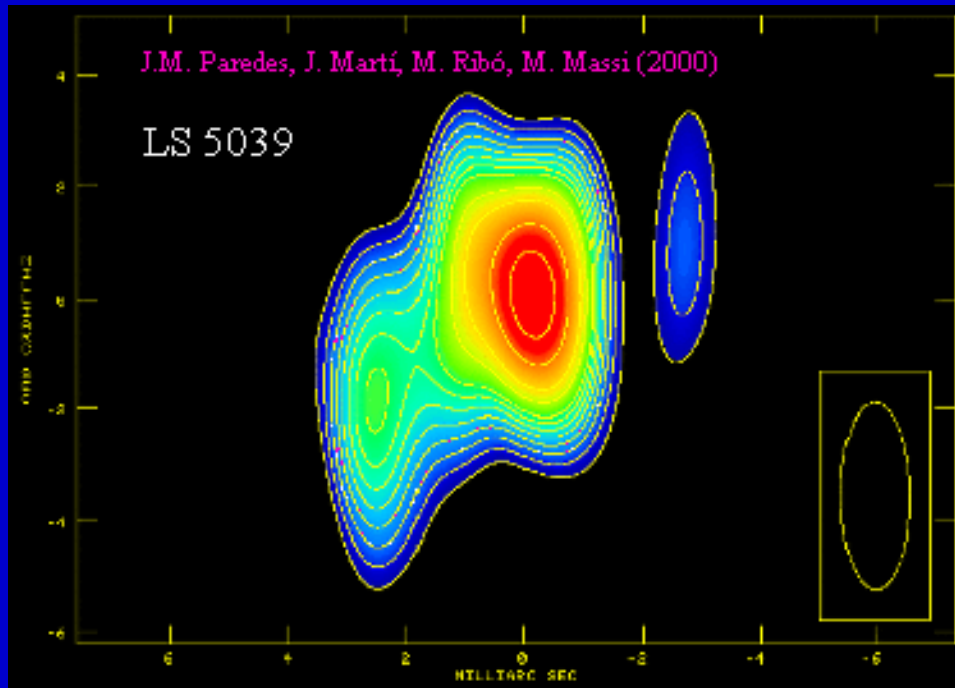
Microquasars



The correlation between X-ray and synchrotron (i.e. between disc and jet emission) is observed.

GRS 1915

Microquasars jets in radio



LS 5039/RX J1826.2-1450 –
is a galactic massive X-ray binary.

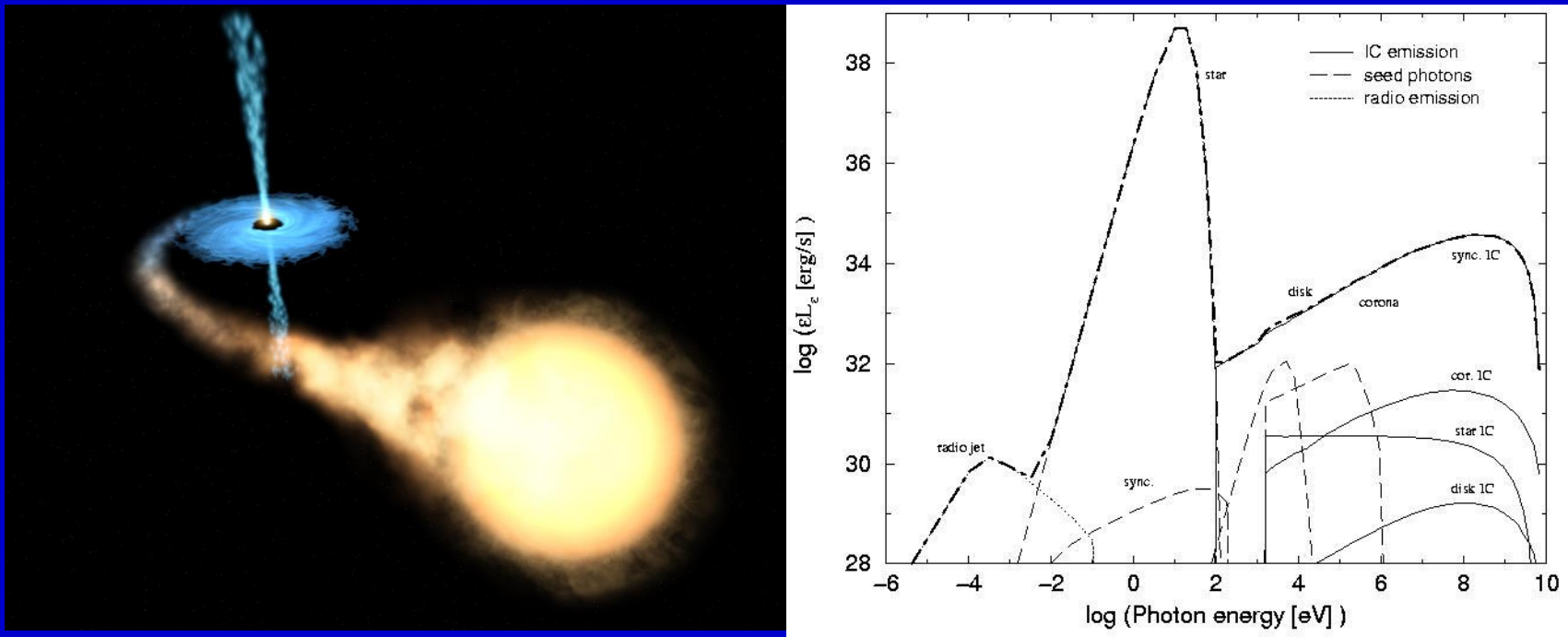
The jet length is ~ 1000 a.e.

Probably, the source was
observed by EGRET
as 3EG J1824-1514.

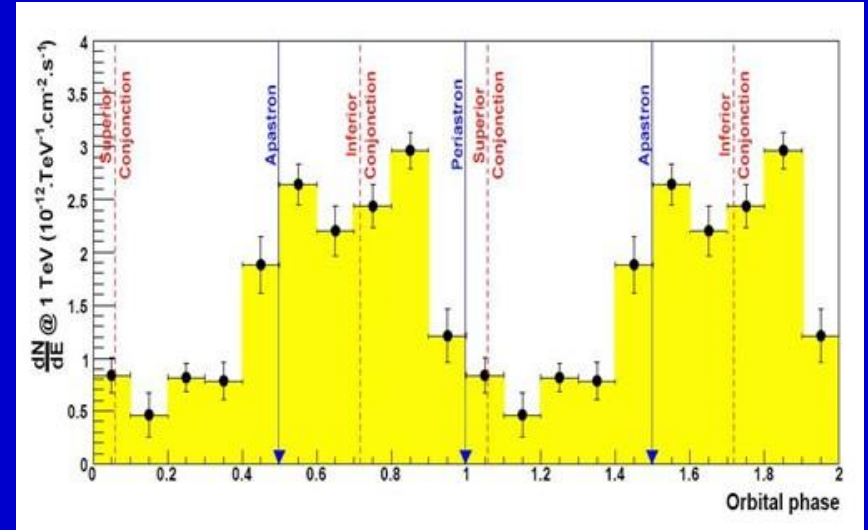
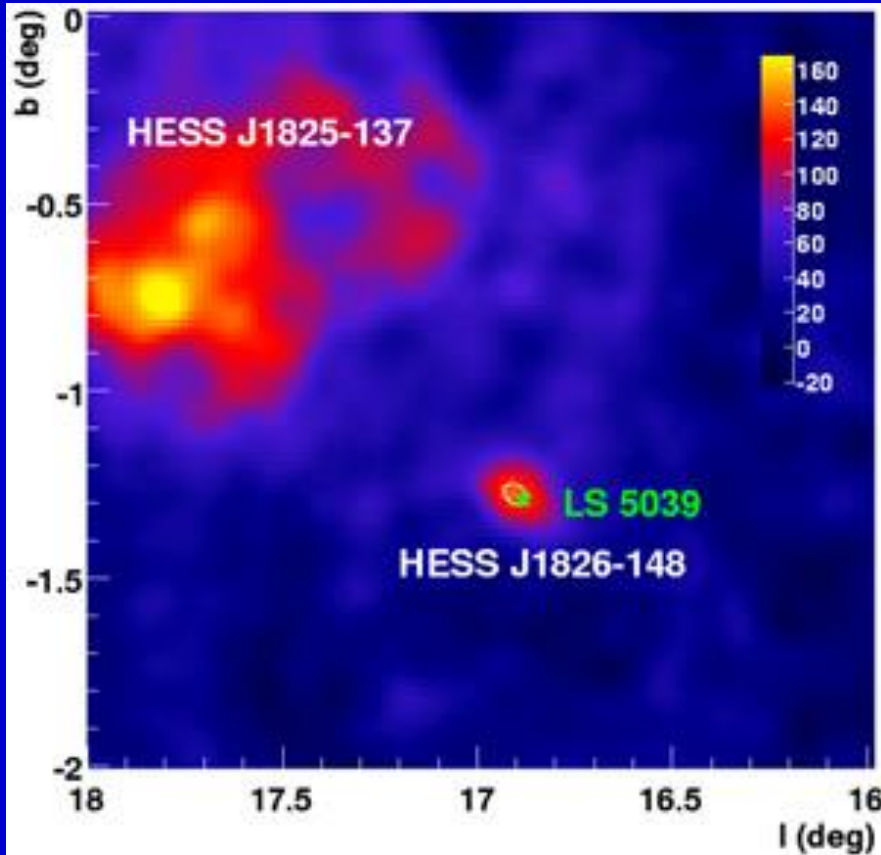
Rem: check <https://ui.adsabs.harvard.edu/abs/2012MNRAS.421.1351B/abstract>

The role of a donor

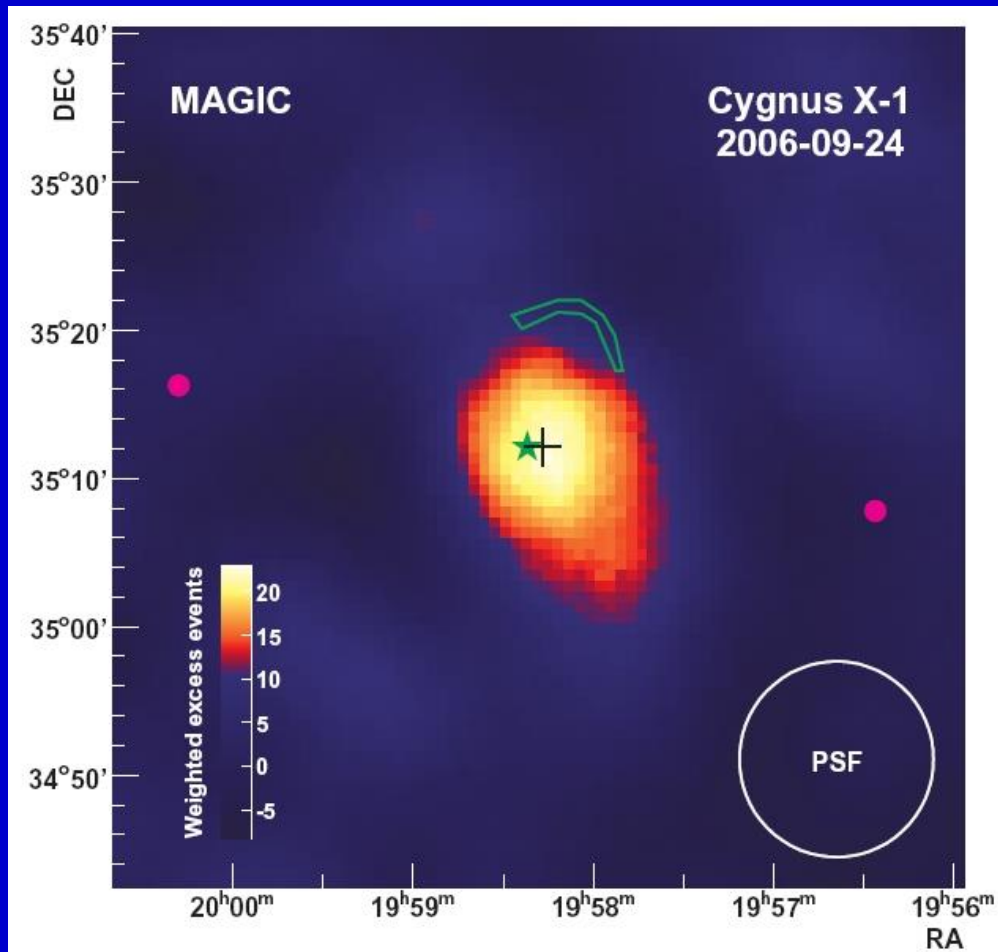
An important difference between the microquasars case and AGNs is related to the existence of a donor-star. Especially, if it is a giant, then the star can inject matter and photons into the jet.



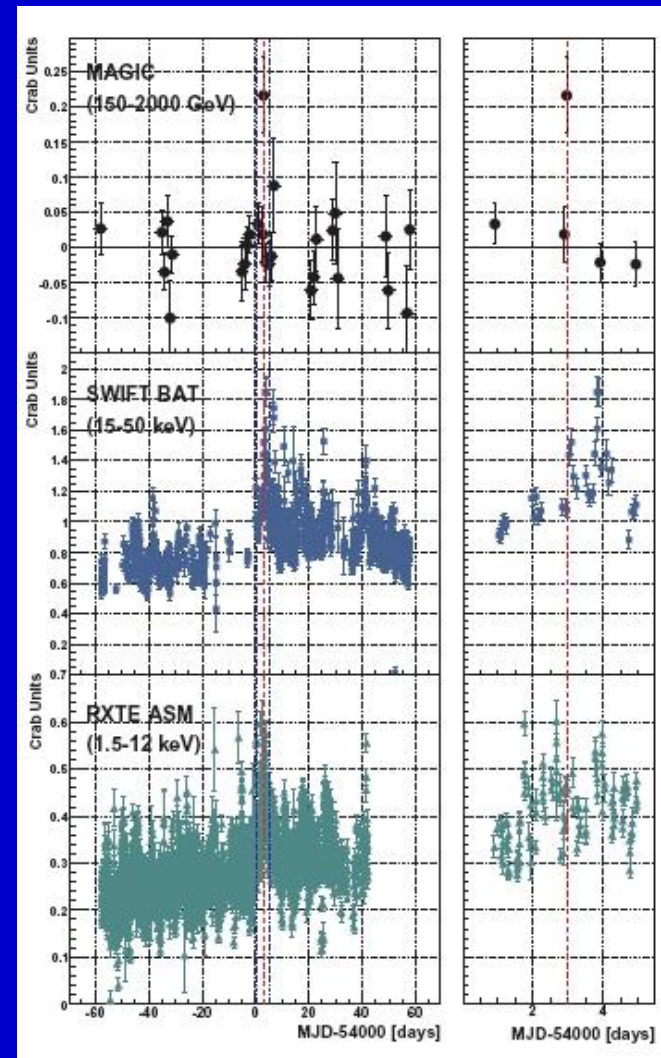
Microquasars in gamma-rays: TeV range



TeV emission from Cyg X-1



arxiv:0706.1505



See a review on jets in binaries in 1407.3674

Jet models

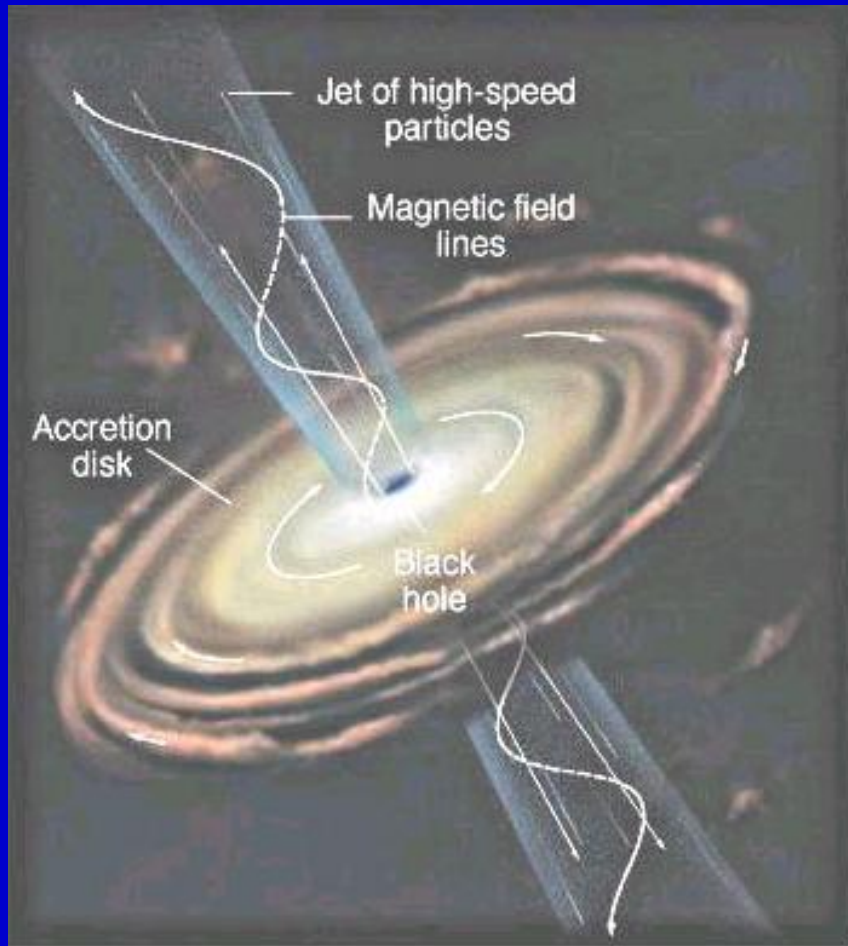


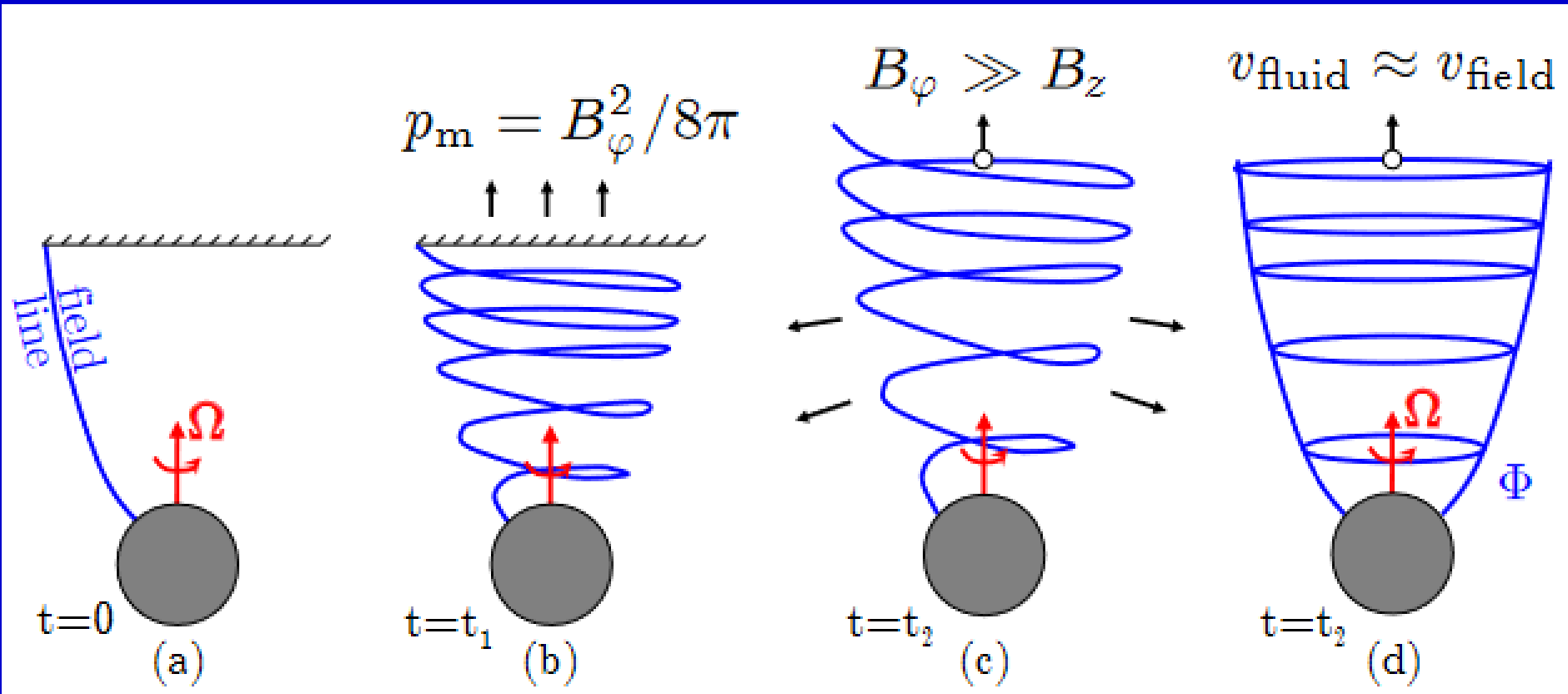
Table 1. Characteristic parameters of relativistic jet sources.

	L_j (erg/s)	Γ	Δt
GRB	10^{47} - 10^{50}	$10^2 - 10^3$	millisec - min.
AGN	10^{42} - 10^{47}	5 - 50	hours - years
MQ	10^{37} - 10^{40}	1 - 10	days
GF	10^{43} - 10^{46}	1	seconds

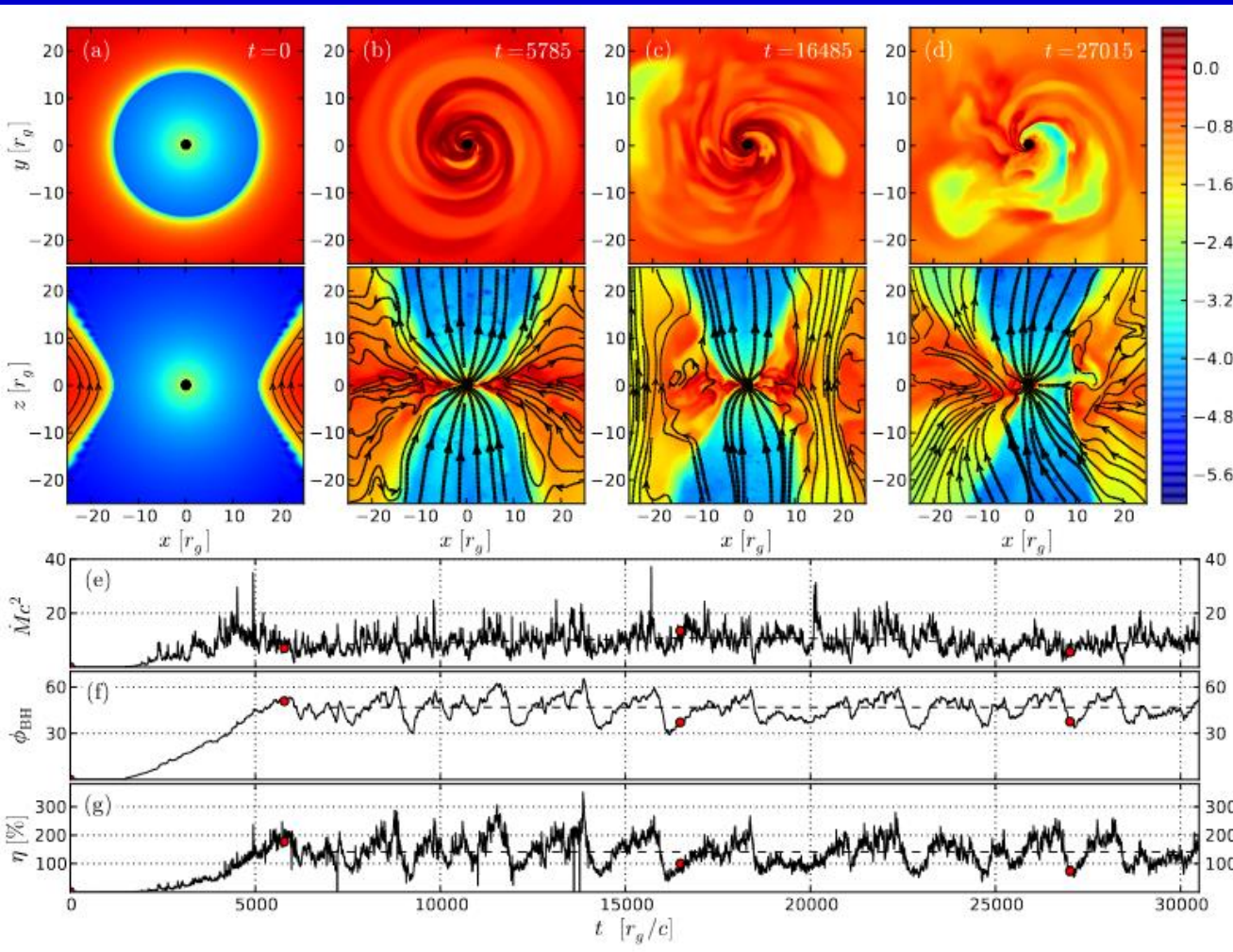
In all models jets are related to discs. Velocity at the base of a jet is about the parabolic (escape) velocity.

(the table is from astro-ph/0611521)

Jet formation by magnetic field

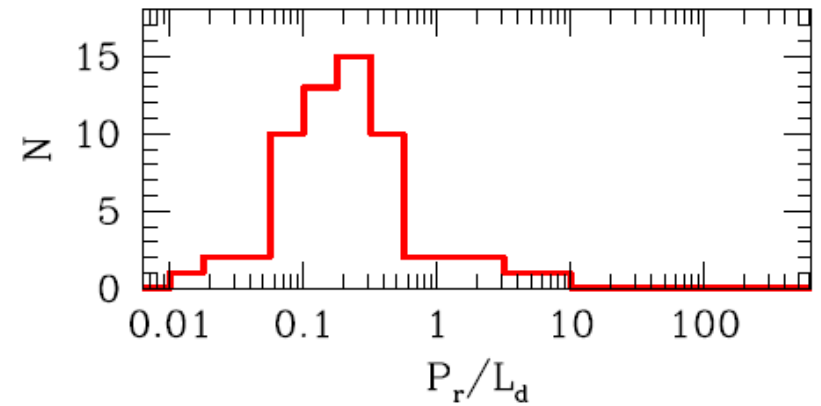
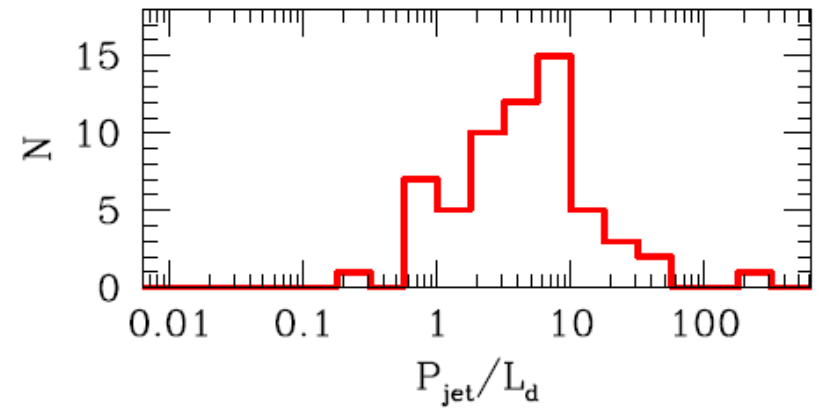
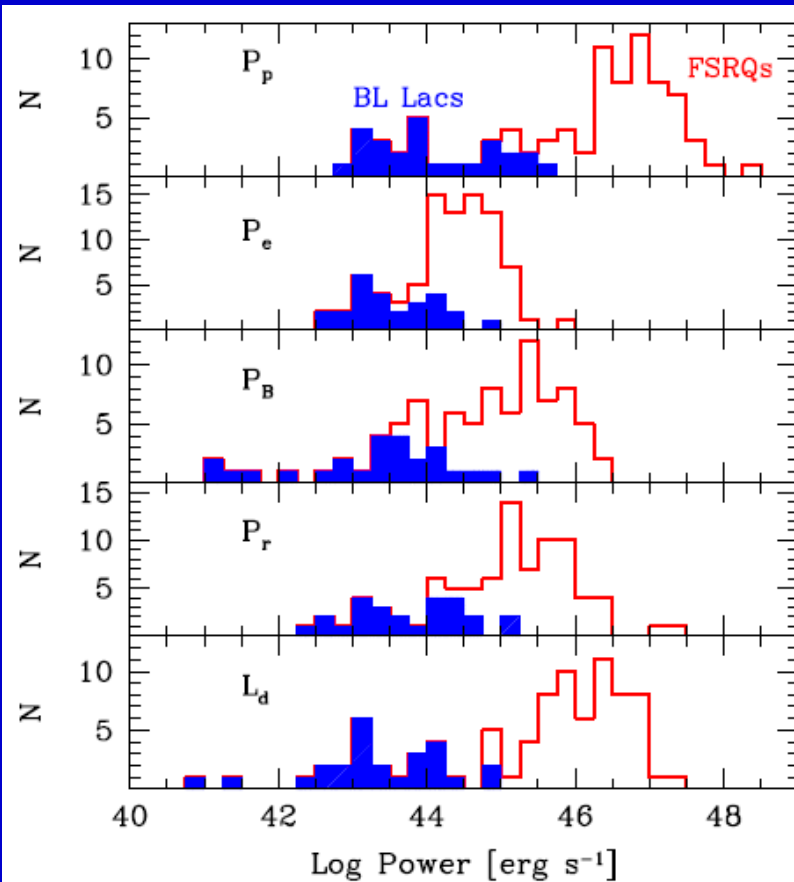


Disk-jet-BH behavior



Large-scale vertical magnetic field accumulates at the center and forms a dynamically important magnetic field that obstructs the accretion flow and leads to a magnetically arrested disk. Color shows the logarithm of density.

Jet power



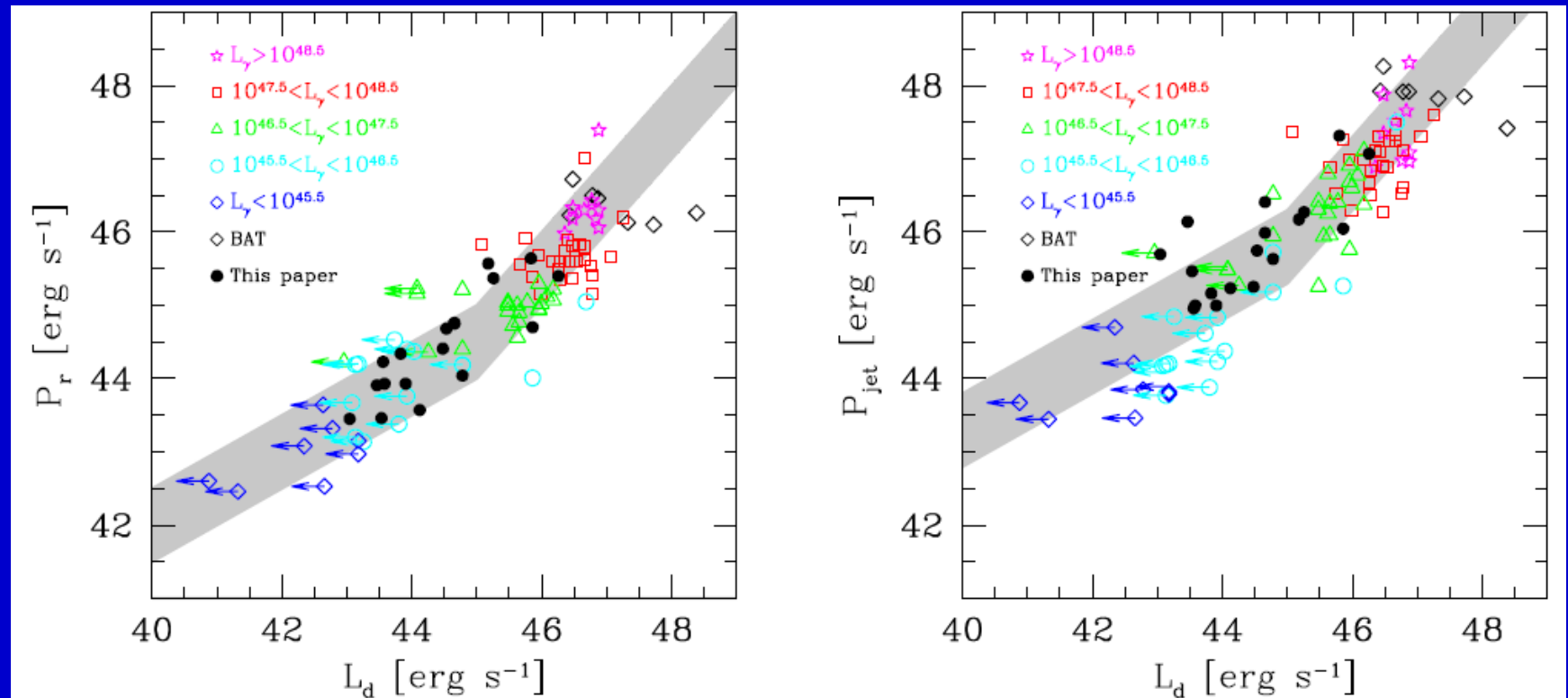
$$P_{\text{jet}} > 2P_r = 2L/\Gamma^2$$

Jet and disc

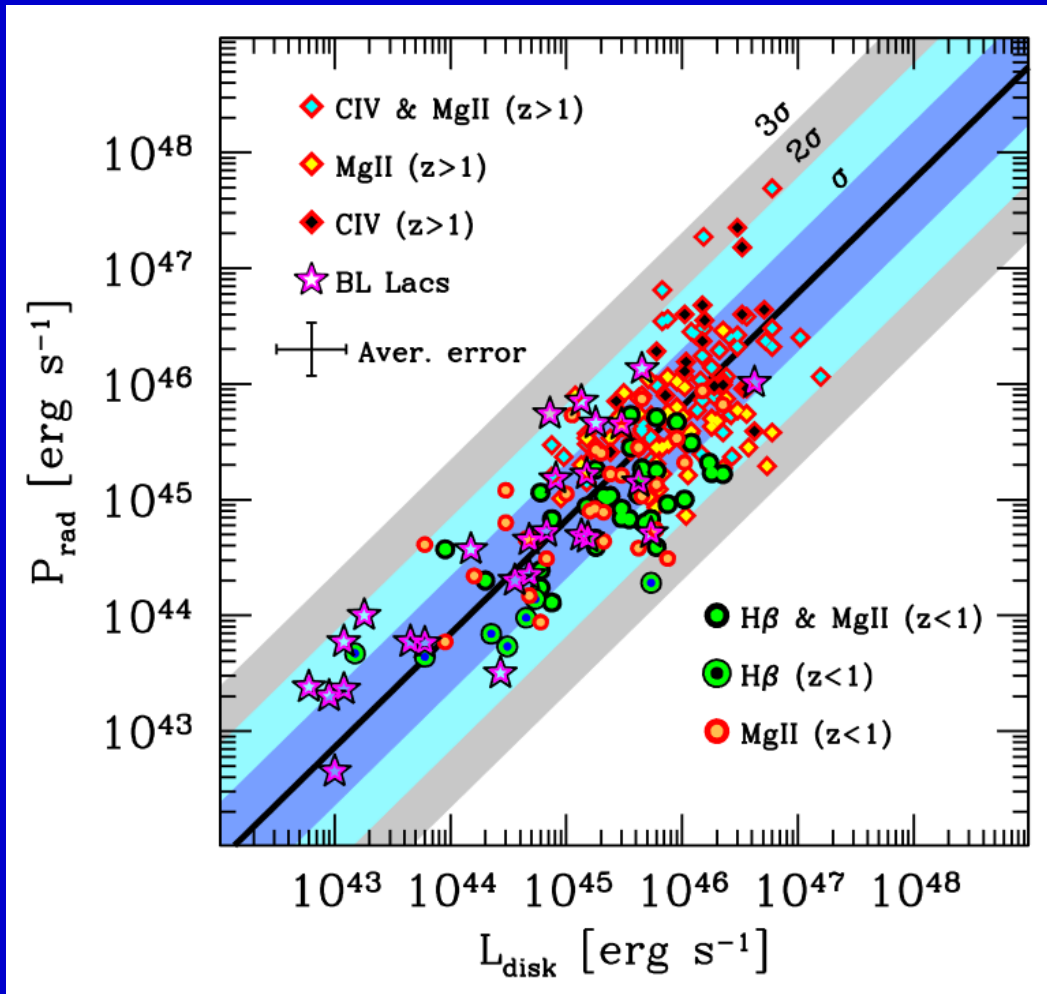
L_d – disc luminosity.

$$P_{\text{jet}} = P_B + P_P + P_e$$

In the gray stripes $P_{\text{jet}} \sim \dot{M}$ and
at low accretion rates $L_d \sim \dot{M}^2$, at large - $L_d \sim \dot{M}$.



Jets are more powerful than discs

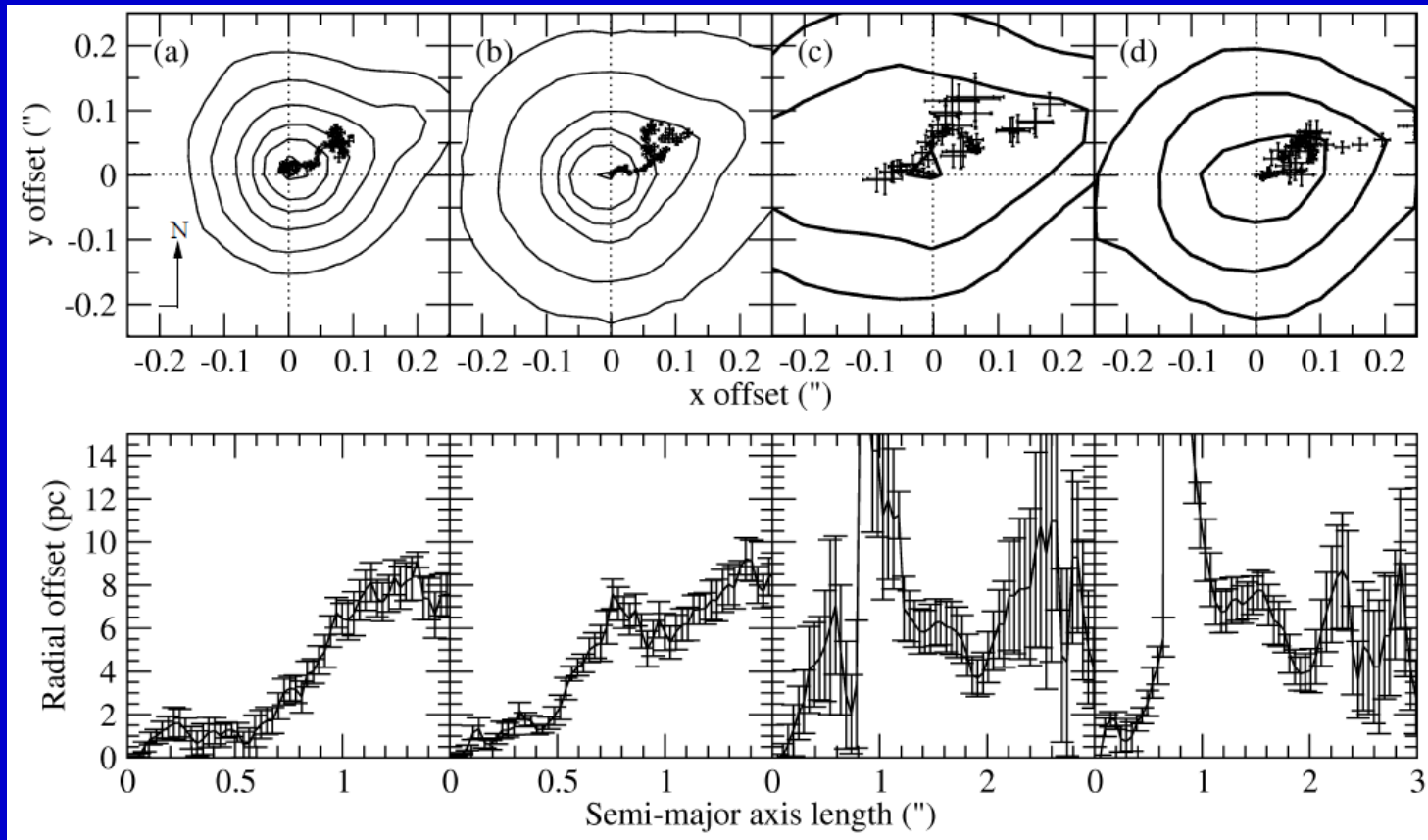


Jets also serve as sites for particle acceleration, see 2003.06587

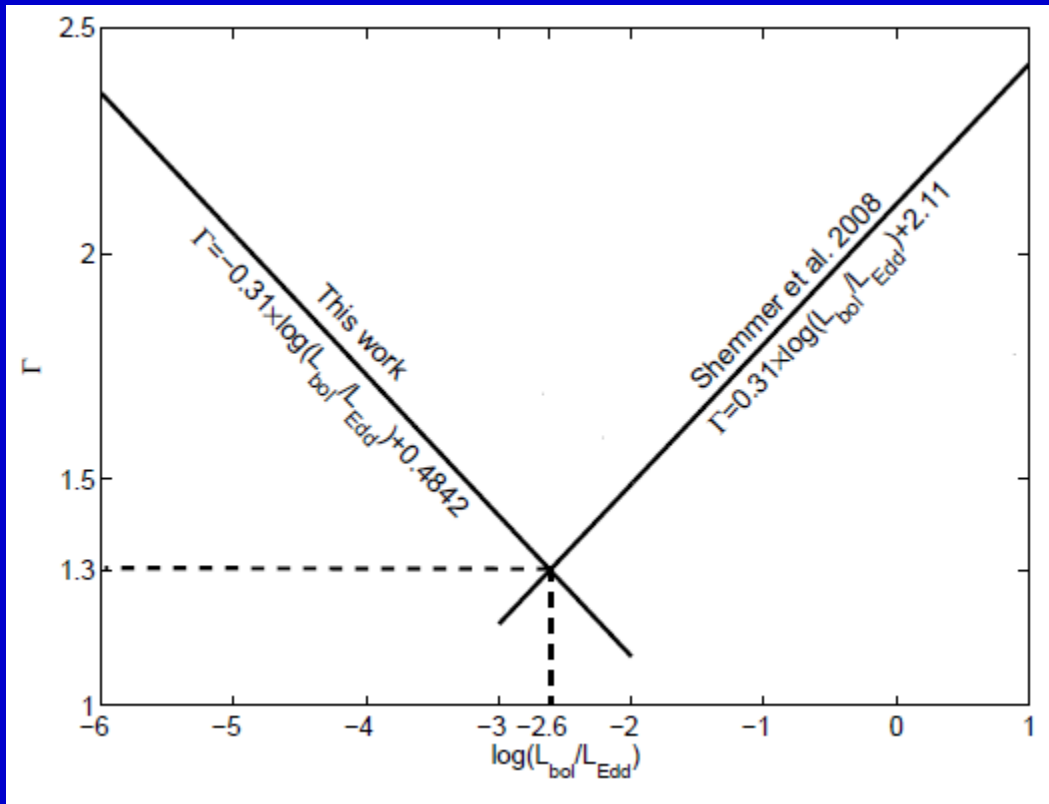
$$P_{\text{rad}} = 2f \frac{L_{\text{jet}}^{\text{bol}}}{\Gamma^2}$$

Displaced SMBH in M87

Projected displacement of 6.8 ± 0.8 pc
consistent with the jet axis
displaced in the counter-jet direction



Different accretion regimes in AGNs



Γ - photon index

Anticorrelation for low-luminosity AGNs (LINERS).

Correlation for luminous AGNs.

In the critical point the accretion regime can be changed: from a standard thin accretion disc to RIAF (radiatively inefficient accretion flow).

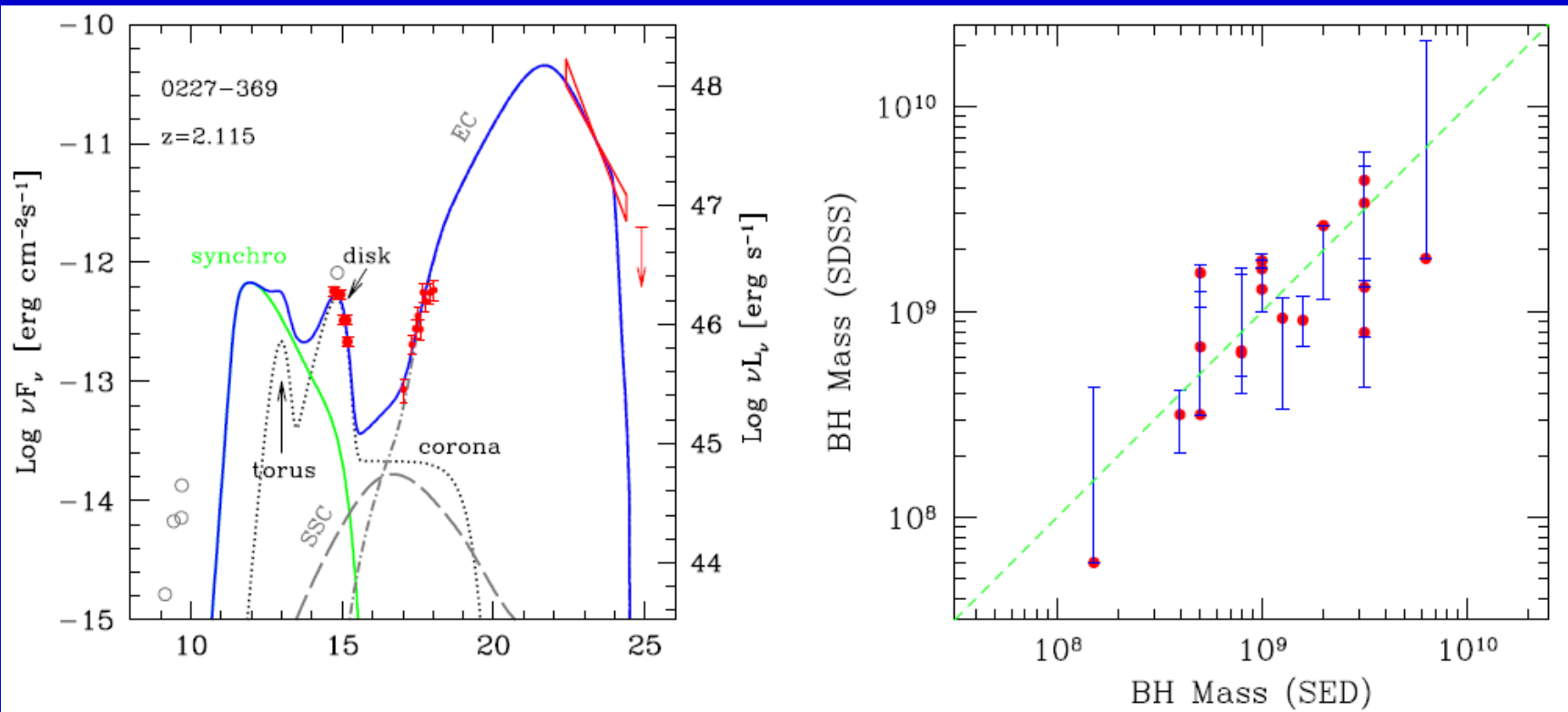
BH mass determination

Accretion disc contribution is visible in opt-UV.

It allows to estimate the BH mass.

It can be compared with emission lines estimates.

Bars correspond to different lines used.



BH mass and jet properties in M87

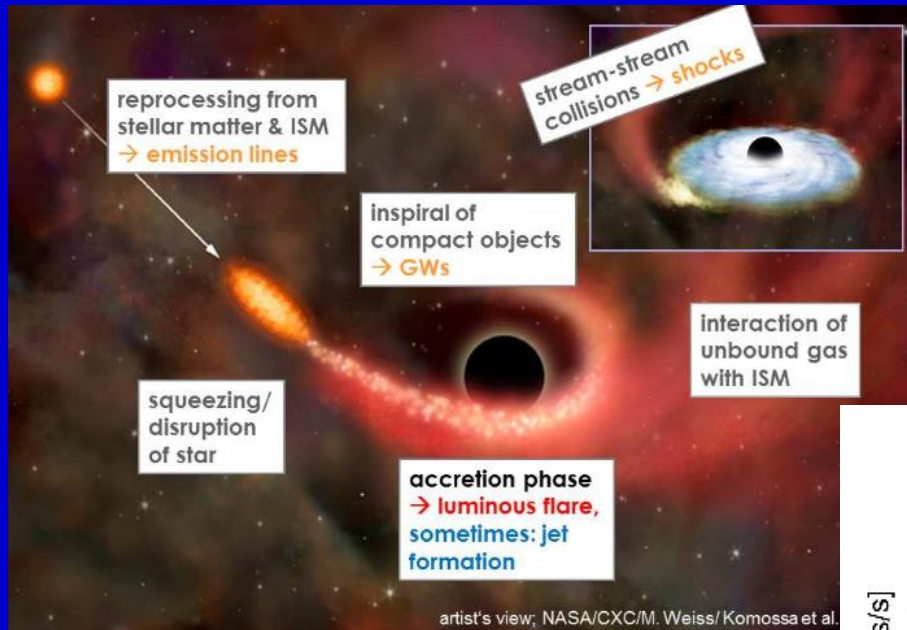
Table 3. Predicted jet and BH parameters for $M = 6.5 \times 10^9 M_{\odot}$.

σ_M	$\Gamma\theta_j$	ϕ	a_*	W_j (10^{42} erg/s)
(1)	(2)	(3)	(4)	(5)
10	0.062	3.2	0.093	1.9
20	0.063	3.3	0.144	4.7

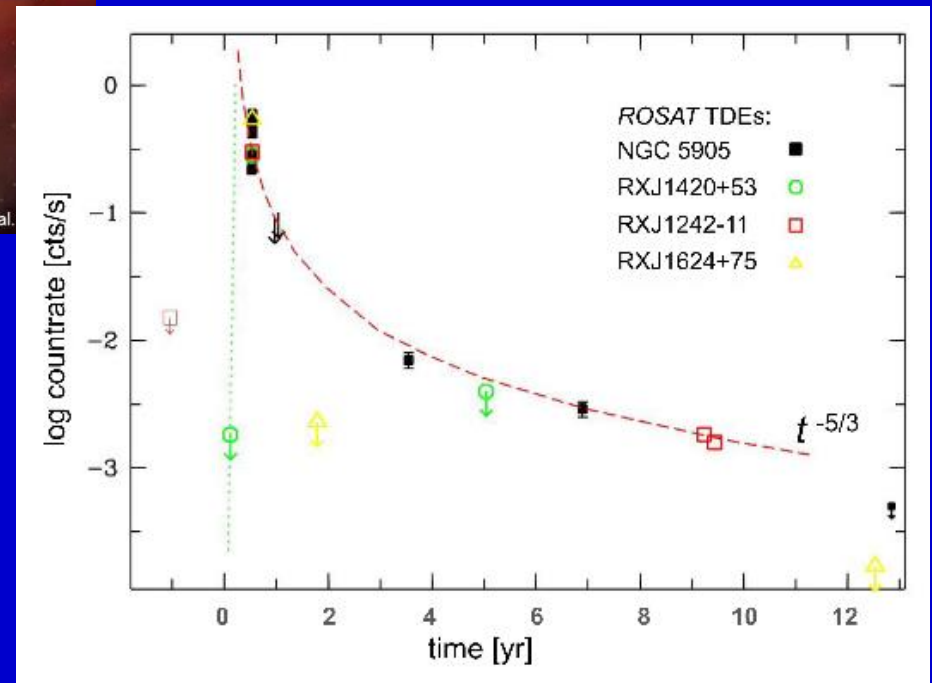
Estimates are in correspondence with the EHT data on the BH mass.

If the mass is assumed to be known,
then the initial magnetization σ_M can be determined.

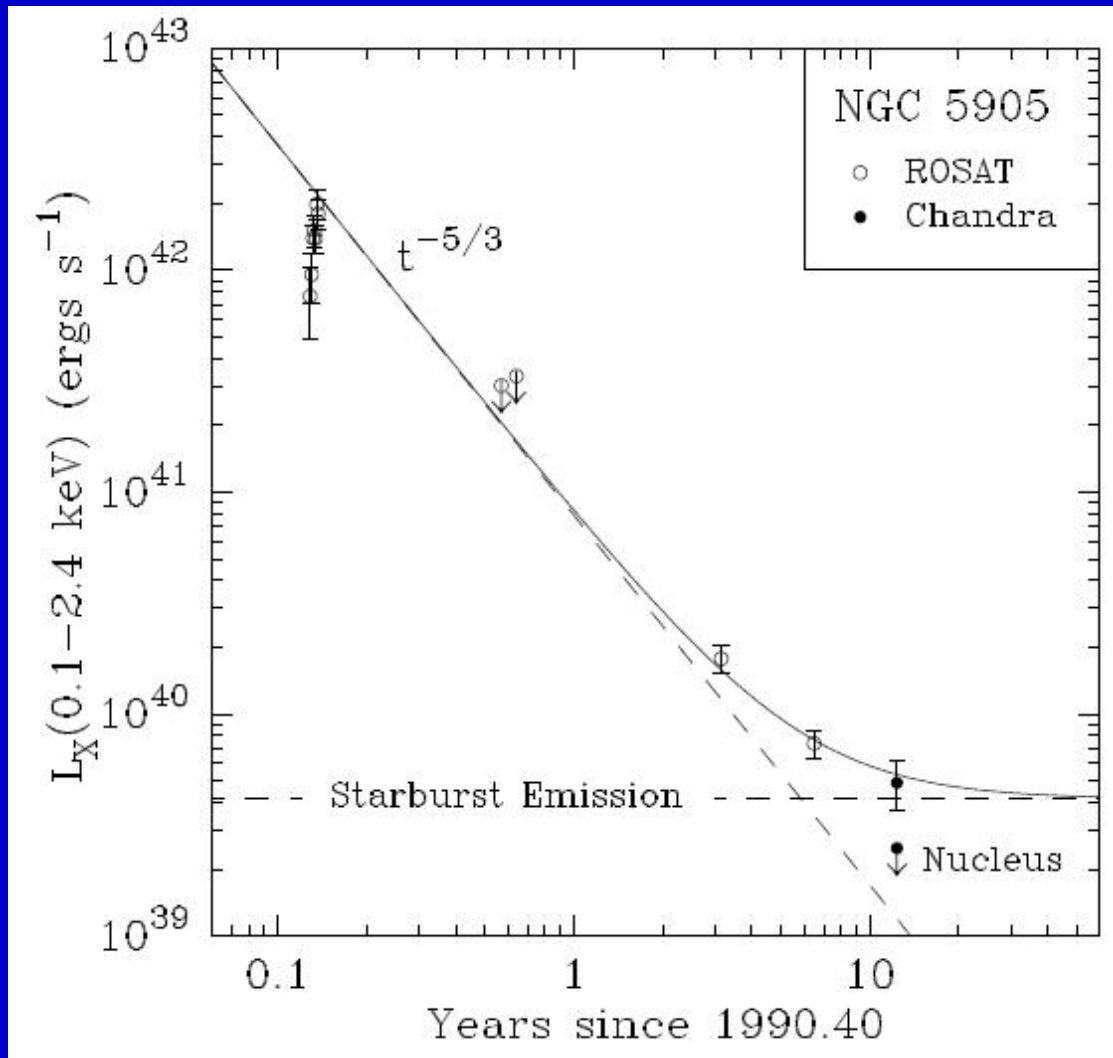
Tidal disruption: general picture



About radiative mechanisms
see 2008.01117



A burst in NGC 5905



The decay was well described by the relation:

$$(t - t_D)^{-5/3}$$

Two other bursts discovered by ROSAT and observed by HST and Chandra:

RX J1624.9+7554
RX J1242.6-1119A

Tidal disruption parameters

The Hills limit: 3×10^8 solar masses. A BH disrupts stars.

After a disruption in

$$(t_0 - t_D) \sim 1.1 M_8^{1/2} \text{ yr}$$

happens a burst with the temperature

$$T_{\text{eff}} \approx (L_{\text{Edd}}/4\pi\sigma R_T^2)^{1/4} = 3.7 \times 10^5 M_8^{1/12} \text{ K}$$

The maximum accretion rate

$$\dot{M}_{\text{max}} \sim 0.14 M_8^{1/2} M_{\odot} \text{ yr}^{-1}$$

This rate corresponds to the moment

$$(t_{\text{max}} - t_D) \sim 1.5 (t_0 - t_D)$$

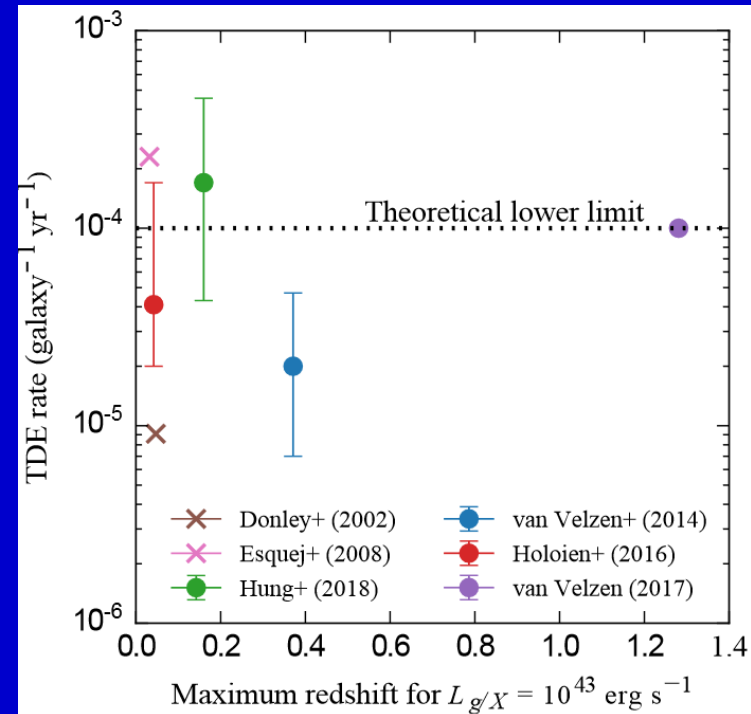
Then the rate can be described as

$$\dot{M}(t) = 0.3 M_8 [(t - t_D)/(t_0 - t_D)]^{-5/3} M_{\odot}$$

For a BH with $M < 10^7 M_{\odot}$ the luminosity at maximum is:

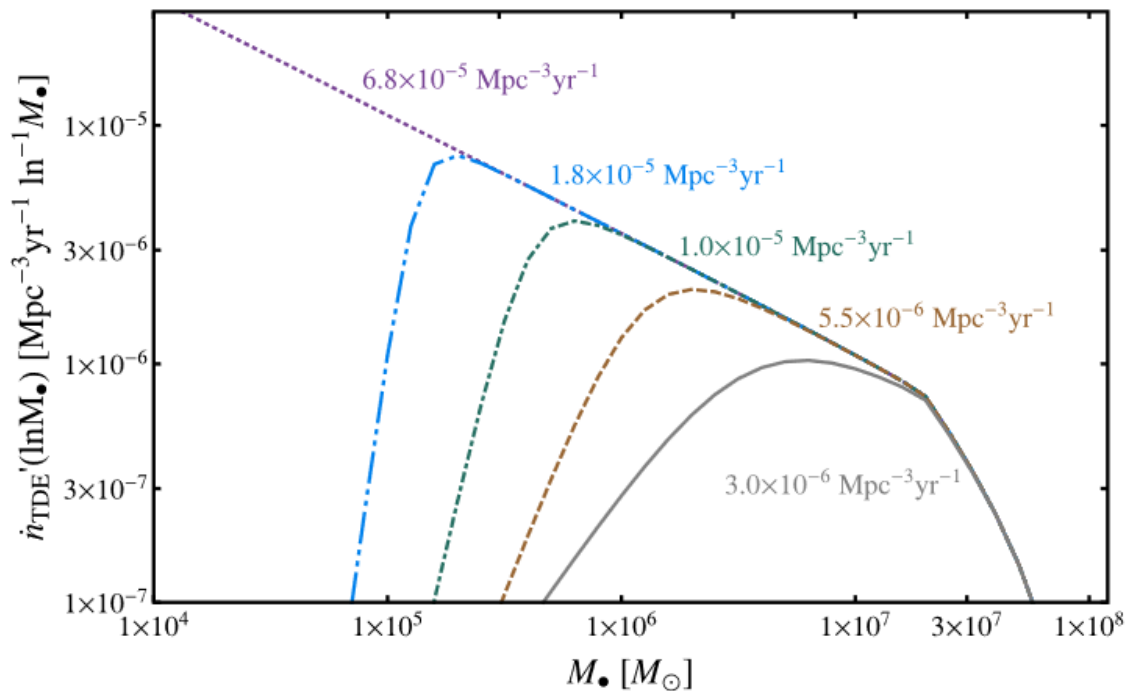
$$L_{\text{flare}} \geq \eta \dot{M}_{\text{Edd}} c^2 > 1.3 \times 10^{45} M_7 \text{ ergs s}^{-1}$$

Rate of TDE

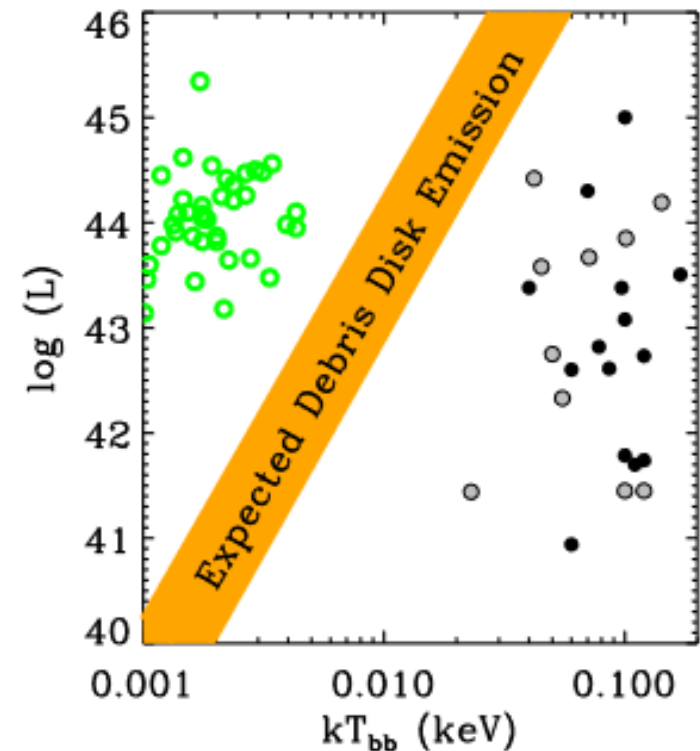
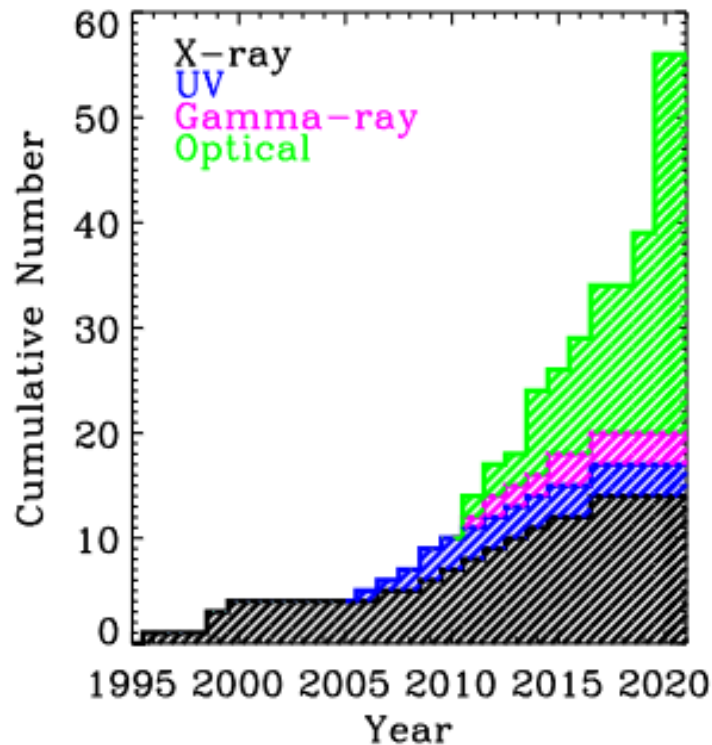


Rate of TDE is $\sim 1/100000$ yrs per galaxy (1407.6425).

Volumetric TDE rates are dominated by the smallest galaxies that typically host SMBHs.

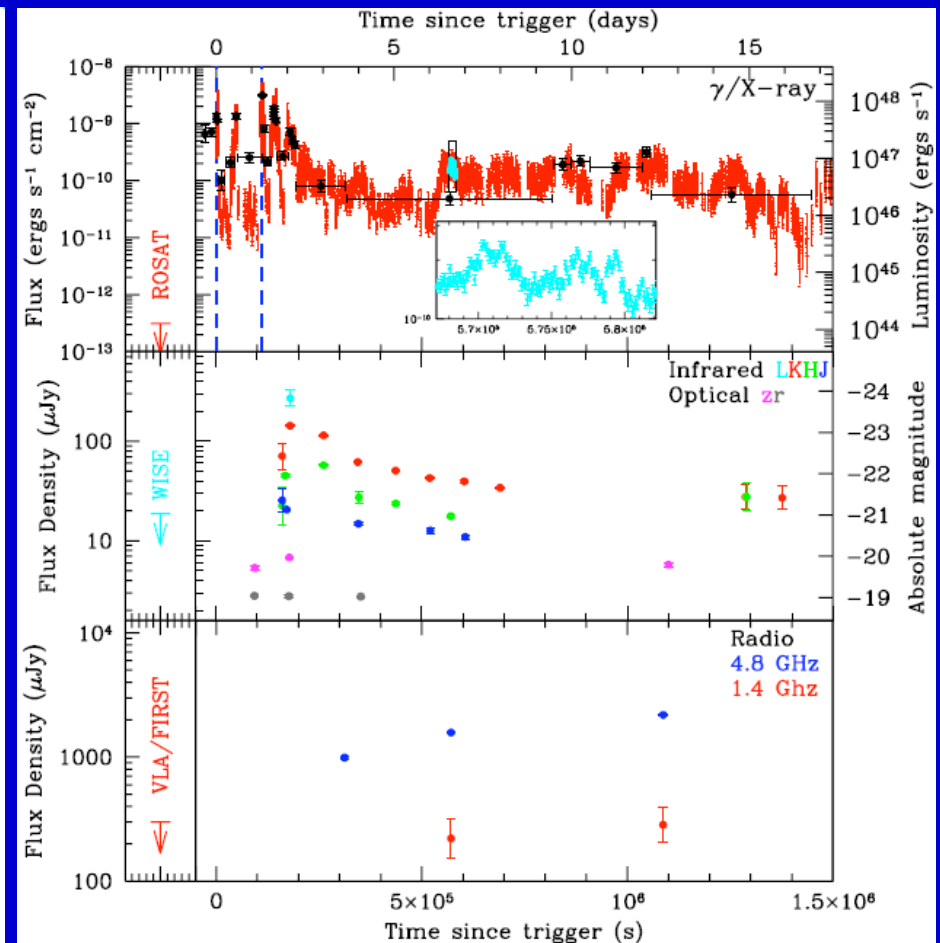
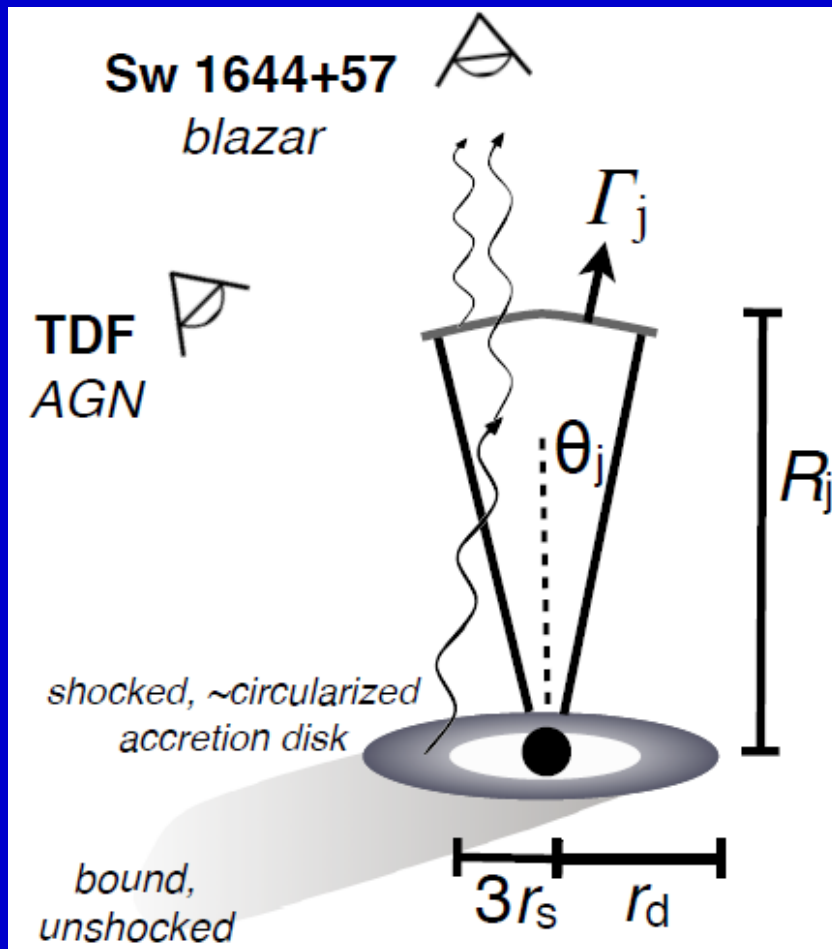


Census



The region of expected thermal emission from a circularized debris disk formed from the tidal disruption of a solar-type star by a 10^6 – $10^8 M_{\text{sun}}$ black hole is shown in orange.

High-energy transient Swift J164449.3+573451

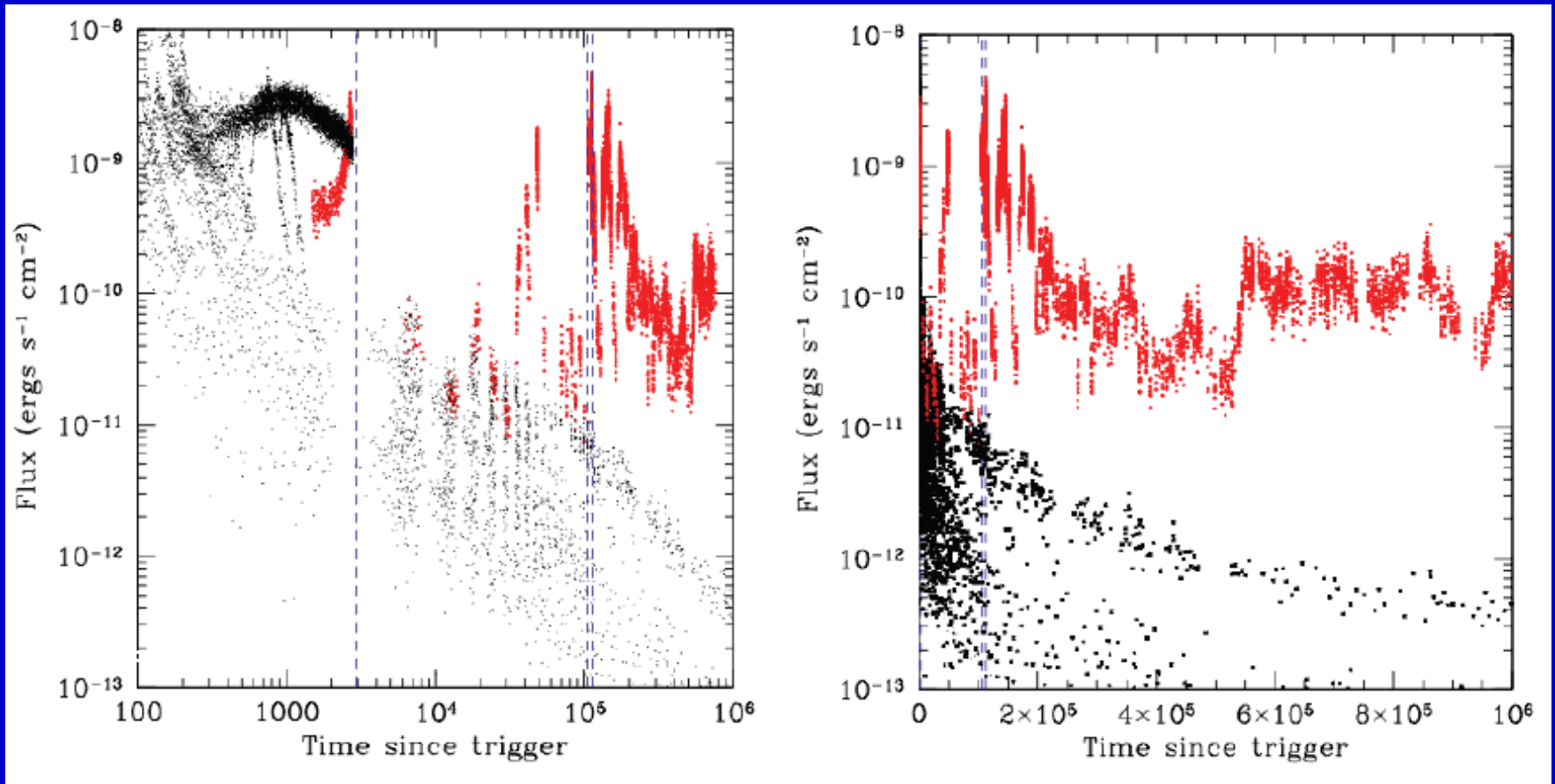


1104.3257

1104.3356

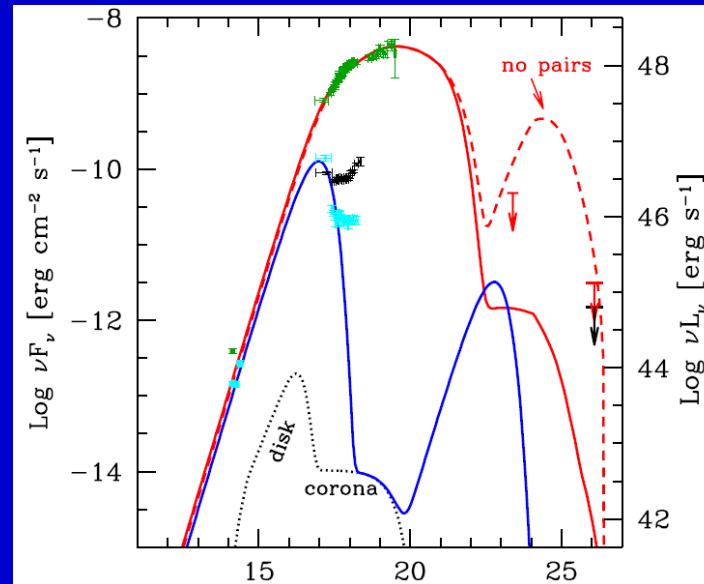
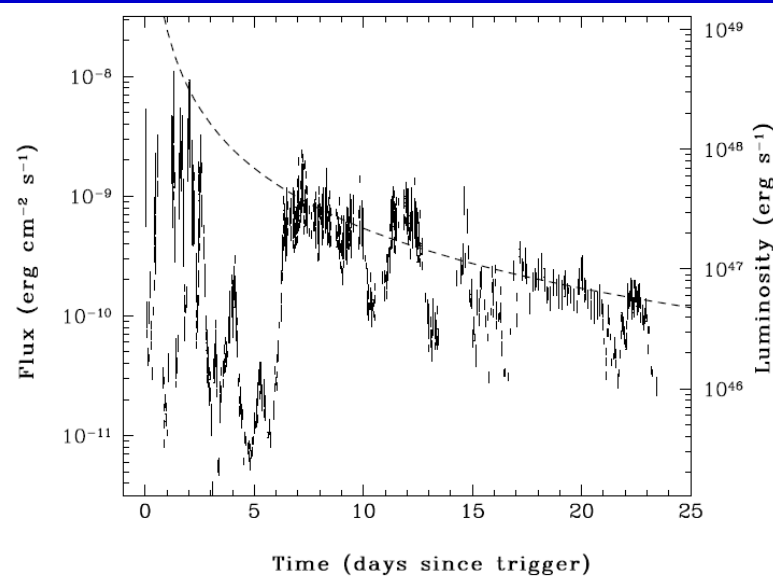
Also known as GRB 110328A

A unique event



The transient does not look similar to GRBs, SN or any other type of event

A tidal disruption event



Light curve fits the prediction for a tidal event. The spectrum is blazar-like.

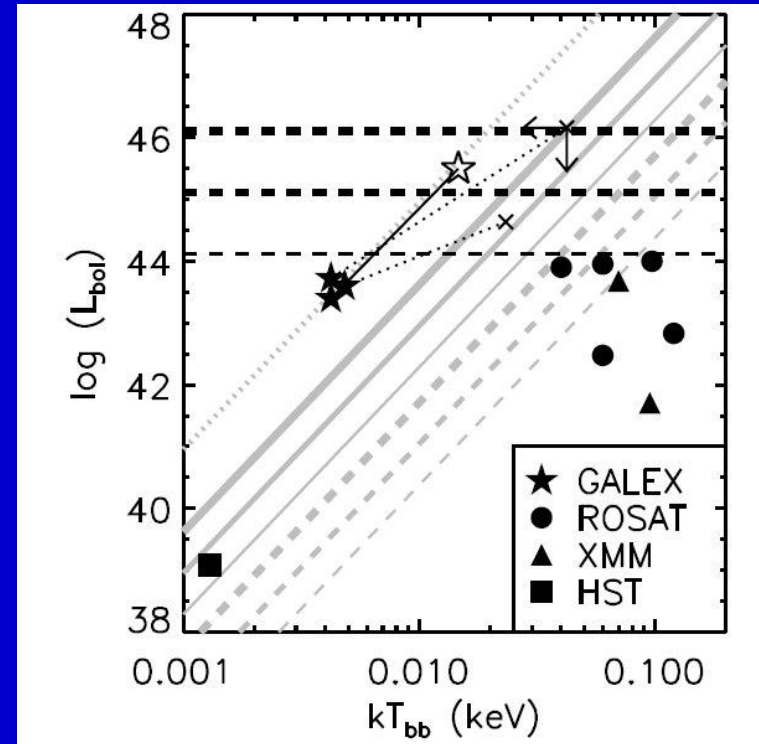
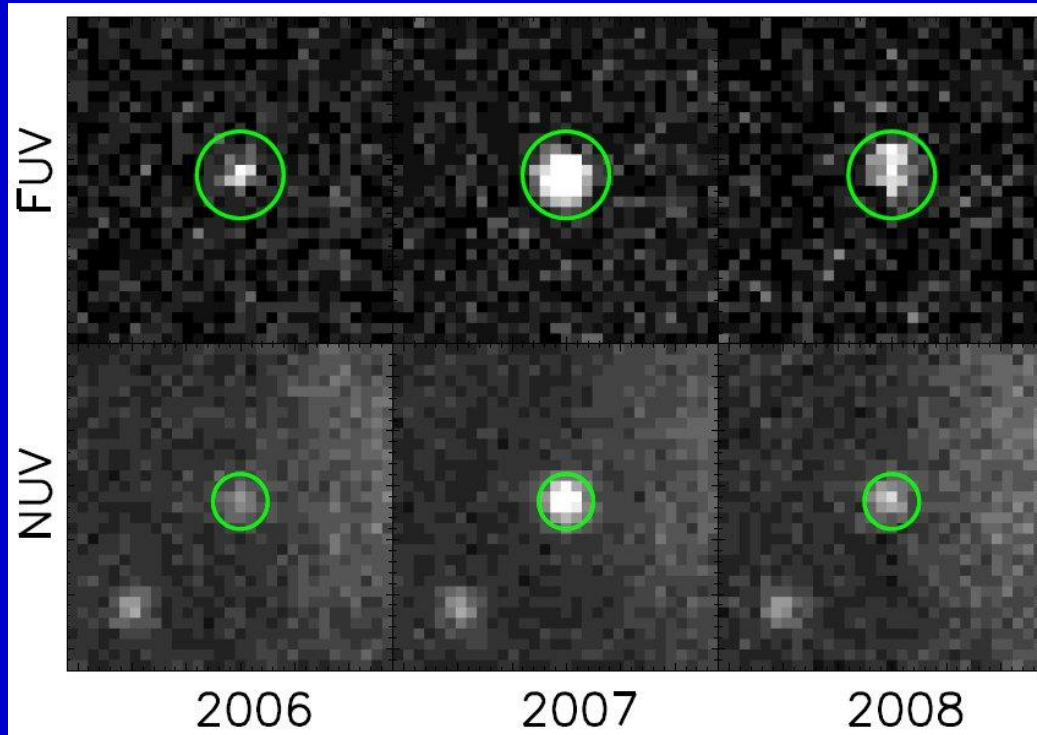
1104.4787

See a review on jets from TDE in 1911.01442.

Name	year	z	X-rays?	
Swift J164449.3+573451	2011/2011	0.3543	non-thermal	On-axis jet
Swift J2058.4+0516	2011/2012	1.1853	non-thermal	On-axis jet
Swift J1112.2-8238	2011/2015	0.89	non-thermal	On-axis jet
Arp 299-B AT1	2005/2018	0.0103	-	Off-axis jet

Optical observations of tidal disruptions

GALEX data



In optics one can observe events far from the horizon.
Surveys like Pan-STARRS
can discover 20-30 events per year.

Two more examples of optical flares due to tidal disruption events

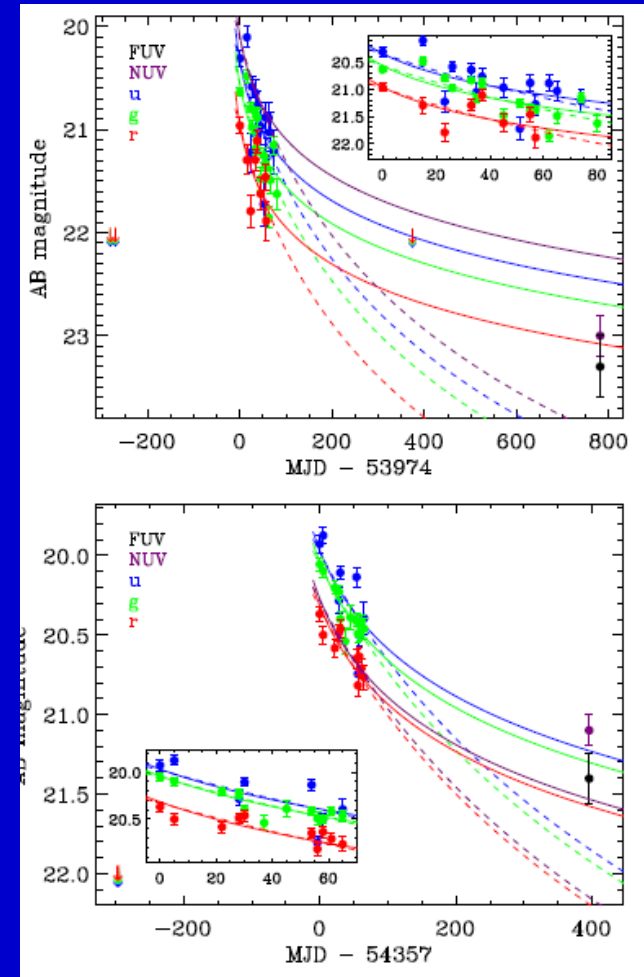
SDSS data

Atypical flares

Rate estimates:

$\sim 10^{-5}$ per year per galaxy
or slightly more

In 2020 ~ 33 TDEs observed in optics/UV
are known, see 2008.05461.

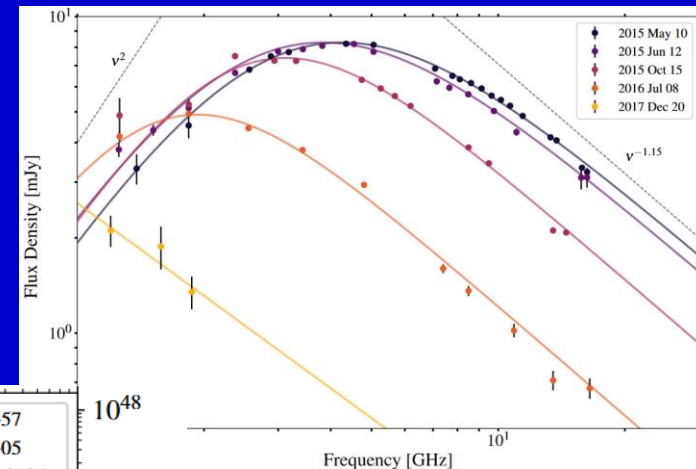


1009.1627

Dashed lines: $-5/3$
Solid lines: $-5/9$

The first radio discovery

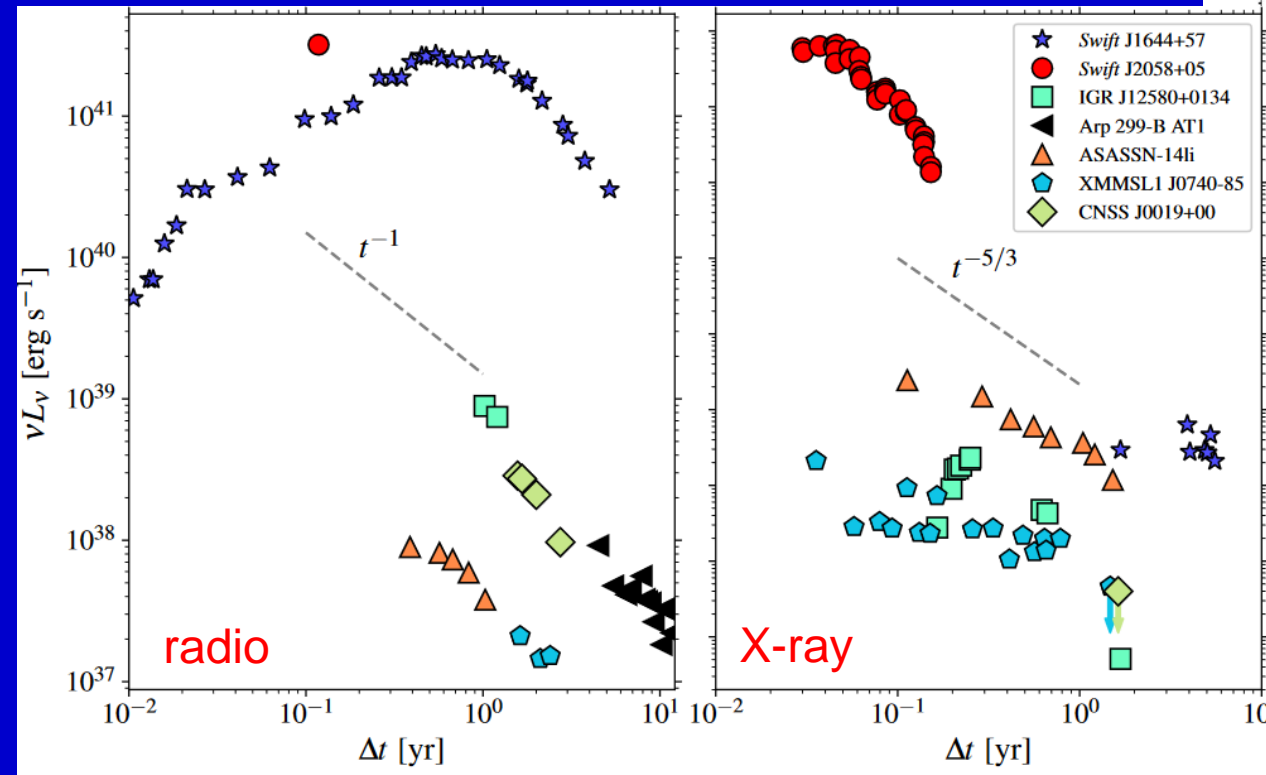
CNSS J001947.3+00352
VLA search for transients
No X-rays detected



Spectral evolution

Comparison with all TDE
with detected
radio emission.

Age obtained by
extrapolation of
expansion.



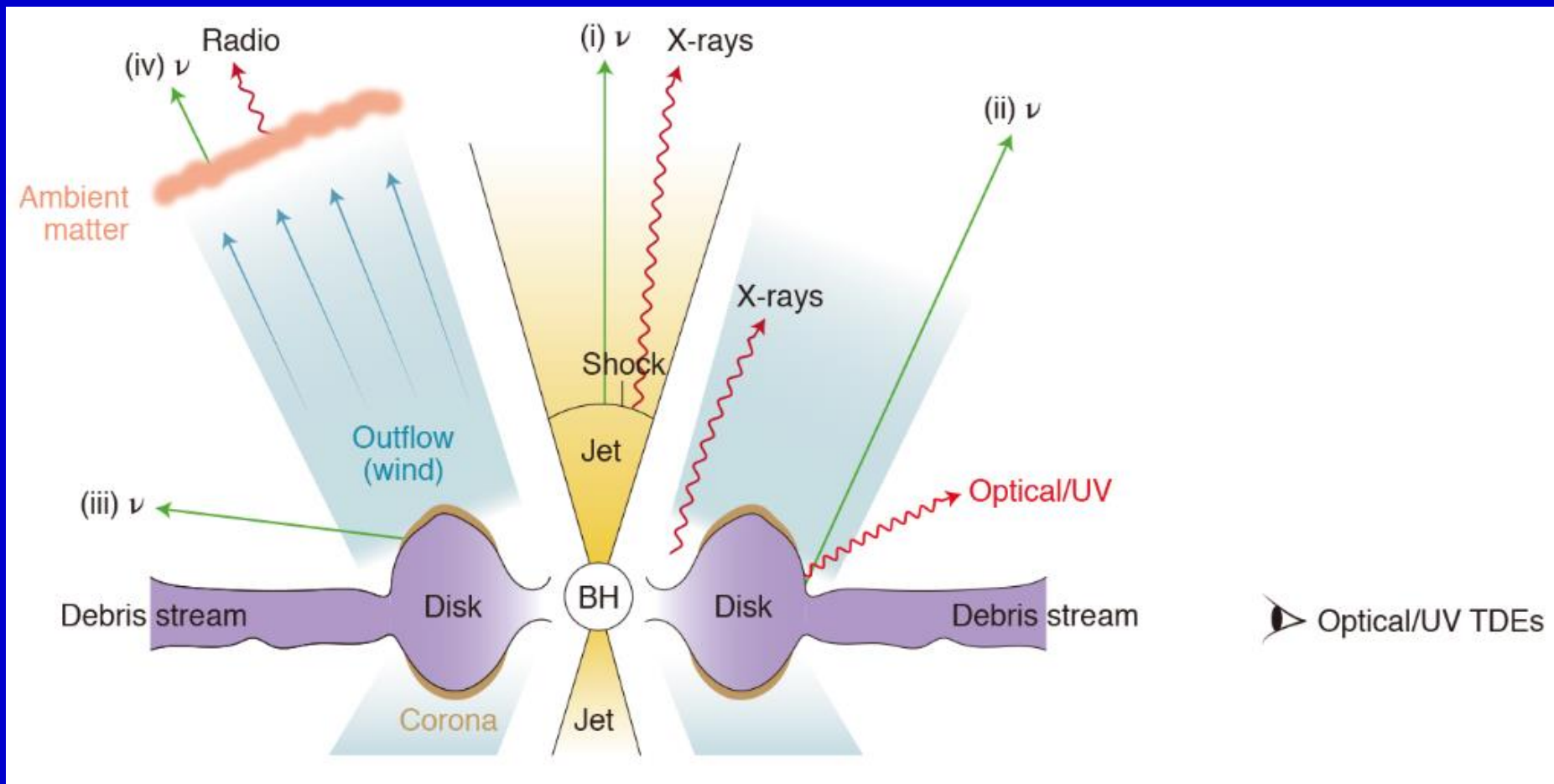
Further observations are necessary to certify that this is indeed a TDE.

1910.11912, see a review on radio observations of TDEs in 2006.01159

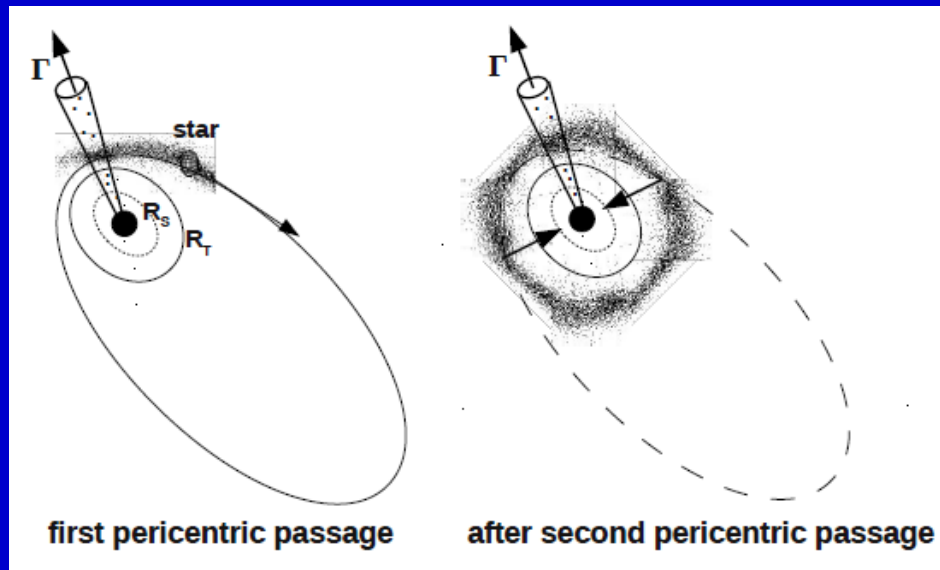
Neutrino from a TDE?

TDE: AT2019dsg

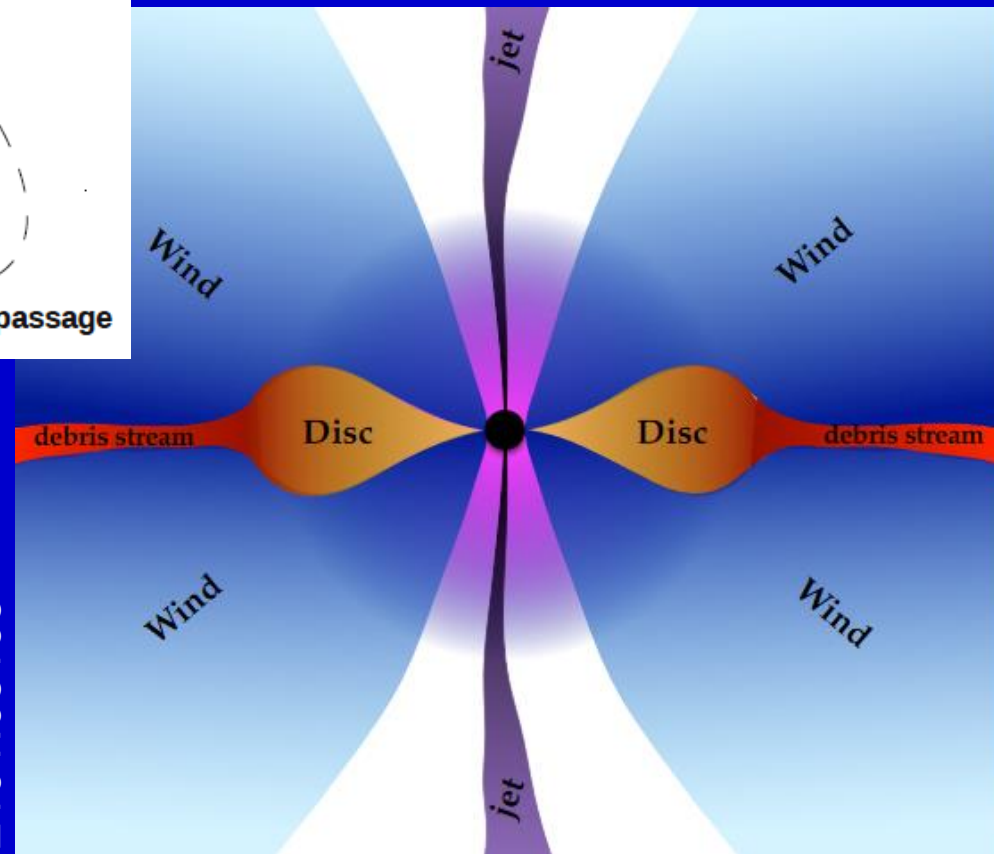
IceCube event: 191001A



Theoretical models

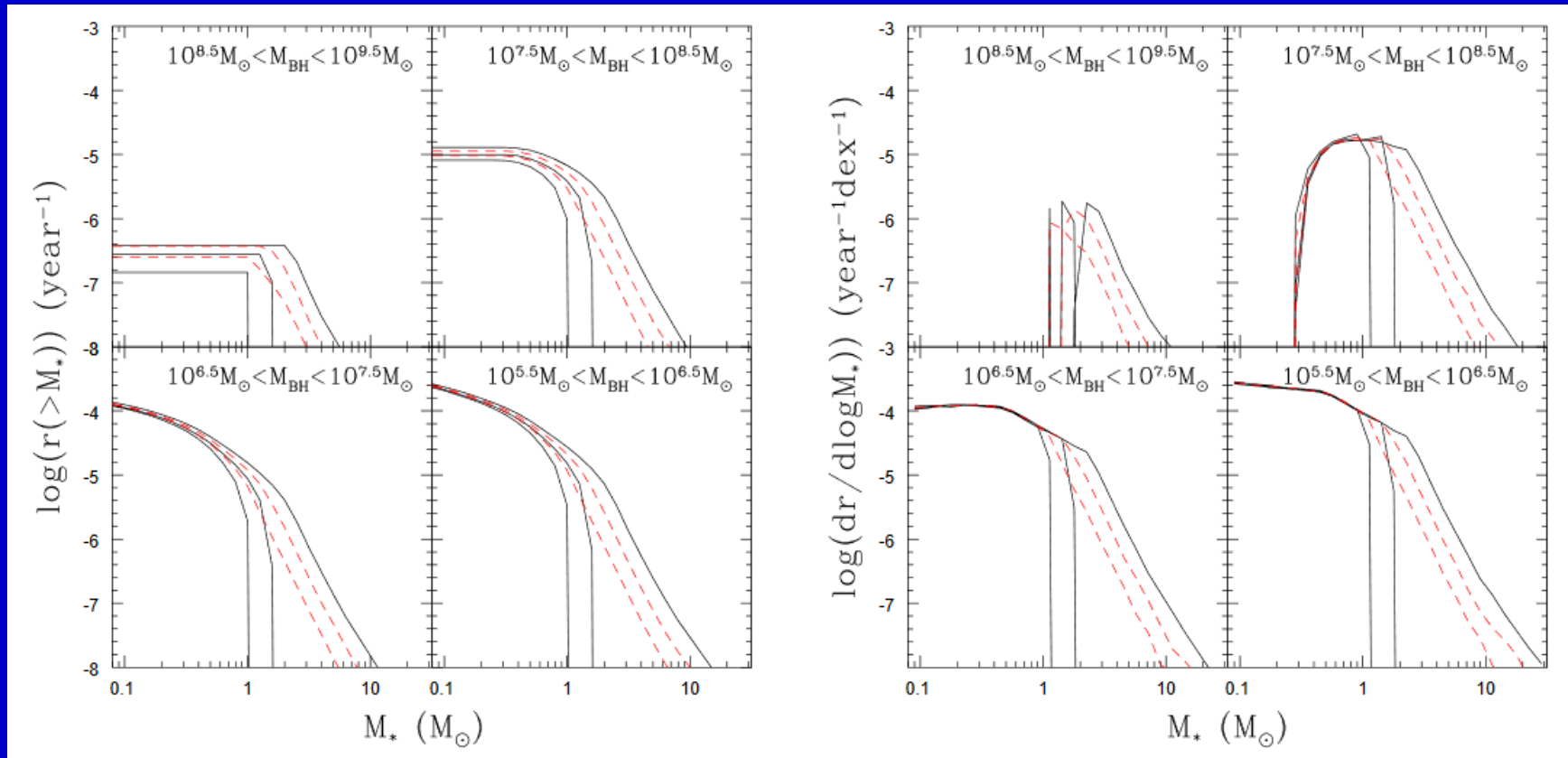


2101.05195



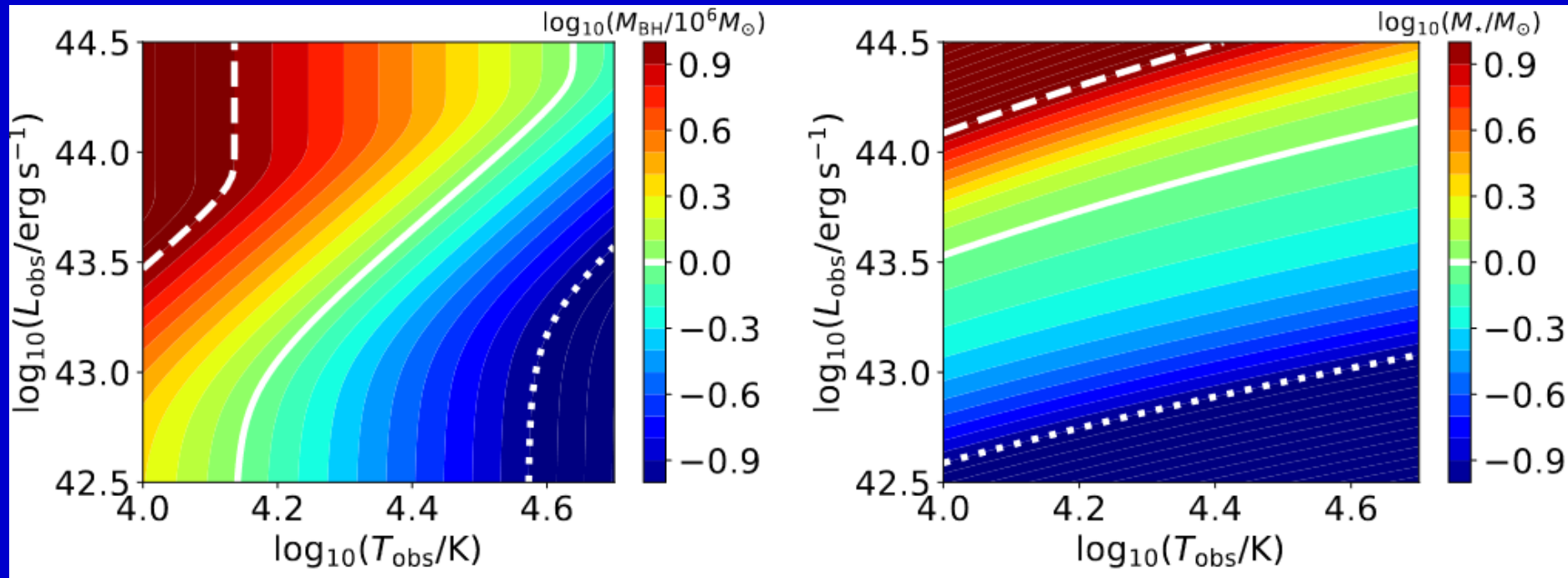
See a review on modeling of TDEs in 2006.03693

Stellar masses



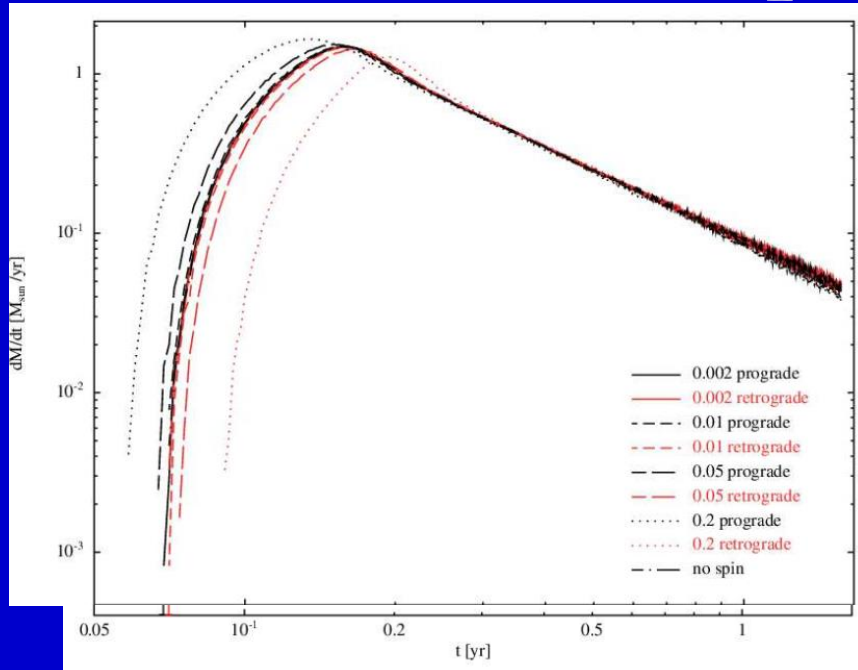
For not too massive BHs the main contribution is due to M-dwarfs (0.3Msolar).
For massive BHs contribution from massive and evolved stars grows.

BH mass and stellar mass estimates

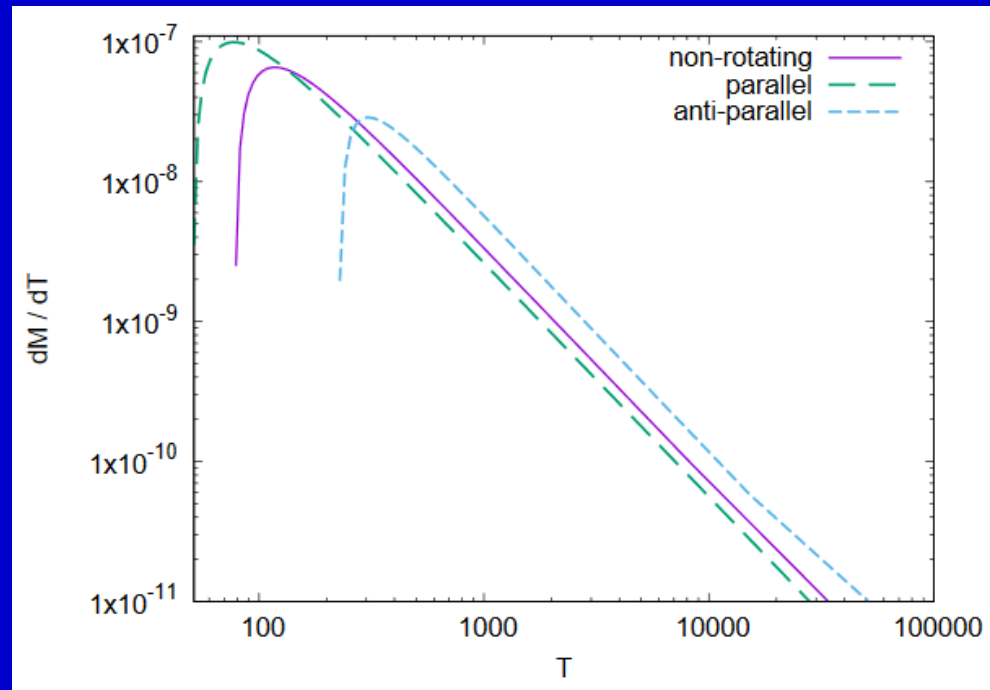


The black hole mass depends mostly on the temperature observed at peak luminosity, while the mass of the disrupted star depends mostly on the peak luminosity.

Role of stellar spin



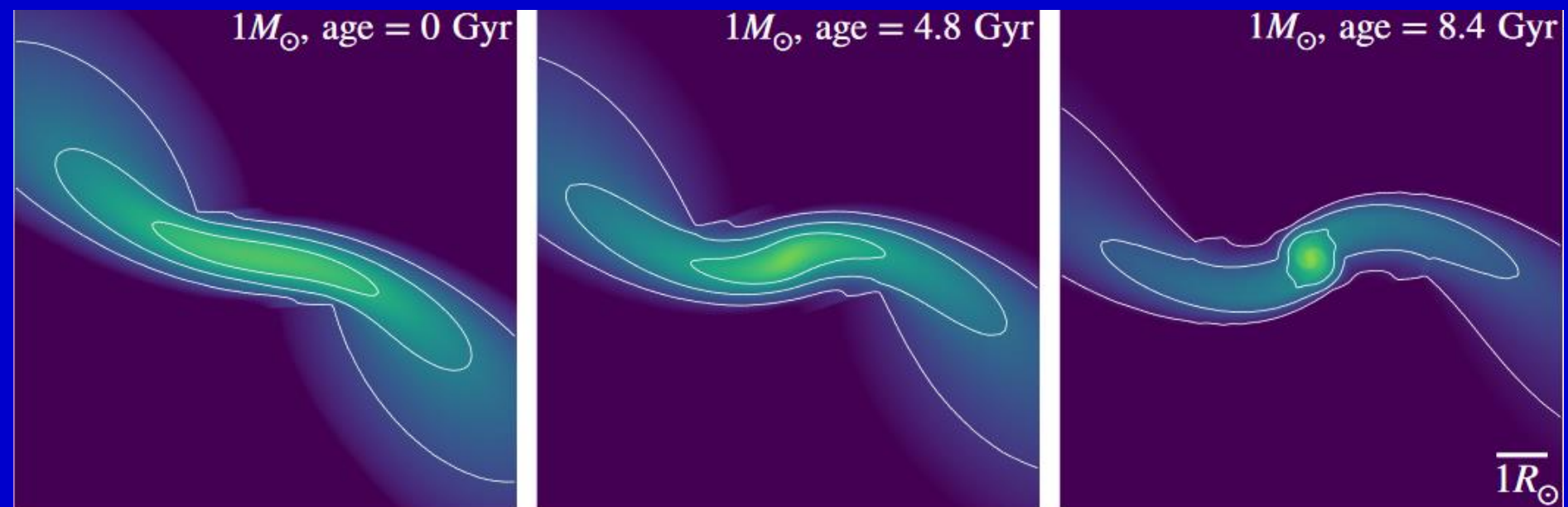
1901.03717



1901.05644

Detailed structure is important

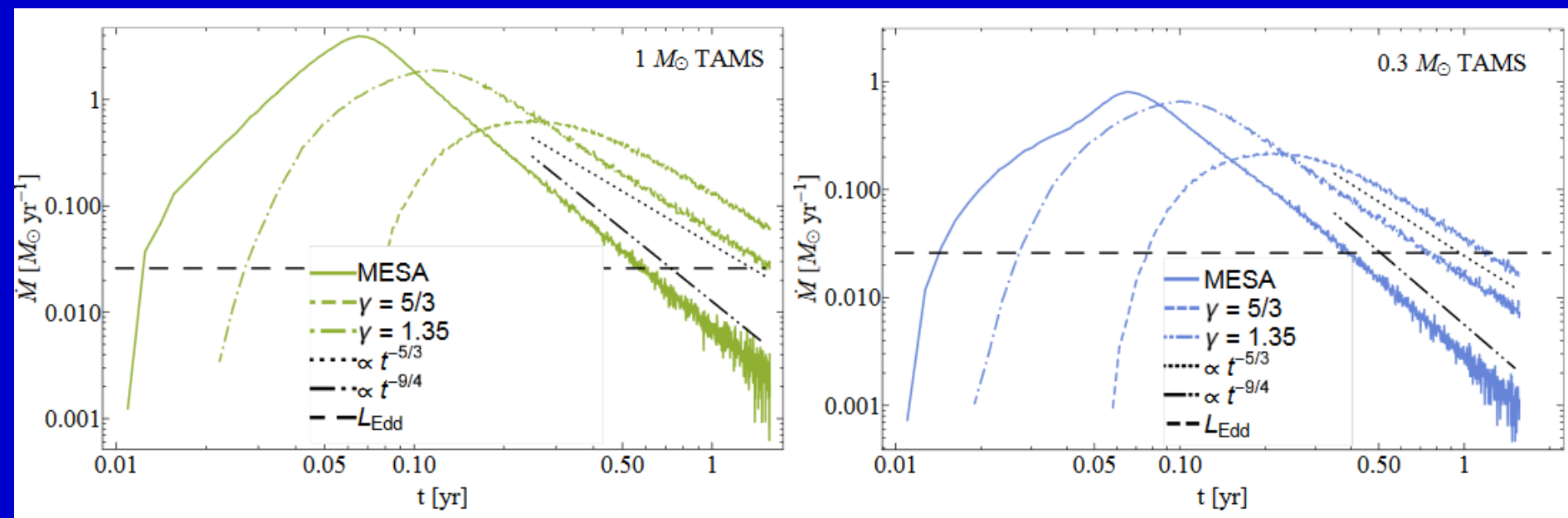
The authors used MESA to model stellar structure before tidal disturbances.



Interaction with a 1 000 000 solar mass BH.

....and again details and MESA

For realistic stellar structure the accretion rate is different from that for polytropic models.



TAMS - terminal-age main sequence

Role of BH spin

For deep encounters rotating BHs accretion rate and mass of the disc can be reduced.

$$r_{\text{tid}} \equiv r_{\star}(M/m_{\star})^{1/3}$$

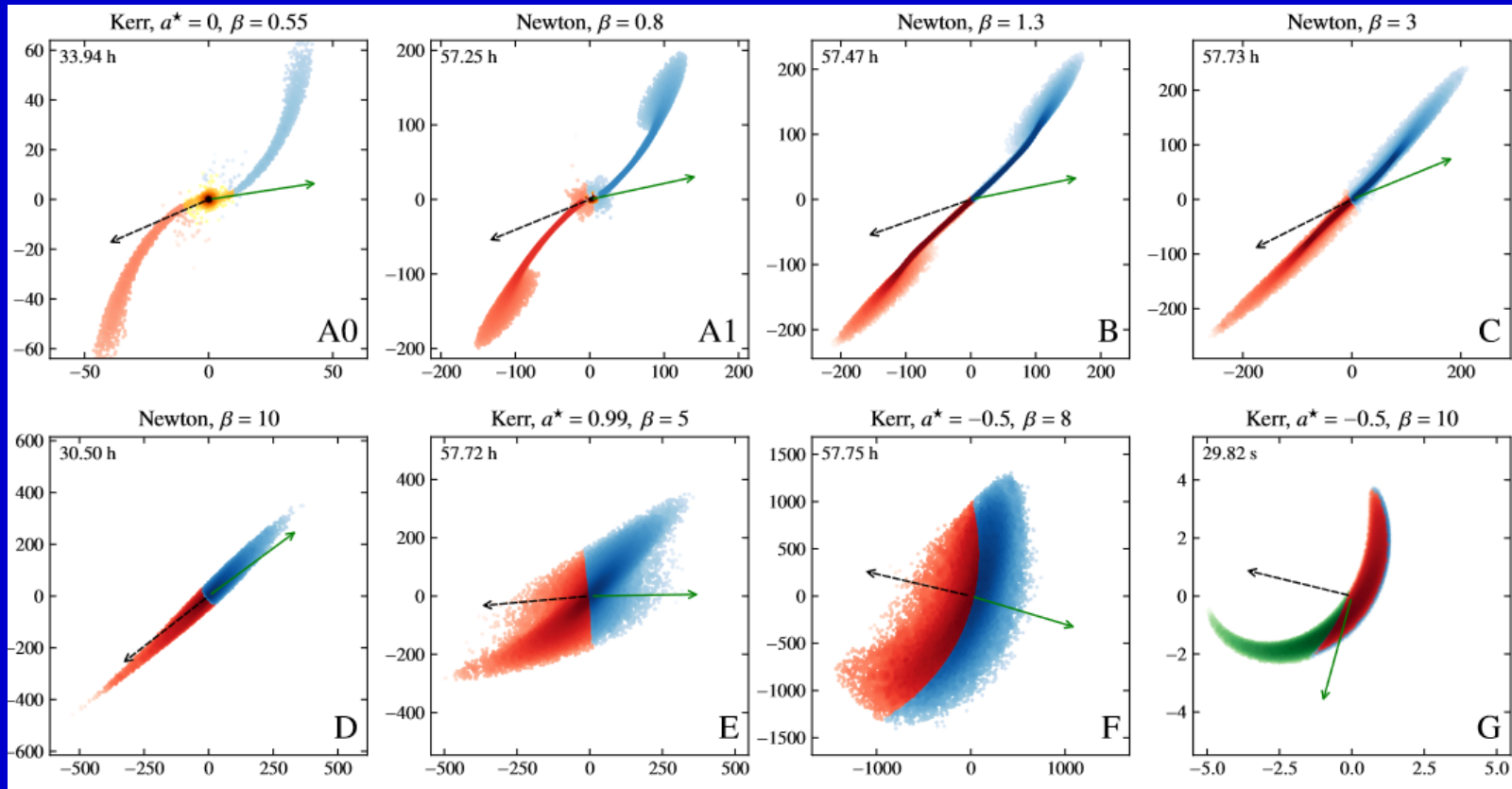
$$M = 10^6 M_{\odot}$$

$$m_{\star} = M_{\odot}, r_{\star} = R_{\odot}$$

$$\beta \equiv r_{\text{tid}}/r_{\text{p}} \quad r_{\text{p}} - \text{periapsis}$$

$$e = 1$$

$$a^{\star} \equiv Jc/GM^2$$



1903.09147

self-bound (yellow), bound (red),
unbound (blue), plunging (green)

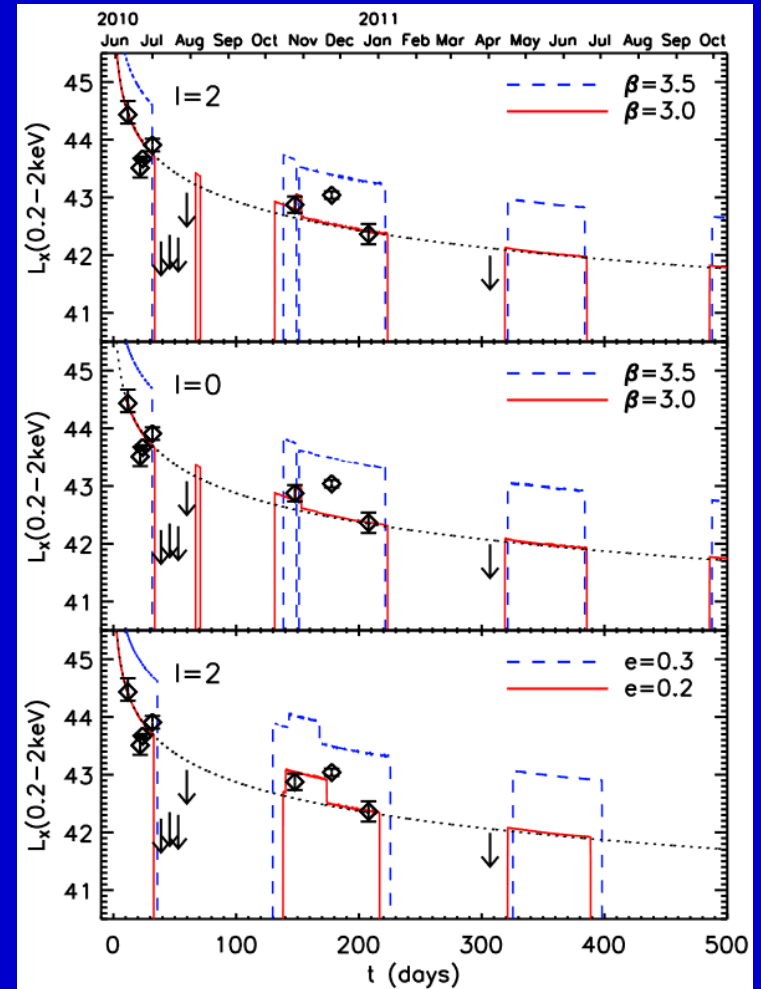
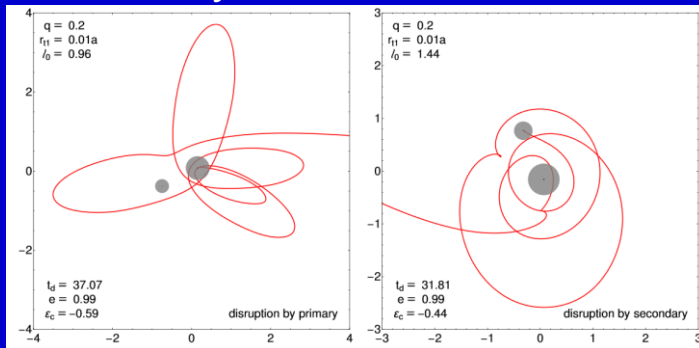
TDE and binary SMBHs

It has been predicted that after a TDE in a system of close SMBH binary there might be particular drops in the light curve. Such phenomena was observed.

SDSS J120136.02+300305.5
XMM-Newton observations

Masses $\sim 10^7$ and 10^6 solar masses,
orbital separation $\sim 10^{-3}$ pc
Eccentricity ~ 0.3

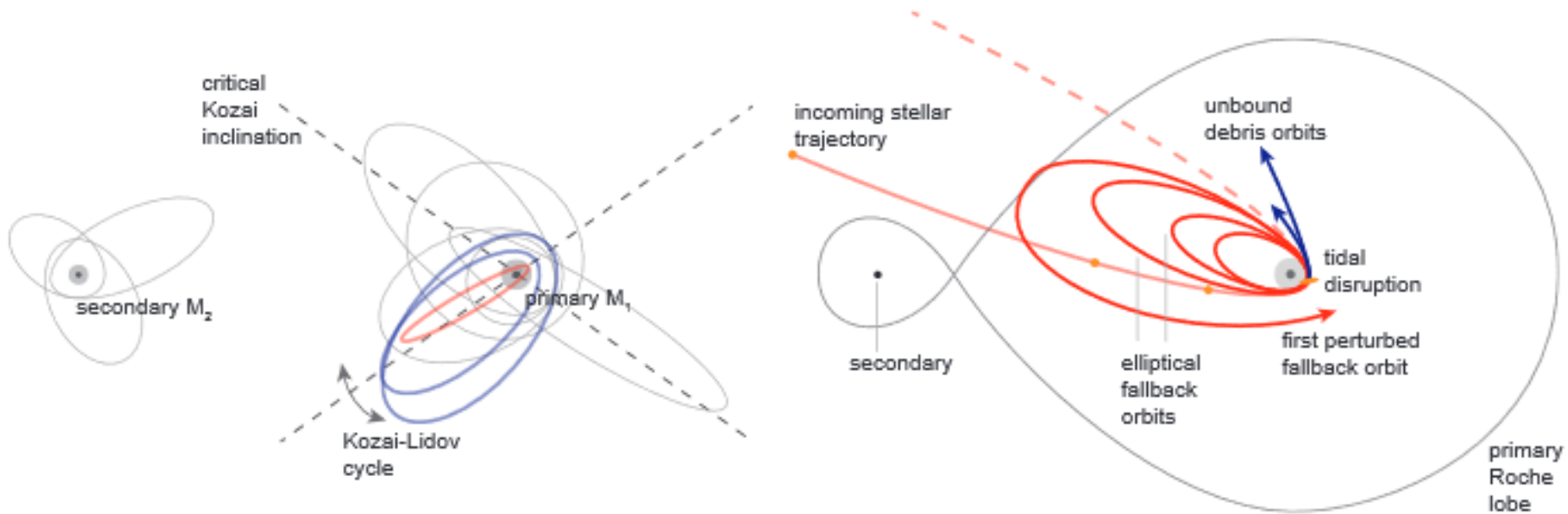
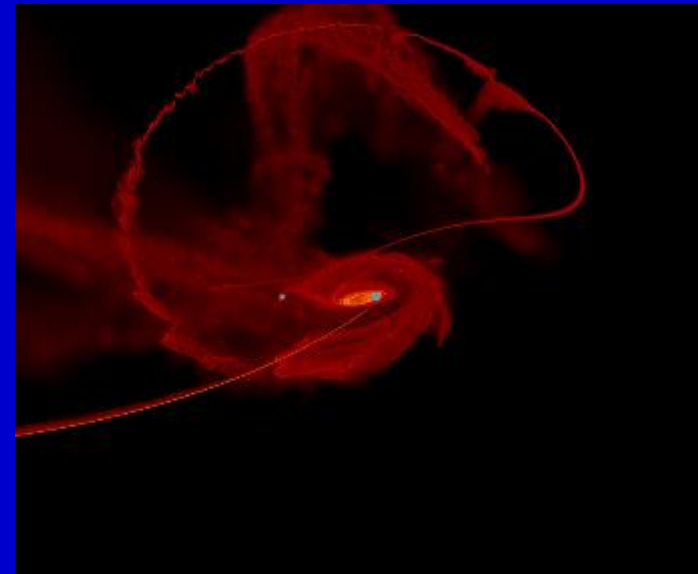
TDEs in supermassive BH binaries
were recently modeled in 1802.07850.



See a review on binary SMBHs and TDEs in 1909.12849

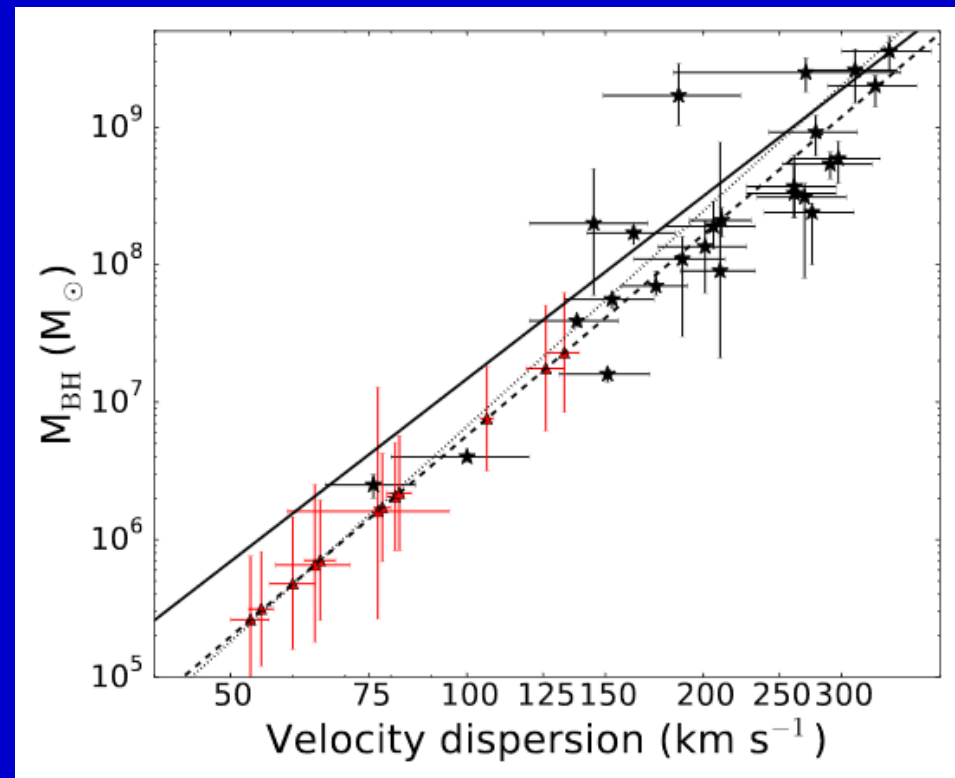
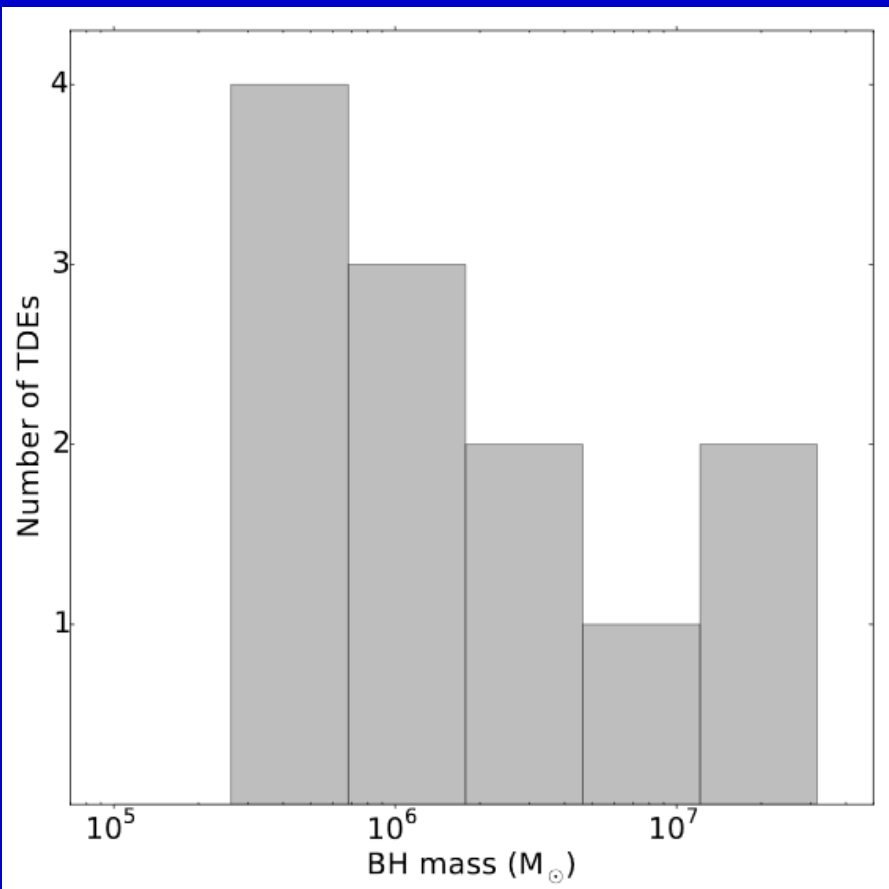
How binarity influences TDE

- Lidov-Kozai influence on the star
- Dynamical influence on the debris



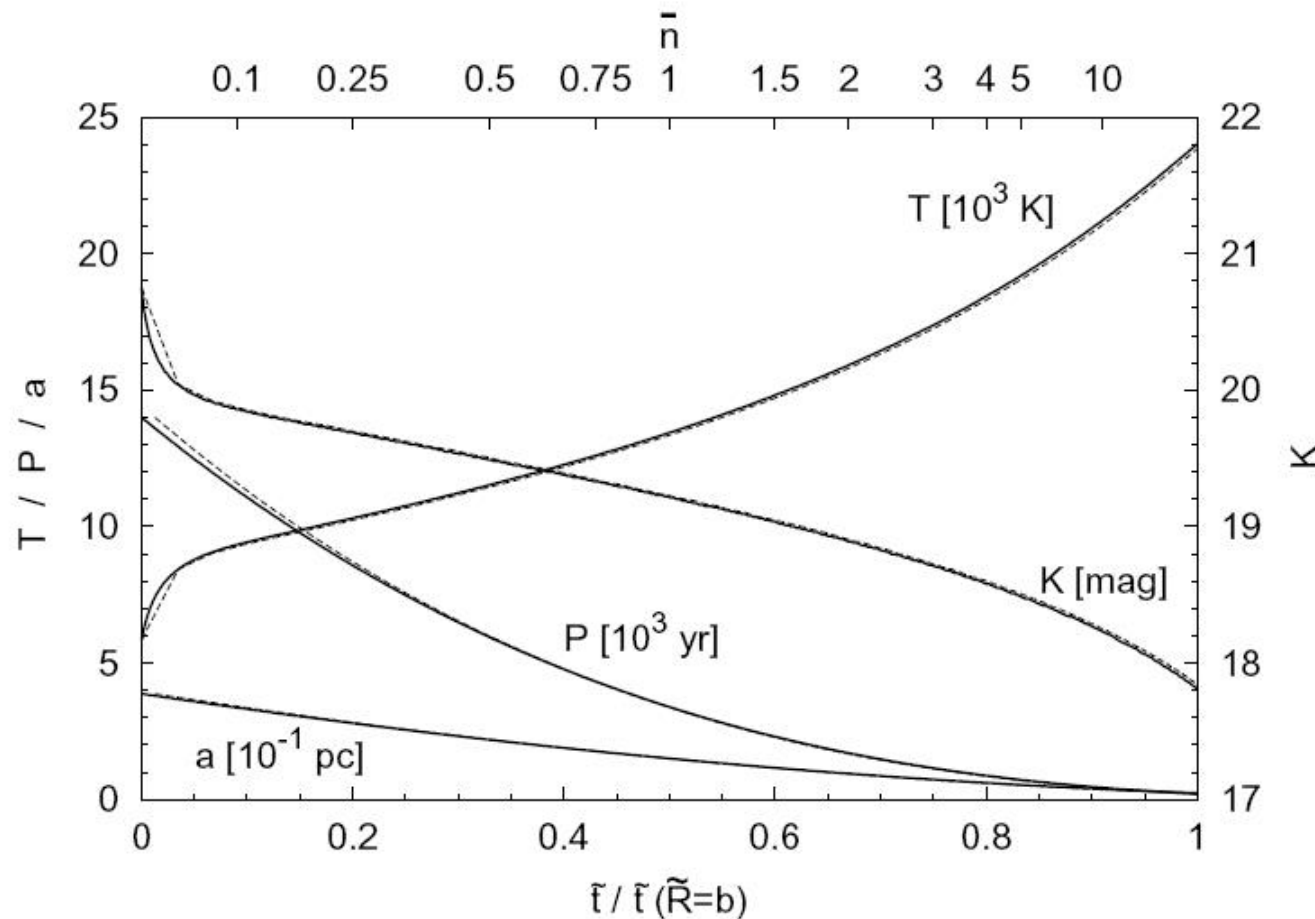
Mass determination of BHs in TDE galaxies

12 optically/UV selected TDE host galaxies



Red- new data, lines – best fits,
black – Ferrarese, Ford (2005).

Squeezars



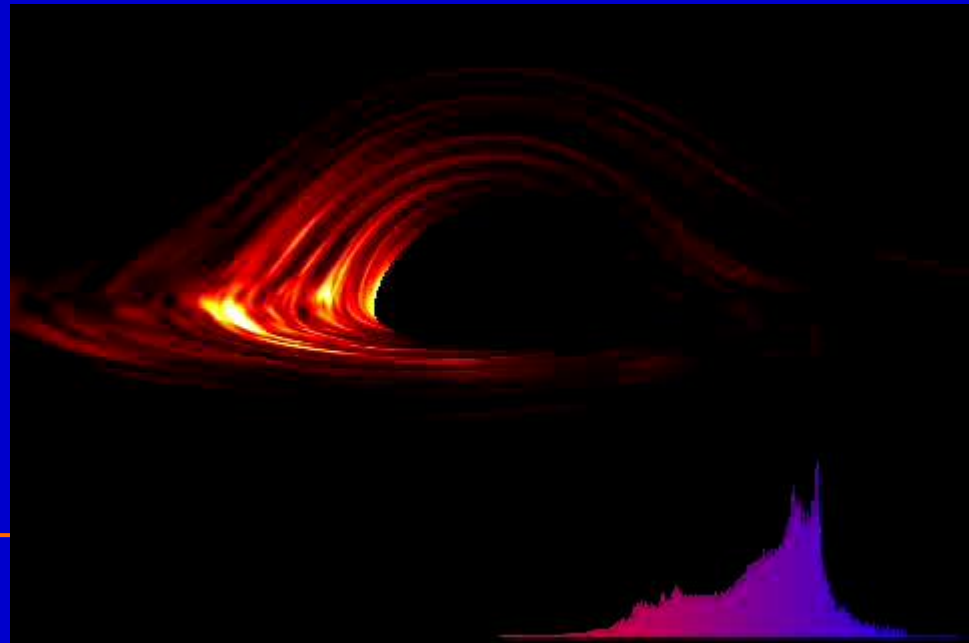
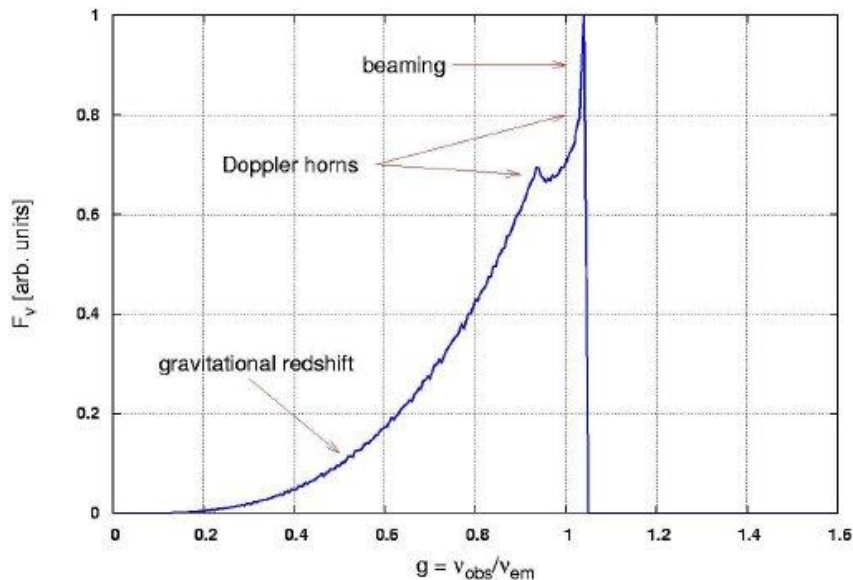
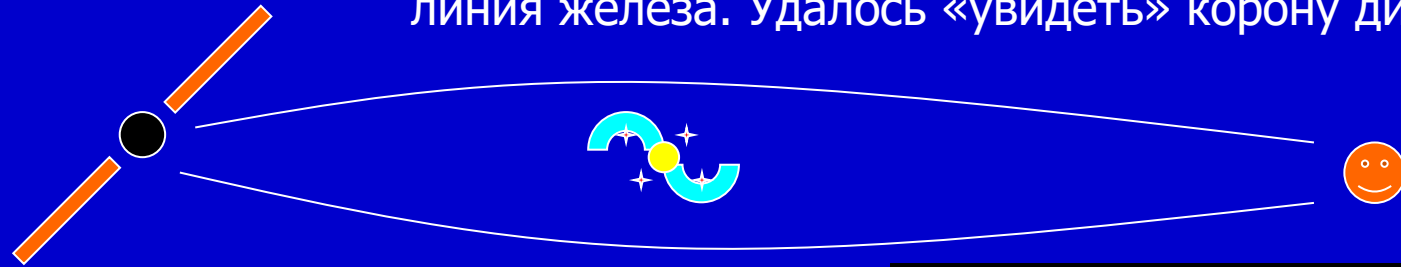
The rate of formation is lower than the rate of tidal disruption events, but the observable time is longer.

Graphs are plotted for a solar-type star orbiting the BH in the center of our Galaxy.

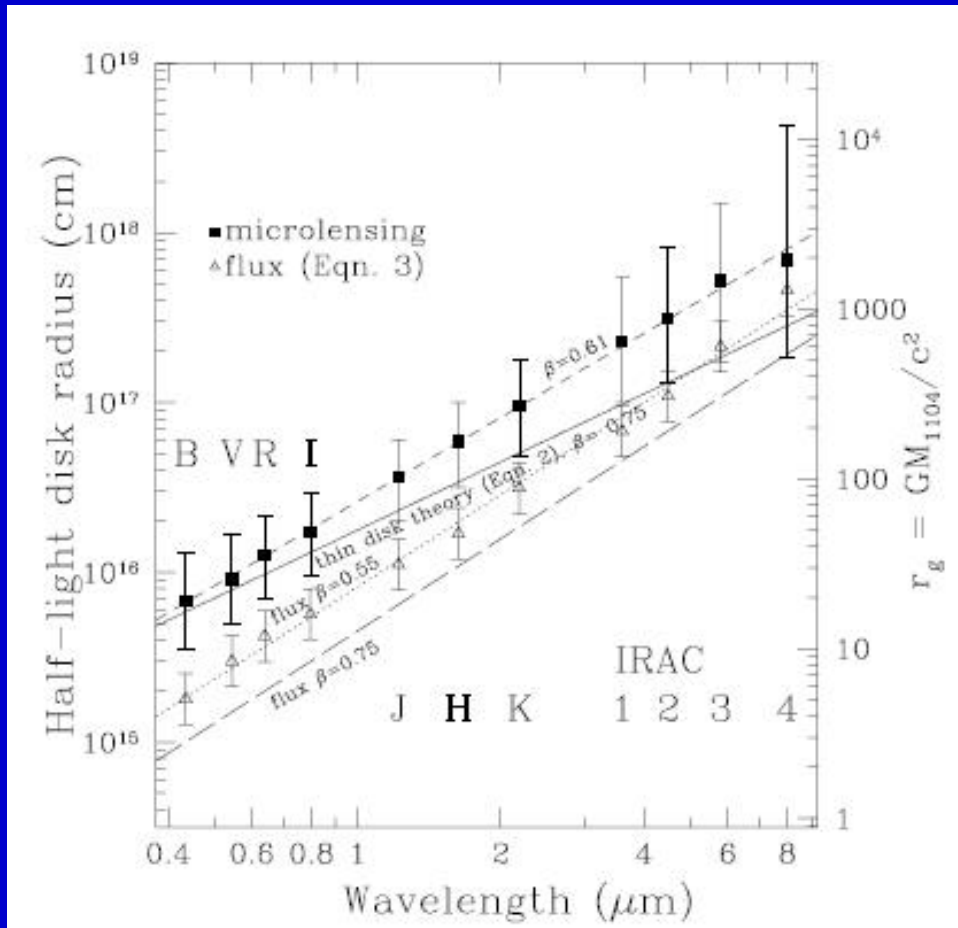
Структура диска вокруг сверхмассивной черной дыры

Наблюдение микролинзирования позволяет
выявлять структуру аккреционного диска.
Кроме этого, наблюдалась линзированная
линия железа. Удалось «увидеть» корону диска.

1204.4480

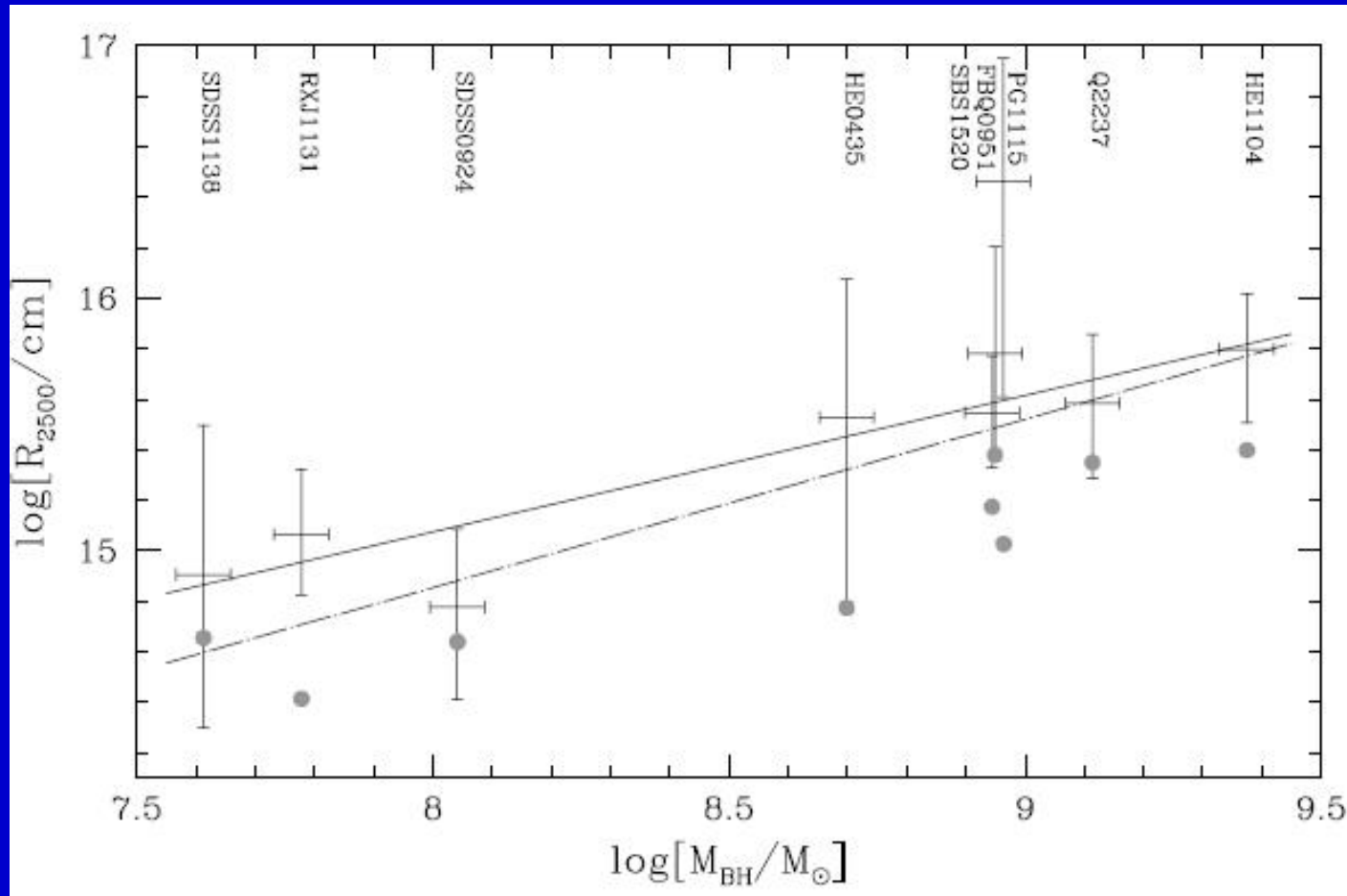


Disc structure from microlensing



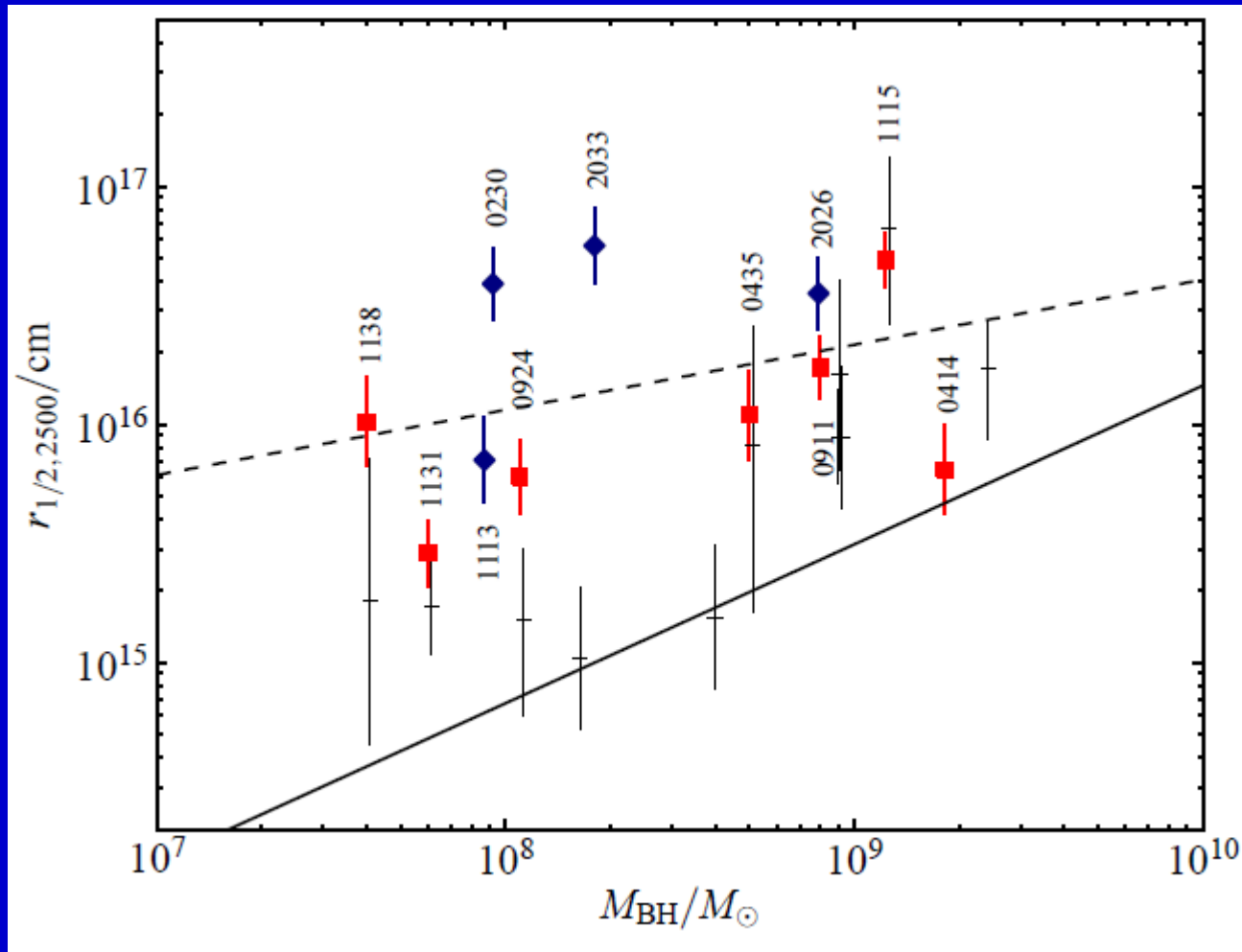
Using the data on microlensing at wavelengths 0.4-8 microns it was possible to derive the size of the disc in the quasar HE1104-1805 at different wavelengths.

Disc size – BH mass



Disc size can be determined from microlensing.

More data



IR and optics.

Chromatic microlensing:
blue light from
the inner regions
is more strongly
microlensed than
red light from farther out

Solid line is
the prediction
of the thin disk model.

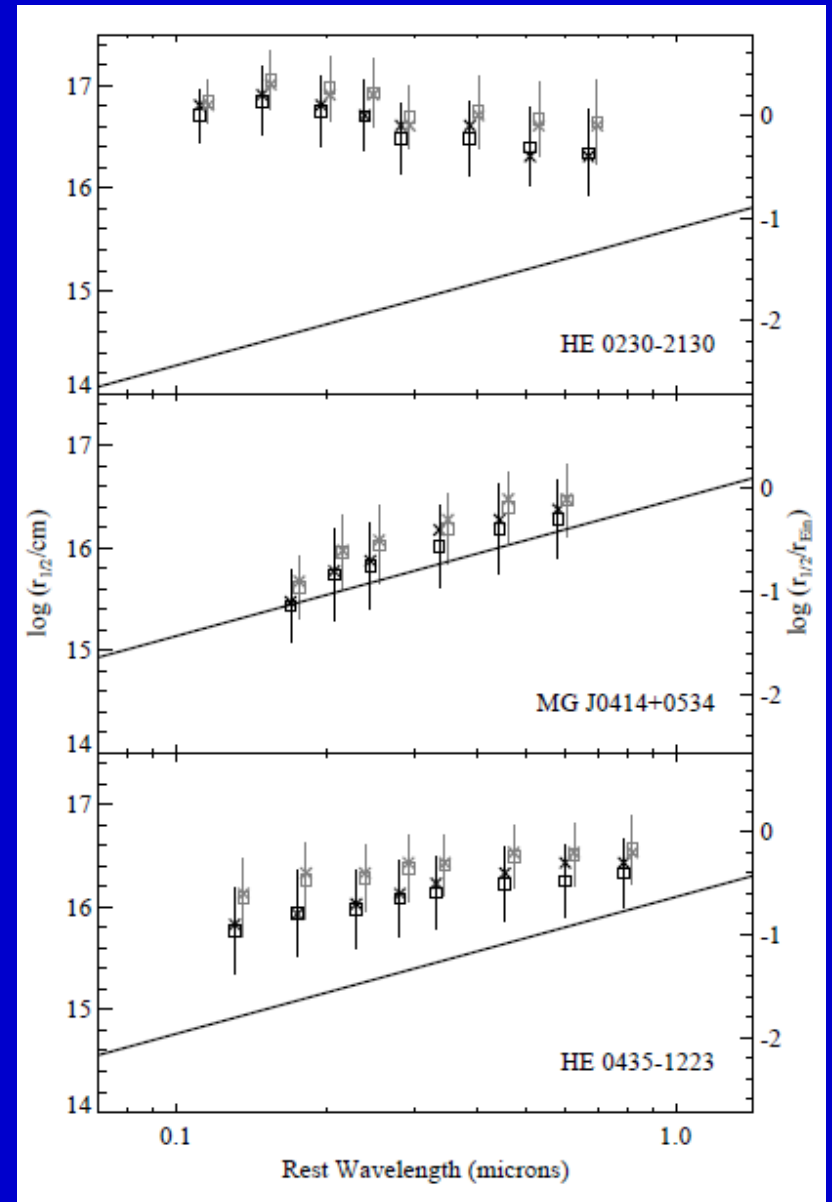
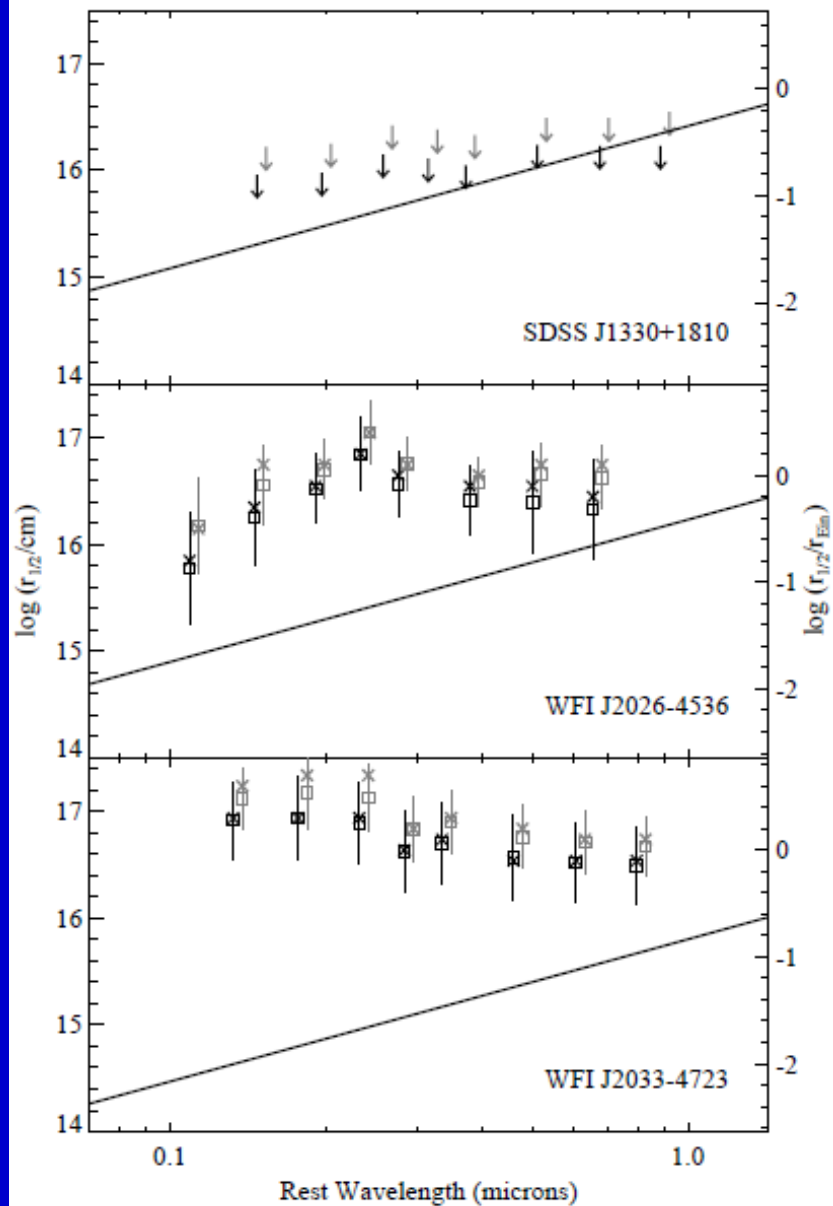
Standard disc properties

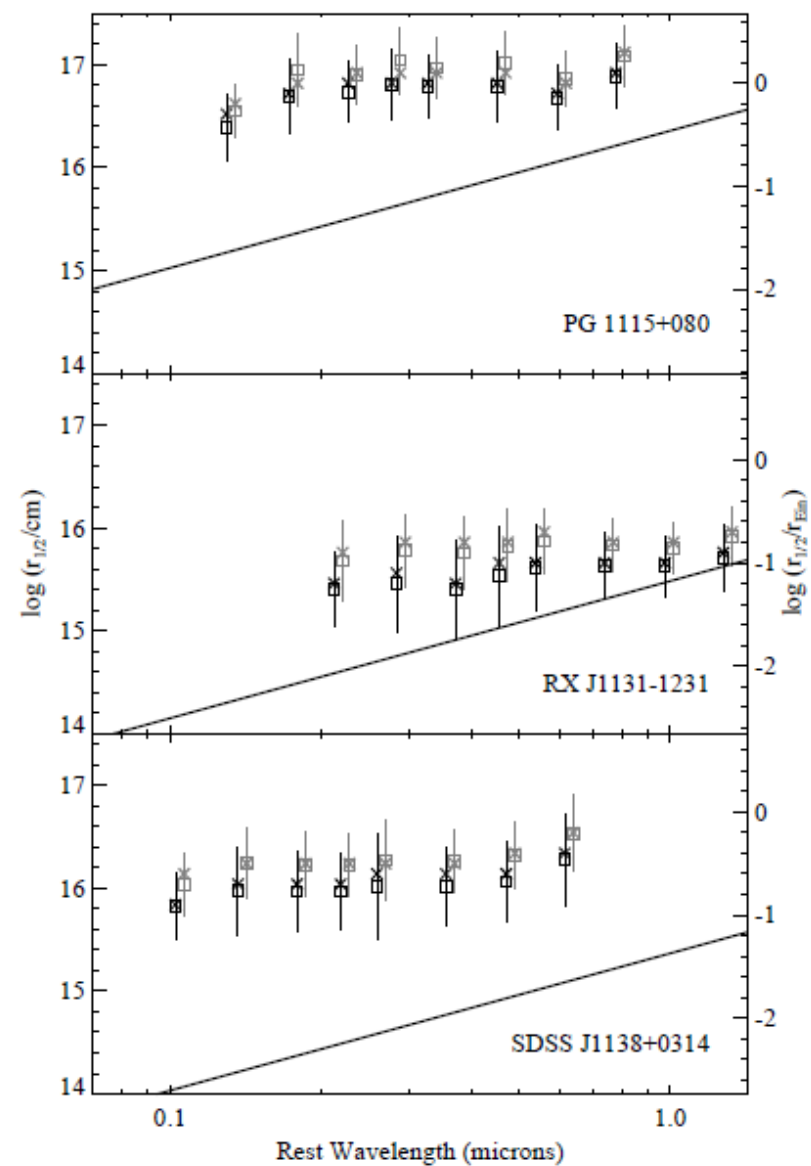
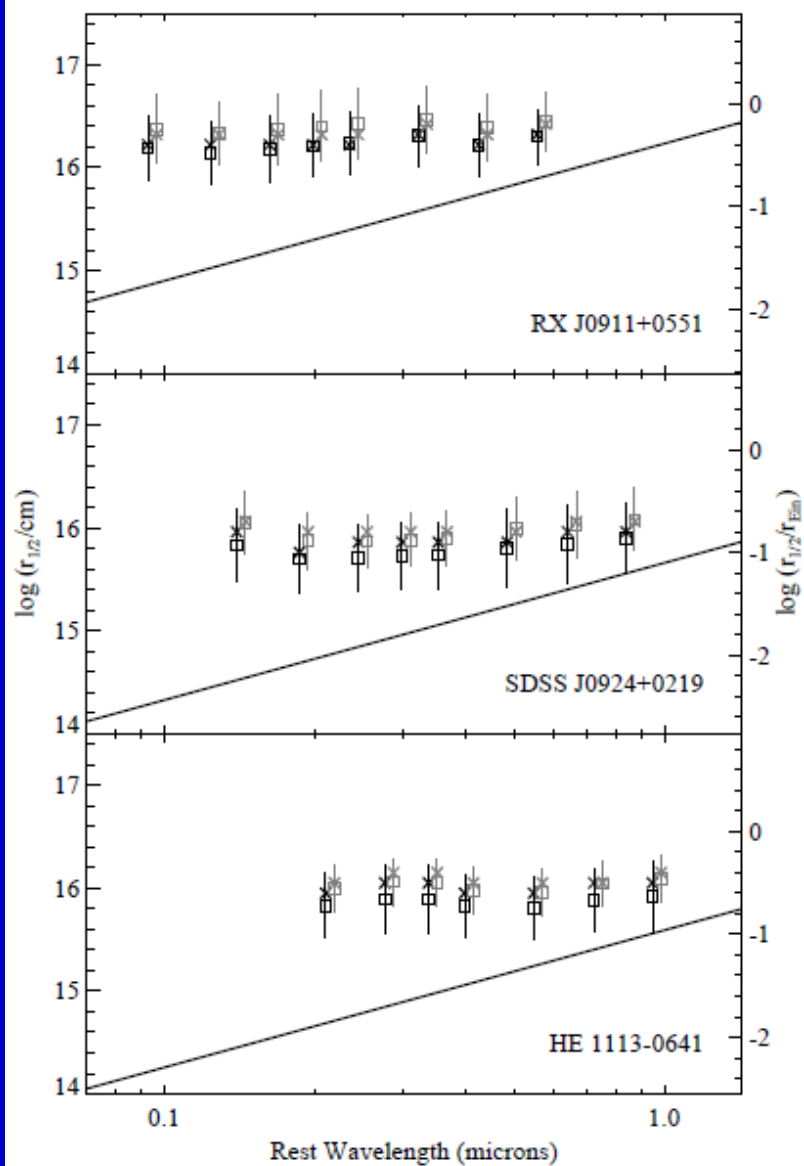
$$T_{\text{eff}}(r) = \left(\frac{3G^2 M_{\text{BH}}^2 m_p f_{\text{Edd}}}{2c\sigma_B \sigma_T \eta r^3} \right)^{1/4} g(r_{\text{in}}/r)^{1/4}$$

Standard disc model

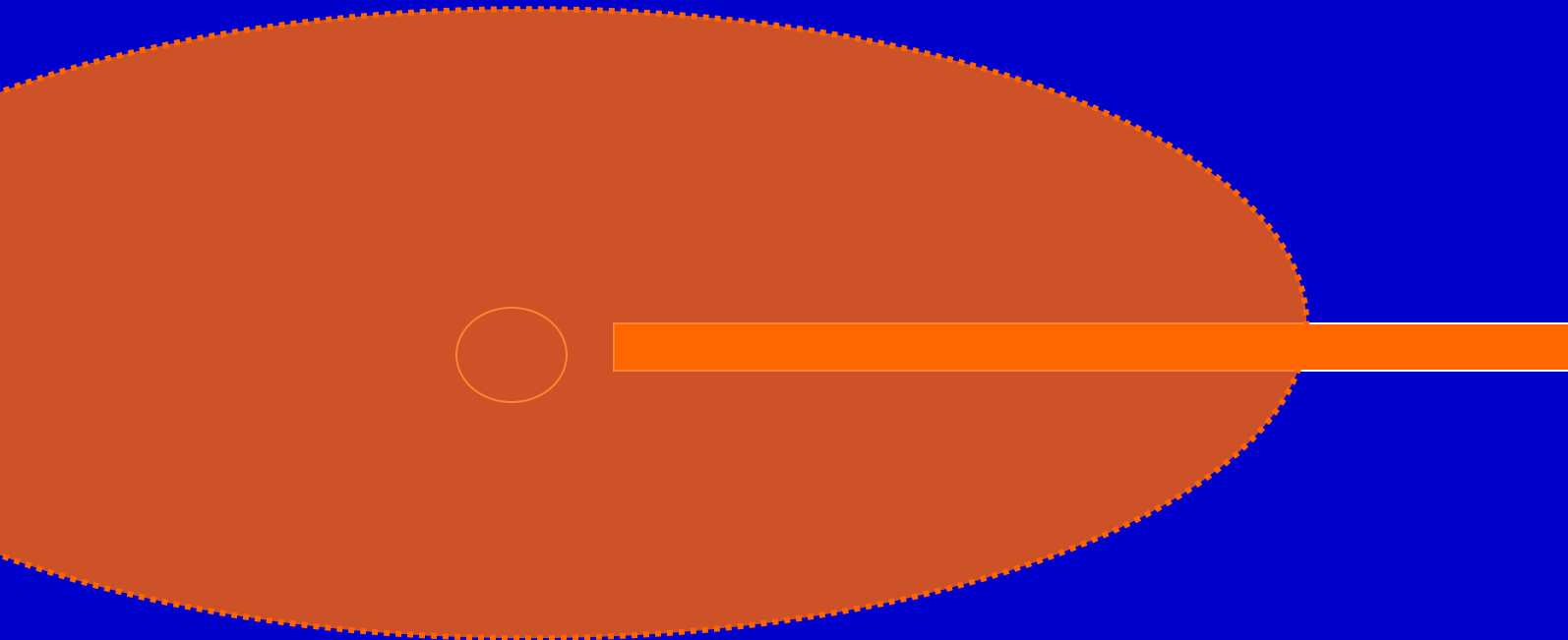
$$\begin{aligned} r_{1/2} &= 2.44 \left[\frac{45G^2 M_{\text{BH}}^2 m_p f_{\text{Edd}} \lambda^4}{4\pi^5 h_P c^3 \sigma_T \eta} \right]^{1/3} \sqrt{\cos i} \\ &= 1.68 \times 10^{16} \text{cm} \left(\frac{M_{\text{BH}}}{10^9 M_{\odot}} \right)^{2/3} \left(\frac{f_{\text{Edd}}}{\eta} \right)^{1/3} \left(\frac{\lambda}{\mu\text{m}} \right)^{4/3} \end{aligned}$$

$$r_{1/2} \sim \lambda^{4/3}$$





Super-Eddington discs



Super-Eddington accretion leads to formation of an optically-thick envelope scattering the radiation formed in the disc.

This makes the apparent disc size larger and practically independent of wavelength

Disc reverberation mapping

super-Eddington AGN

Mrk 142 (PG1022+519)

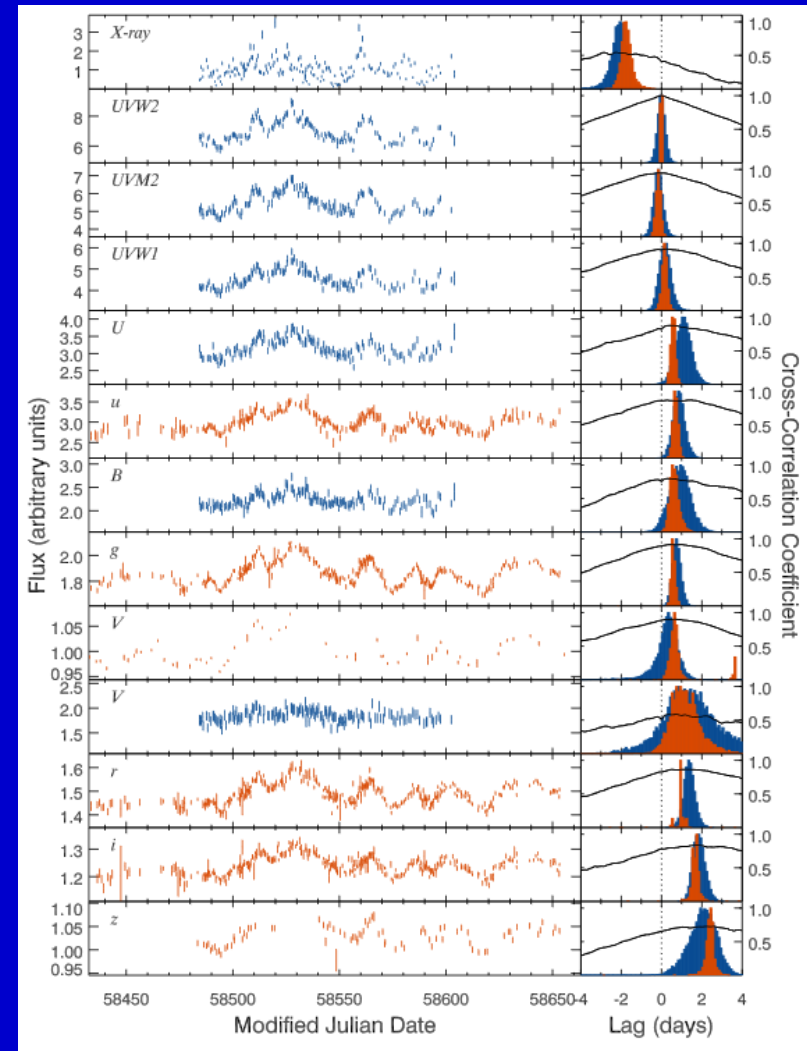
$z = 0.045$

Accretion disk RM uses time lags between the continuum at different wavelengths to probe the size and temperature of the accretion disk.

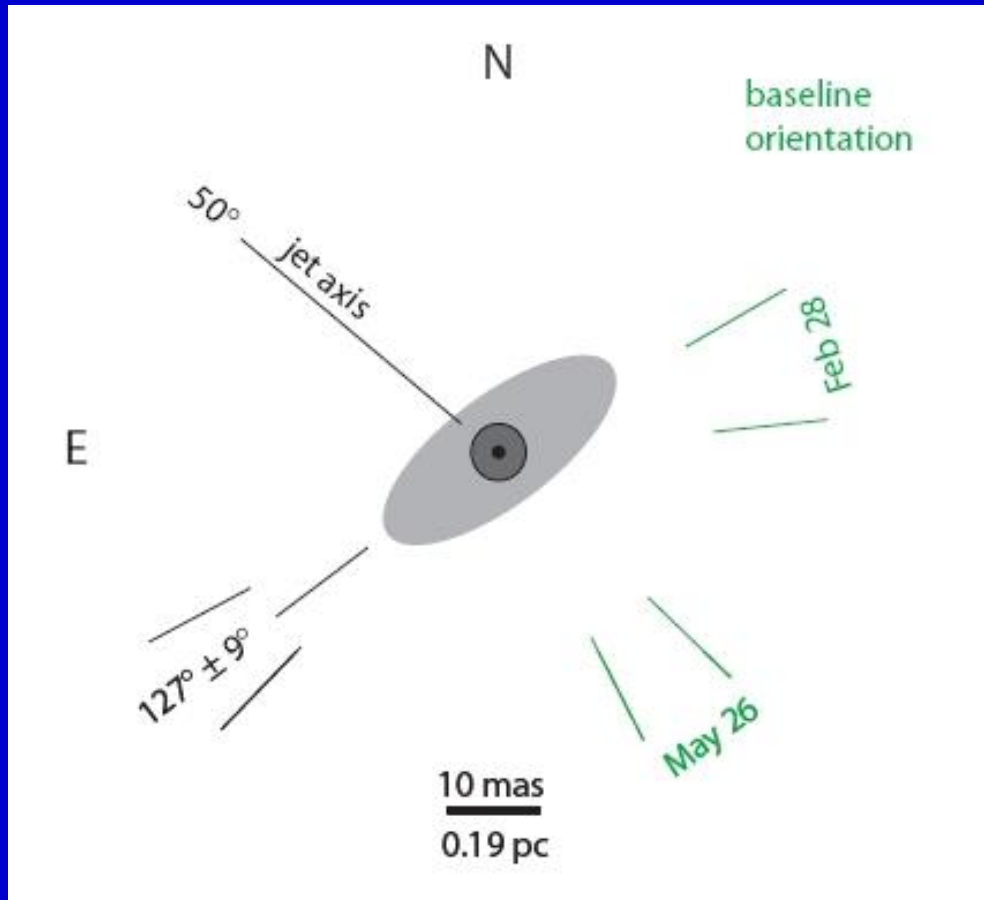
High energy photons from a central corona irradiate the accretion disk, driving variability at longer wavelengths.

The hotter, inner disk will respond to variability in the irradiating photons before the cooler, outer disk.

This then leads to correlated continuum light curves with longer wavelengths lagging shorter wavelengths.



Discs observed by VLTI



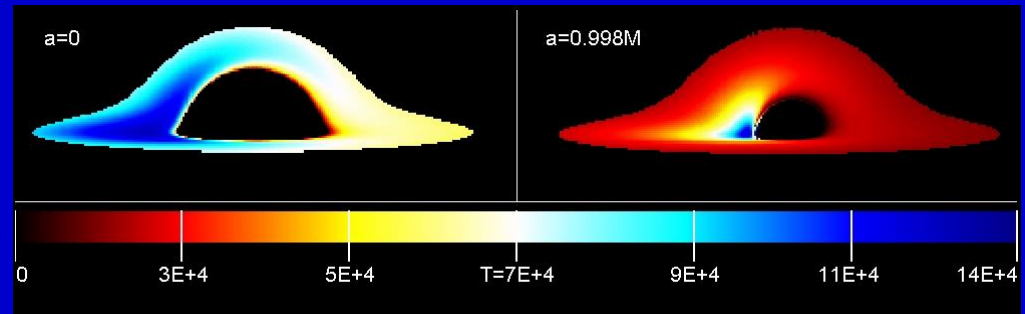
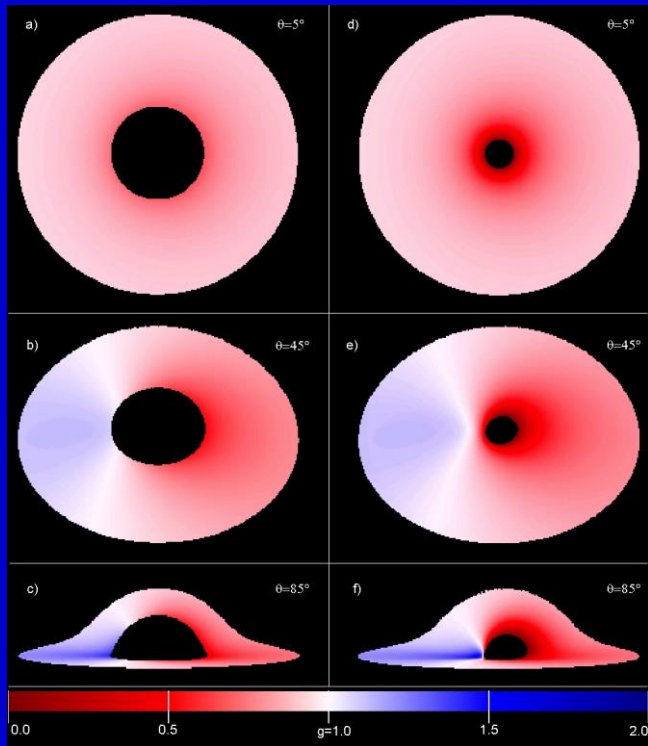
The structure of the disc in Cen A was studied in IR for scales <1 pc.

The data is consistent with a geometrically thin disc with diameter 0.6 pc.

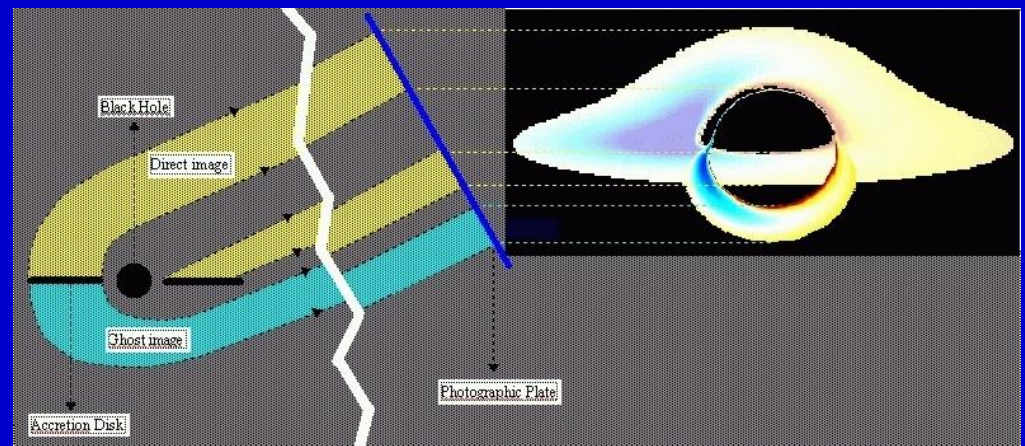
Observations on VLTI.

arXiv:0707.0177 K. Meisenheimer et al.
«Resolving the innermost parsec of Centaurus A at mid-infrared wavelengths»

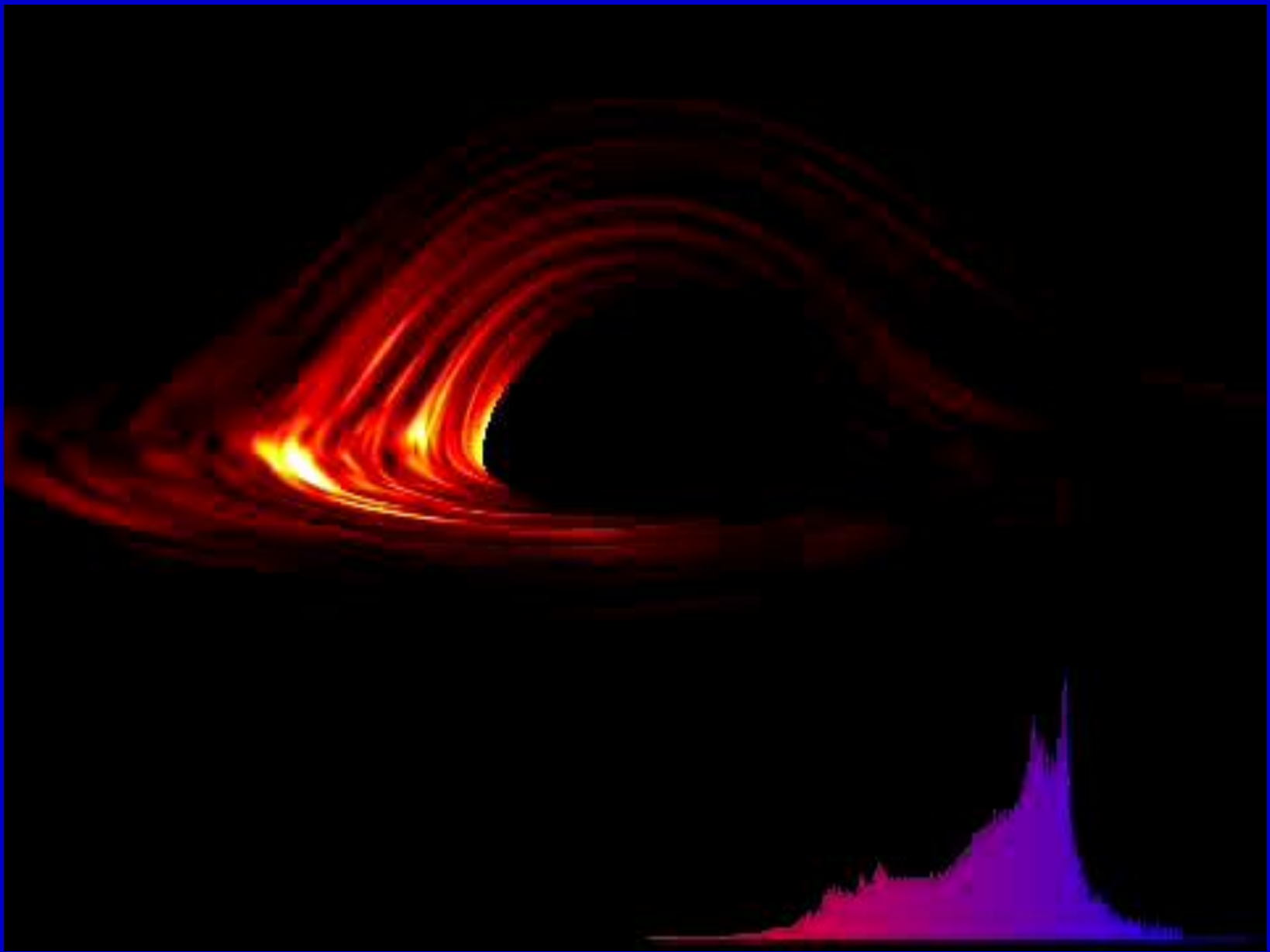
Discs around black holes: a look from aside



Disc temperature

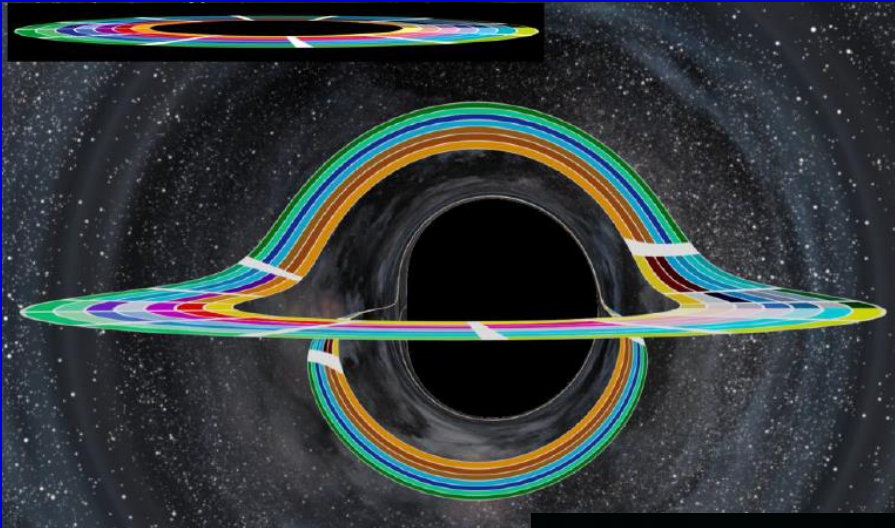


Discs observed from infinity.
Left: non-rotating BH,
Right: rotating.

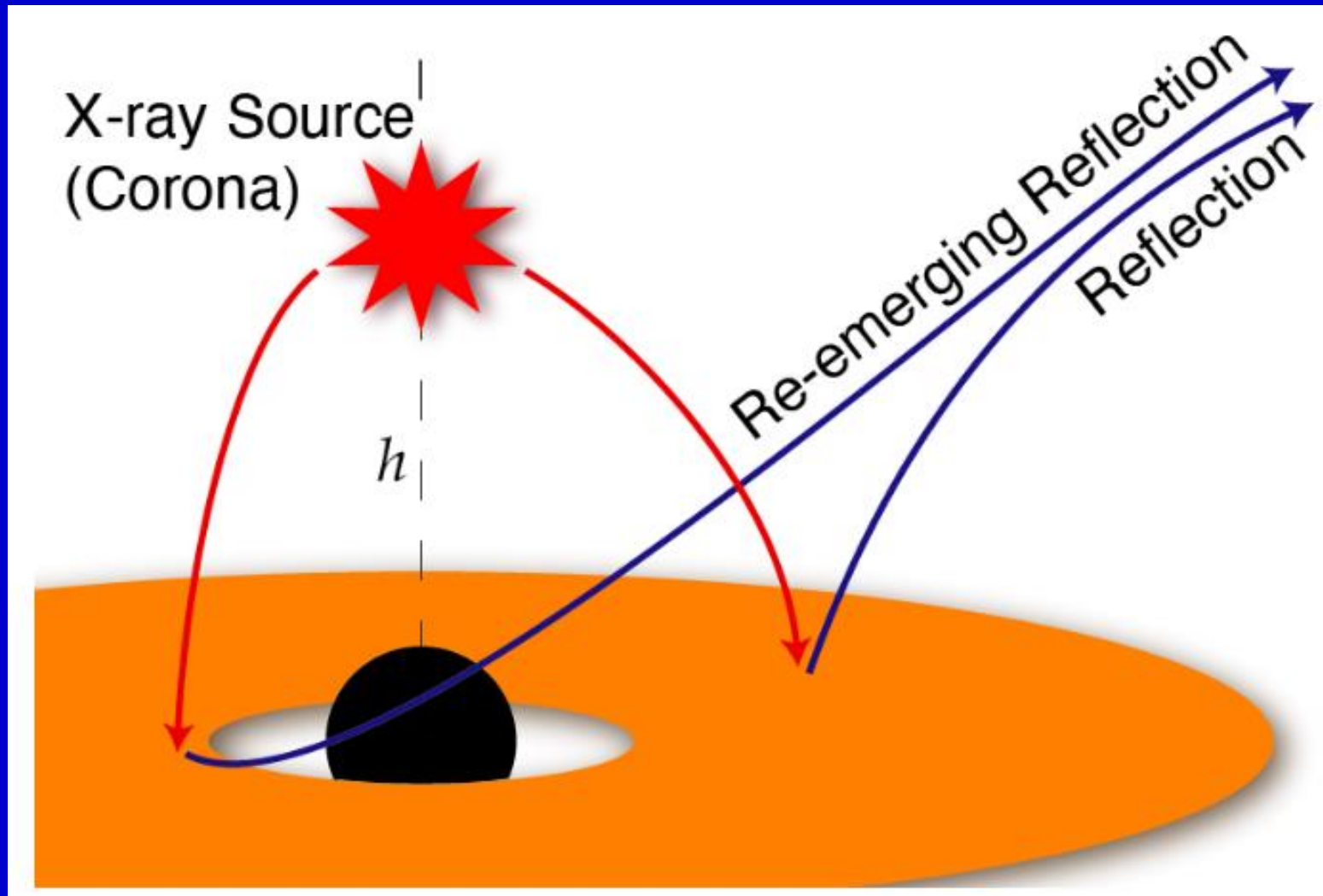


from gr-qc/0506078

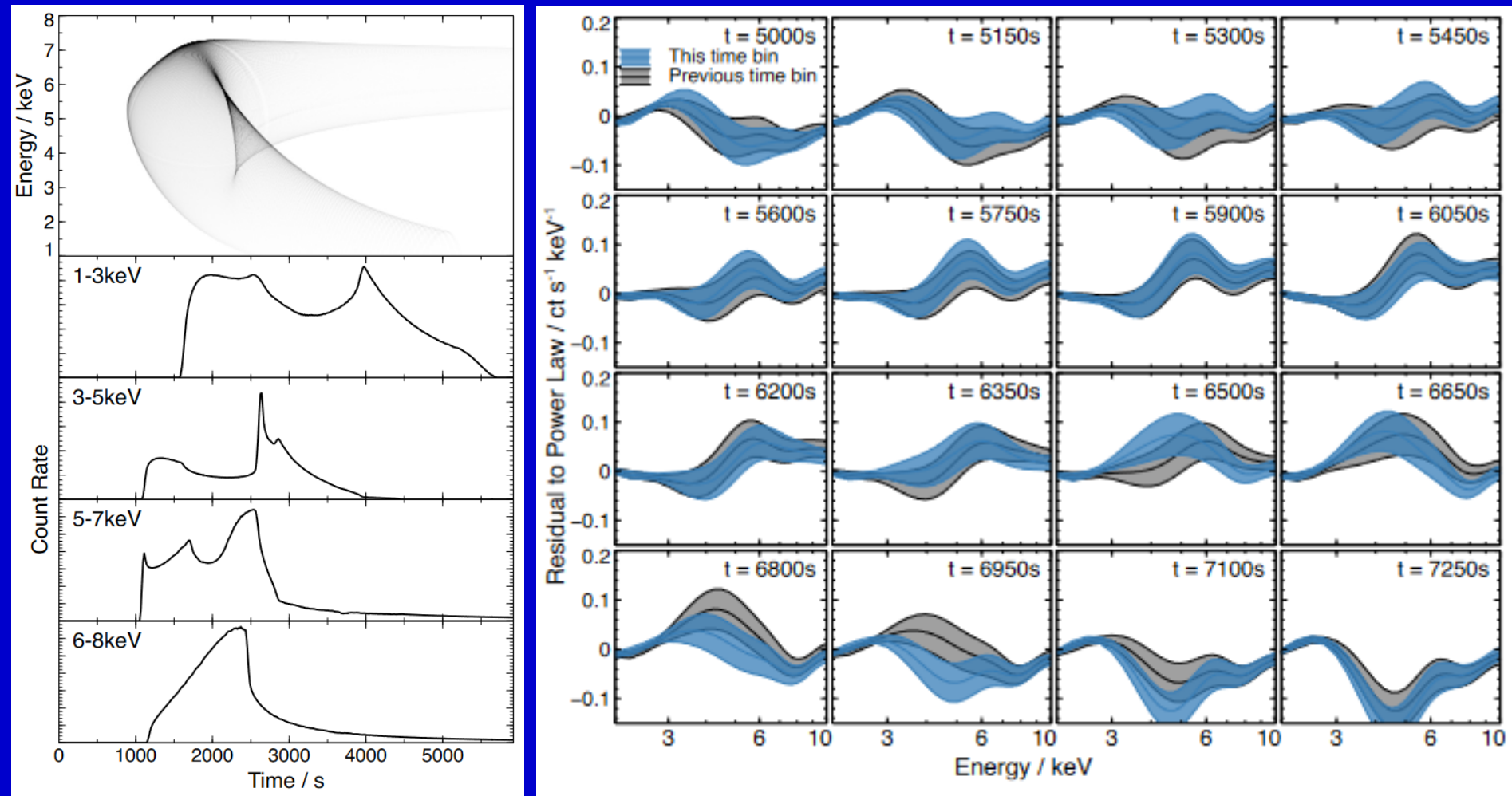
Discs from Interstellar movie



X-ray reverberation

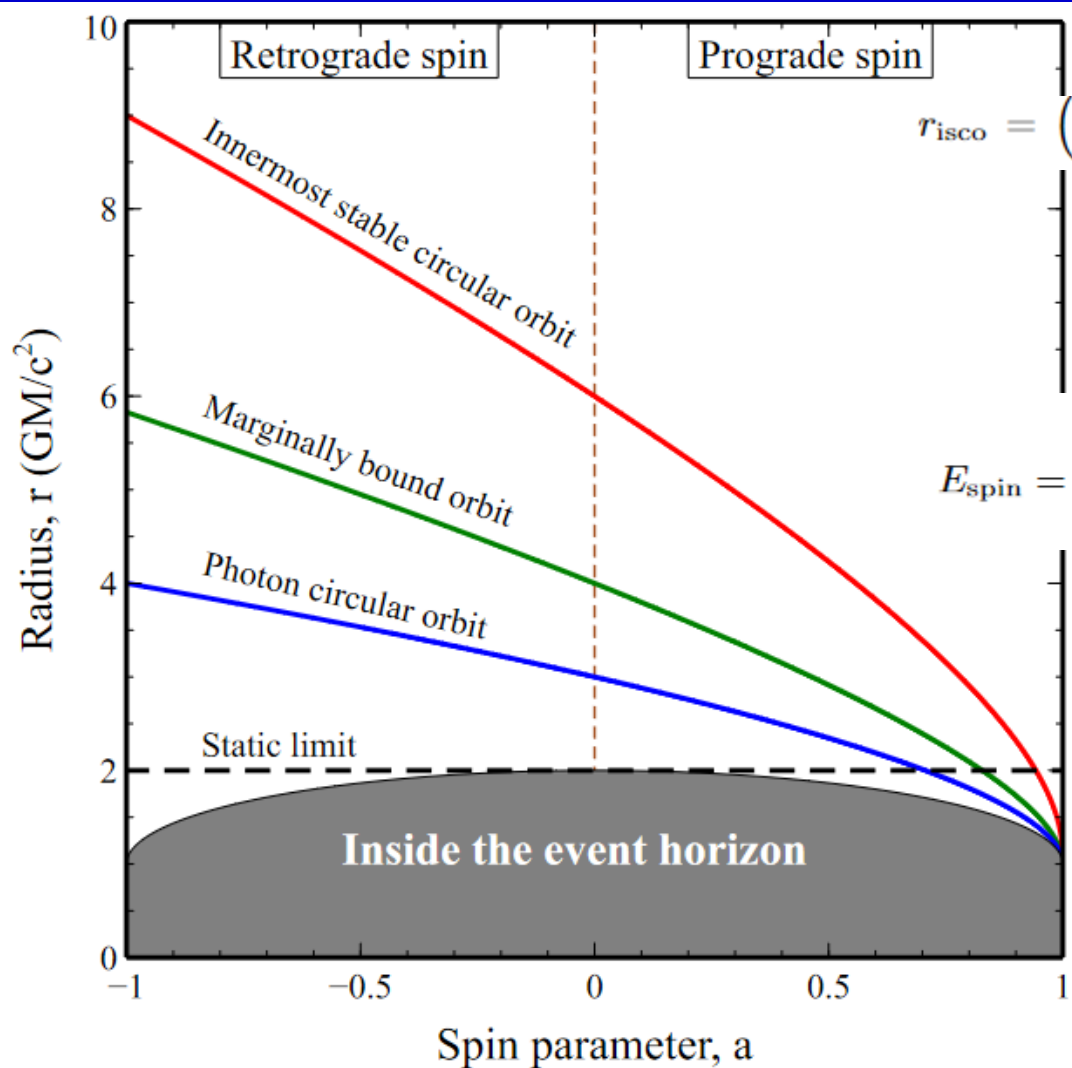


Model and observations for I Zw 1



2107.13555

Rotation and ISCO



$$r_{\text{isco}} = \left(3 + Z_2 \mp [(3 - Z_1)(3 + Z_1 + 2Z_2)]^{1/2} \right) r_g,$$

$$r_{\text{mb}} = (2 \mp a + 2\sqrt{1 \mp a}) r_g,$$

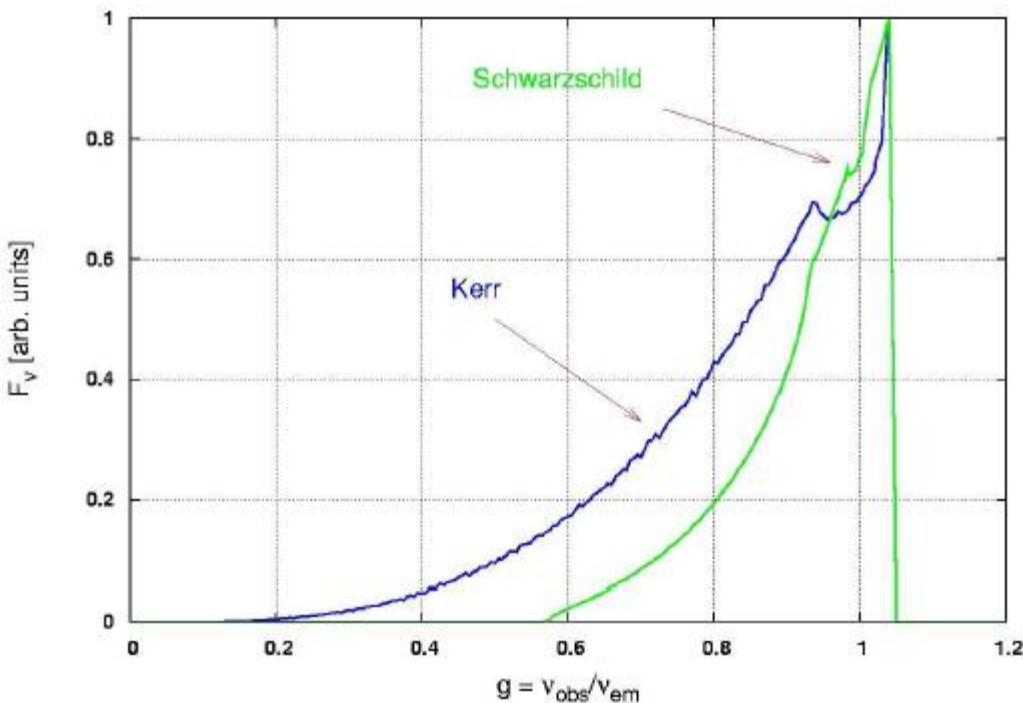
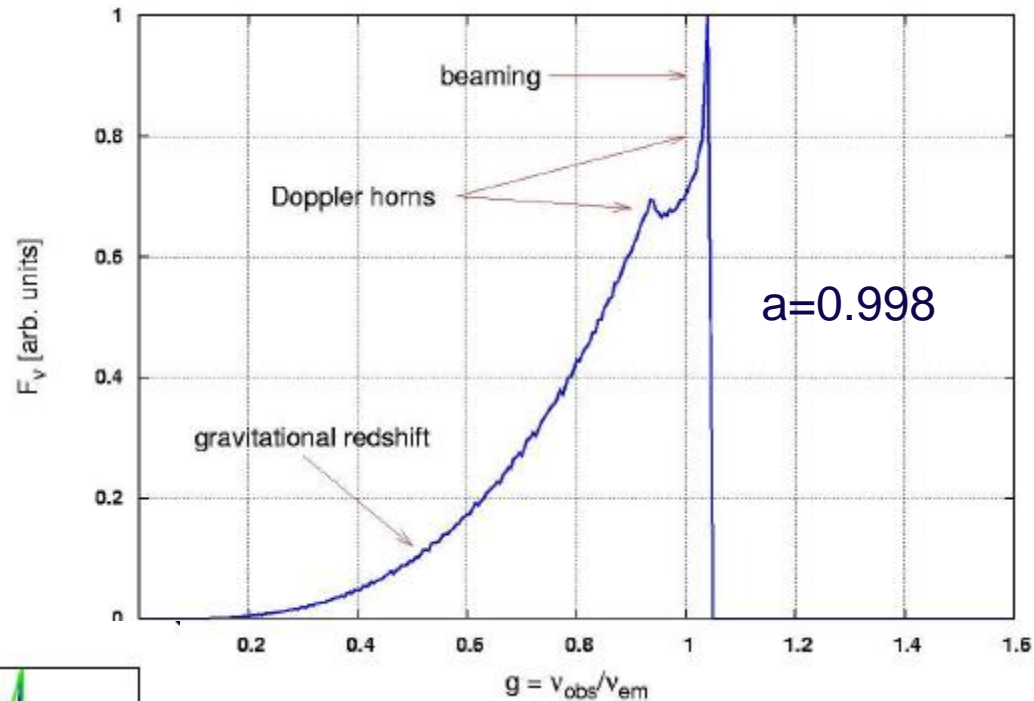
$$r_{\text{ph}} = 2 \left(1 + \cos \left[\frac{2}{3} \cos^{-1}(\mp a) \right] \right) r_g,$$

$$E_{\text{spin}} = \left[1 - \frac{1}{2} \left(\left[1 + \sqrt{1 - a^2} \right]^2 + a^2 \right)^{1/2} \right] Mc^2,$$

Different effects

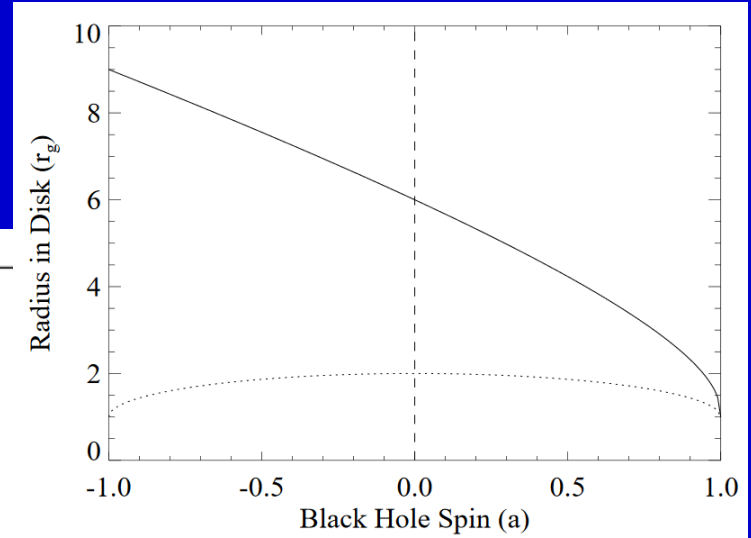
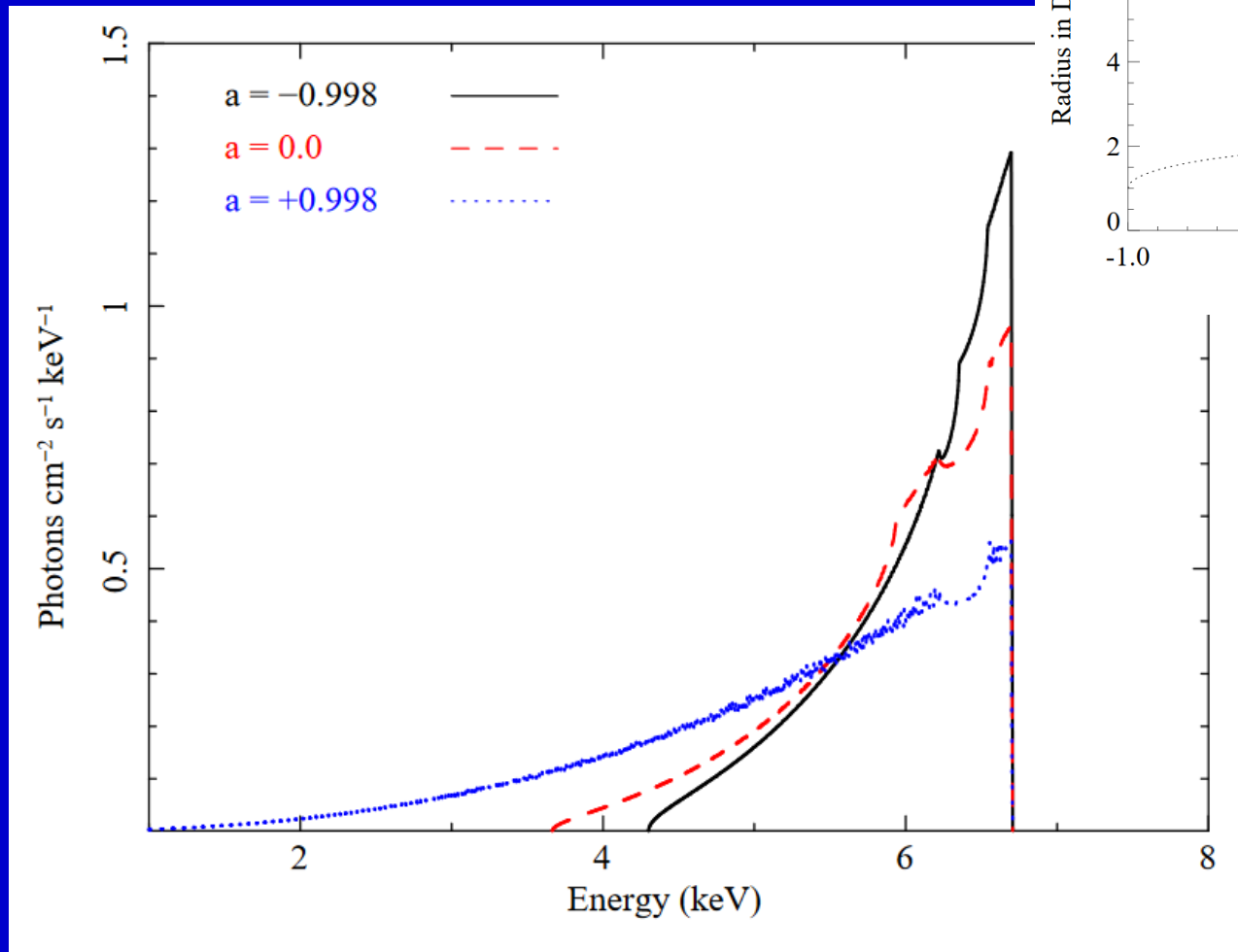
$$r_+ = \frac{GM}{c^2} + \left[\left(\frac{GM}{c^2} \right)^2 - \left(\frac{J}{Mc} \right)^2 \right]^{\frac{1}{2}}$$

For maximal rotation $r_{\text{ISCO}}=r_+$

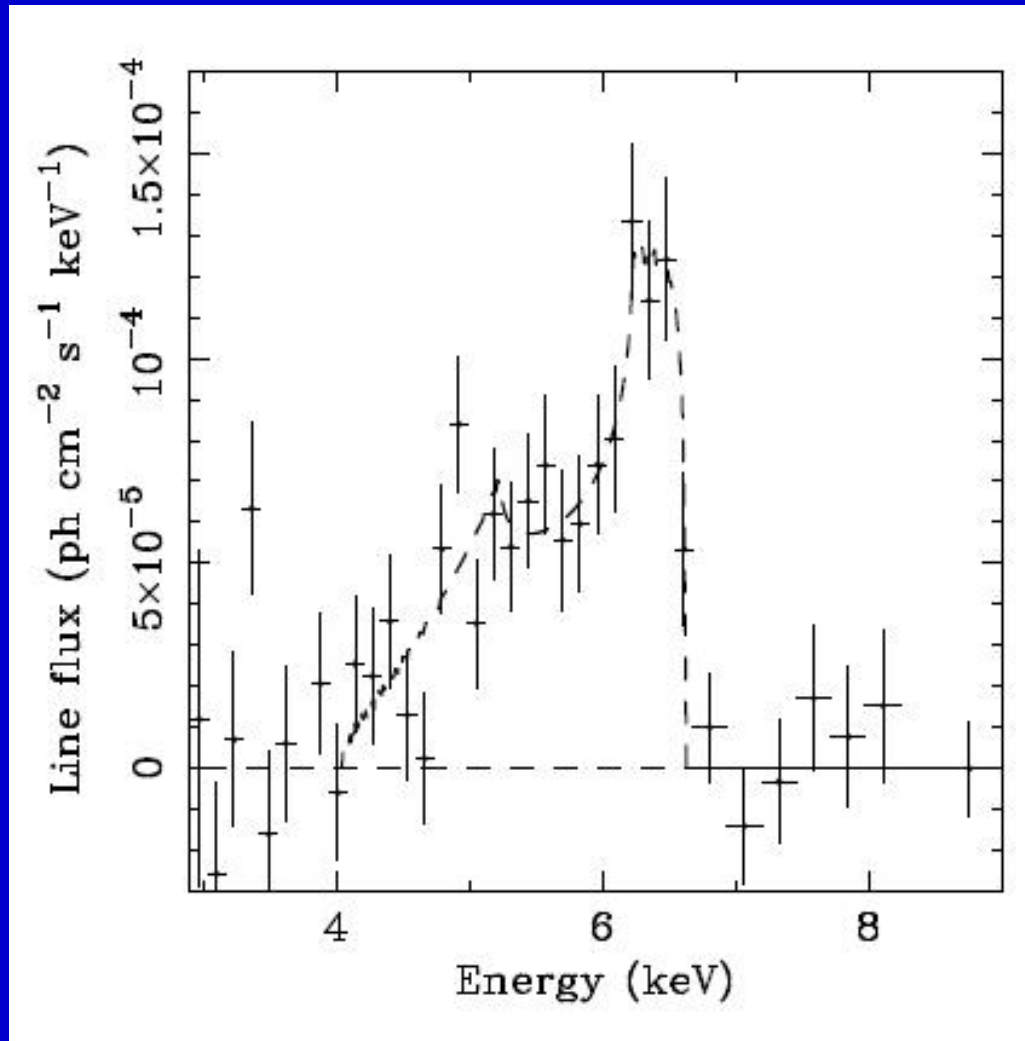


- Doppler effect
- Relativistic beaming
- GR light bending
- GR grav. redshift

Rotation direction



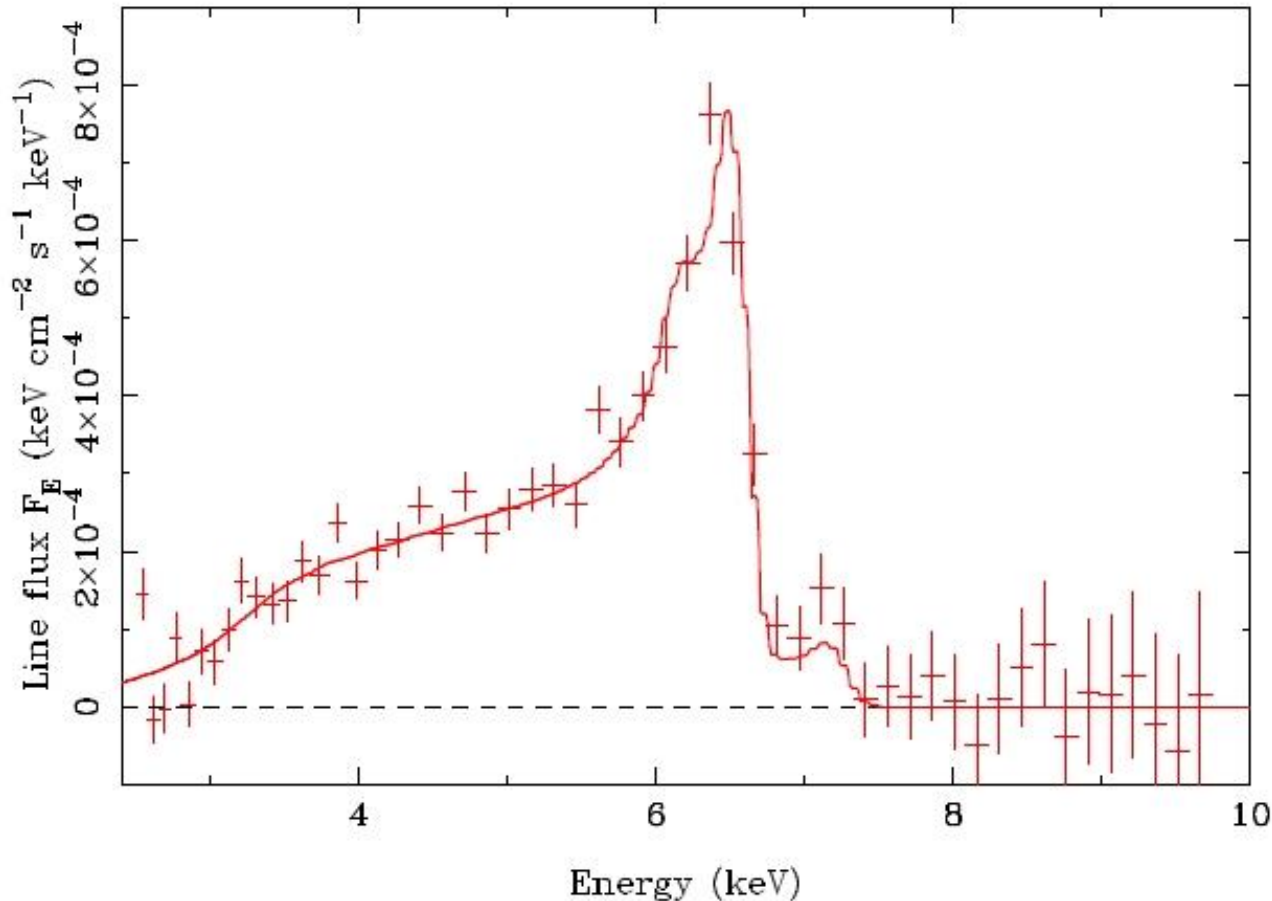
Fluorescent lines



The K α iron line observed by
ASCA (1994 r.).
Seyfert galaxy MCG-6-30-15

Dashed line: the model with
non-rotating BH,
disc inclination 30 degrees.

Lines and rotation of BHs



XMM-Newton data
(astro-ph/0206095)

The fact that the line extends to the red side below 4 keV is interpreted as the sign of rapid rotation (the disc extends inside $3R_g$).

see astro-ph/0212065

Suzaku spin measurements program

NGC 3783 $z = 0.00973$

A very complicated model.
 $a > 0.93$ (90% confidence)

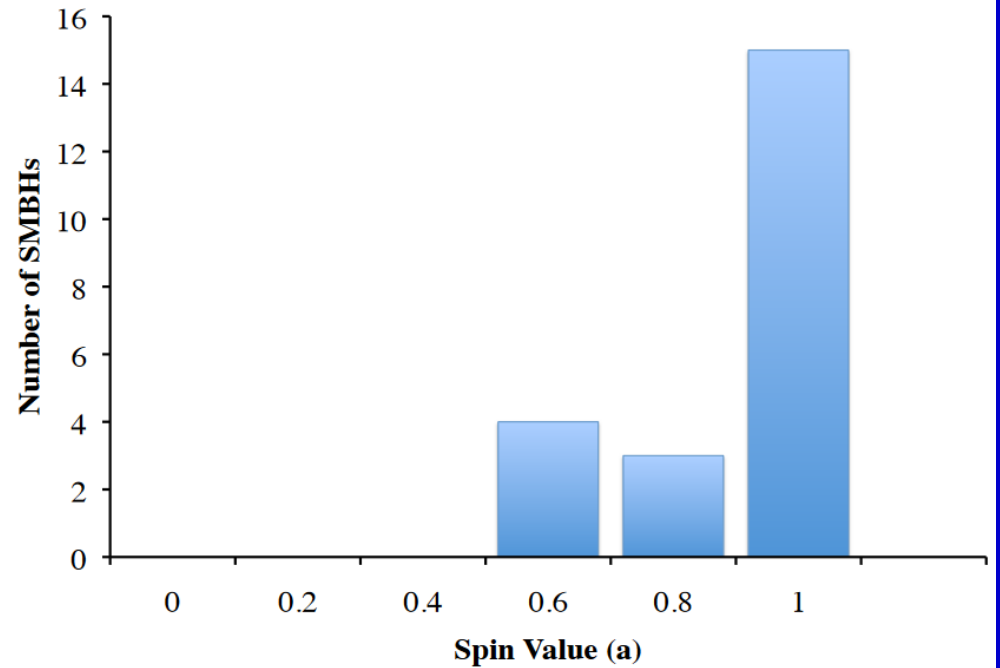
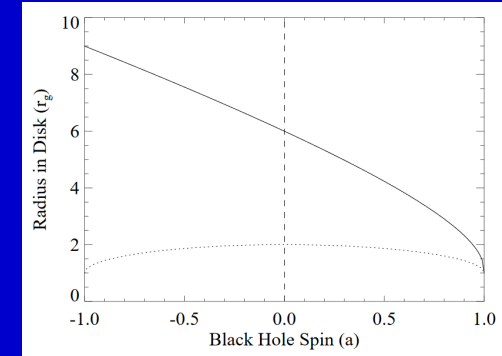
AGN	a
MCG-6-30-15 ^a	≥ 0.98
Fairall 9 ^b	$0.65^{+0.05}_{-0.05}$
SWIFT J2127.4+5654 ^c	$0.6^{+0.2}_{-0.2}$
1H0707-495 ^d	≥ 0.98
Mrk 79 ^e	$0.7^{+0.1}_{-0.1}$
Mrk 335 ^f	$0.70^{+0.12}_{-0.01}$
NGC 7469 ^f	$0.69^{+0.09}_{-0.09}$
NGC 3783 ^g	≥ 0.98

A little bit more data
in 1307.3246
and a big review in 1309.6334

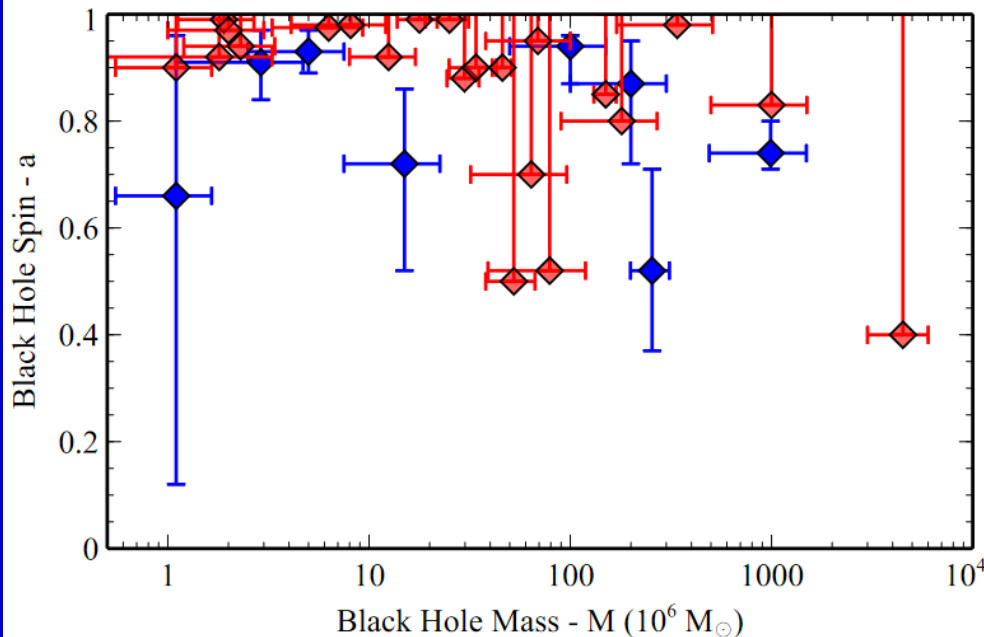


Relativistic reflection fitting of spectra

AGN	a	log M	$L_{\text{bol}}/L_{\text{Edd}}$	Host
MCG 6-30-15 ^a	$\geq +0.98$	$6.65^{+0.17}_{-0.17}$	$0.40^{+0.13}_{-0.13}$	E/S0
Fairall 9 ^b	$+0.52^{+0.19}_{-0.15}$	$8.41^{+0.11}_{-0.11}$	$0.05^{+0.01}_{-0.01}$	Sc
SWIFT J2127.4+5654 ^c	$+0.6^{+0.2}_{-0.2}$	$7.18^{+0.07}_{-0.07}$	$0.18^{+0.03}_{-0.03}$	—
1 H0707-495 ^d	$\geq +0.98$	$6.70^{+0.40}_{-0.40}$	$\sim 1.0_{-0.6}$	—
Mrk 79 ^e	$+0.7^{+0.1}_{-0.1}$	$7.72^{+0.14}_{-0.14}$	$0.05^{+0.01}_{-0.01}$	SBb
Mrk 335 ^f	$+0.70^{+0.12}_{-0.01}$	$7.15^{+0.13}_{-0.13}$	$0.25^{+0.07}_{-0.07}$	S0a
NGC 3783 ^g	$\geq +0.98$	$7.47^{+0.08}_{-0.08}$	$0.06^{+0.01}_{-0.01}$	SB(r)ab
Ark 120 ^h	$+0.94^{+0.1}_{-0.1}$	$8.18^{+0.05}_{-0.05}$	$0.04^{+0.01}_{-0.01}$	Sb/pec
3C 120 ⁱ	≥ 0.95	$7.74^{+0.20}_{-0.22}$	$0.31^{+0.20}_{-0.19}$	S0
1 H0419-577 ^j	$\geq +0.88$	$8.18^{+0.12}_{-0.12}$	$1.27^{+0.42}_{-0.42}$	—
Ark 564 ^j	$+0.96^{+0.01}_{-0.06}$	≤ 6.90	≥ 0.11	SB
Mrk 110 ^j	$\geq +0.99$	$7.40^{+0.09}_{-0.09}$	$0.16^{+0.04}_{-0.04}$	—
SWIFT J0501.9-3239 ^j	$\geq +0.96$	—	—	SB0/a(s) pec
Ton S180 ^j	$+0.91^{+0.02}_{-0.09}$	$7.30^{+0.60}_{-0.40}$	$2.15^{+3.21}_{-1.61}$	—
RBS 1124 ^j	$\geq +0.98$	8.26	0.15	—
Mrk 359 ^j	$+0.66^{+0.30}_{-0.54}$	6.04	0.25	pec
Mrk 841 ^j	$\geq +0.52$	7.90	0.44	E
IRAS 13224-3809 ^j	$\geq +0.995$	7.00	0.71	—
Mrk 1018 ^j	$+0.58^{+0.36}_{-0.74}$	8.15	0.01	S0
IRAS 00521-7054 ^l	$\geq +0.84$	—	—	—
NGC 4051 ^m	$\geq +0.99$	6.28	0.03	SAB(rs)bc
NGC 1365 ^k	$+0.97^{+0.01}_{-0.04}$	$6.60^{+1.40}_{-0.30}$	$0.06^{+0.06}_{-0.04}$	SB(s)b

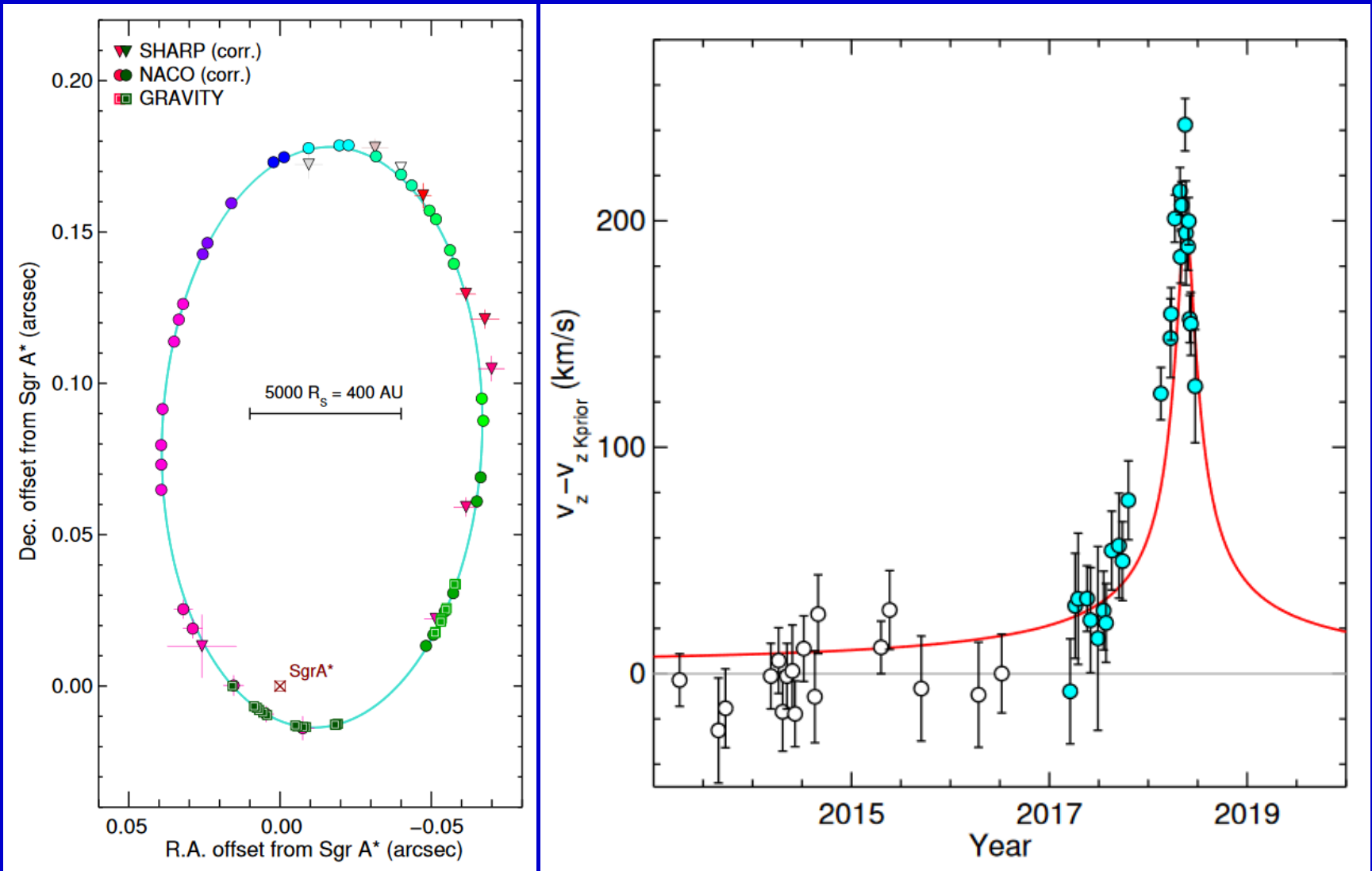


Spins of SMBHs | in AGNs



Object	Mass ($\times 10^6 M_{\odot}$)	Spin	Mass/Spin References
Mrk359	~ 1.1	$0.66^{+0.30}_{-0.54}$	Va16+
Ark564	~ 1.1	> 0.9	Va16+/Ji19
Mrk766	$1.8^{+1.6}_{-1.4}$	> 0.92	Be06/Bu18
NGC4051	1.91 ± 0.78	> 0.99	Va16+
NGC1365	~ 2	> 0.97	Va16+/Wa14
1H0707-495	~ 2.3	> 0.94	Va16+/Ka15
MCG-6-30-15	$2.9^{+1.8}_{-1.6}$	$0.91^{+0.06}_{-0.07}$	Va16+/Ma13
NGC5506	~ 5	0.93 ± 0.04	Ni09/Su18
IRAS13224-3809	~ 6.3	> 0.975	Va16+/Ji18
Tons180	~ 8.1	> 0.98	Va16+/Ji19
ESO 362-G18	12.5 ± 4.5	> 0.92	Va16+
Swift J2127.4+5654	~ 15	$0.72^{+0.14}_{-0.20}$	Va16+/Ji19
Mrk335	$17.8^{+4.6}_{-3.7}$	> 0.99	Gr18/Ji19
Mrk110	25.1 ± 6.1	> 0.99	Va16+/Ji19
NGC3783	29.8 ± 5.4	> 0.88	Va16+
1H0323+342	34^{+9}_{-6}	> 0.9	Wa16/Gh18
NGC 4151	$45.7^{+5.7}_{-4.7}$	> 0.9	Be06/Ke15
Mrk79	52.4 ± 14.4	> 0.5	Va16+/Ji19
PG1229+204	57 ± 25	$0.93^{+0.06}_{-0.02}$	Ji19/Ji19
IRAS13197-1627	~ 64	> 0.7	Va10/Wa18
3C120	69^{+31}_{-24}	> 0.95	Gr18/Va16+
Mrk841	~ 79	> 0.52	Va16+
IRAS09149-6206	~ 100	$0.94^{+0.02}_{-0.07}$	Wa20/Wa20
Ark120	150 ± 19	> 0.85	Va16+/Ji19
RBS1124	~ 180	> 0.8	Mi10/Ji19
RXS J1131-1231	~ 200	$0.87^{+0.08}_{-0.15}$	Sl12/Re14c
Fairall 9	255 ± 56	$0.52^{+0.19}_{-0.15}$	Va16+
1H0419-577	~ 340	> 0.98	Va16+/Ji19a
PG0804+761	550 ± 60	> 0.97	Ji19/Ji19
Q2237+305	~ 1000	$0.74^{+0.06}_{-0.03}$	Ass11/Re14b
PG2112+059	~ 1000	> 0.83	Ve06/Sc10
H1821+643	4500 ± 1500	> 0.4	Va16+
IRAS 00521-7054	—	> 0.77	-/Wa19
IRAS13349+2438	—	$0.93^{+0.03}_{-0.02}$	-/Pa18
Fairall 51	—	> 0.75	-/Sv15
Mrk 1501	—	> 0.97	-/Ch19

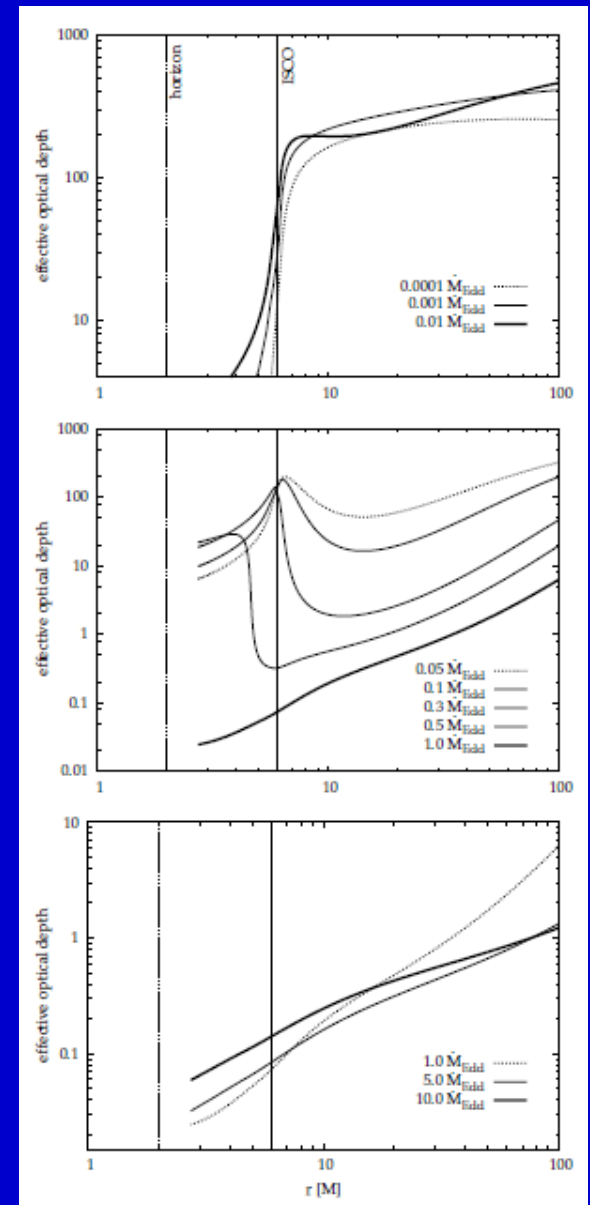
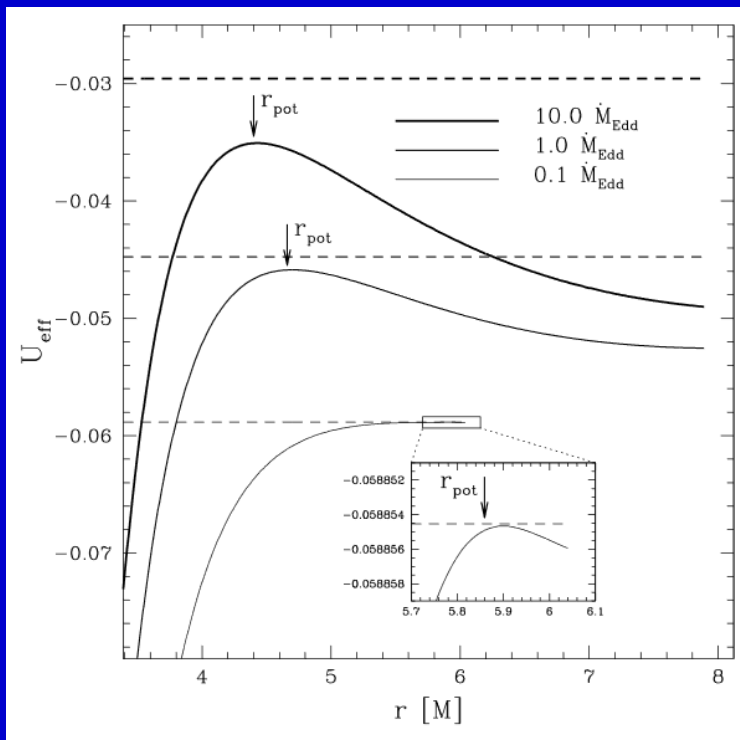
Gravitational redshift of the S2 star



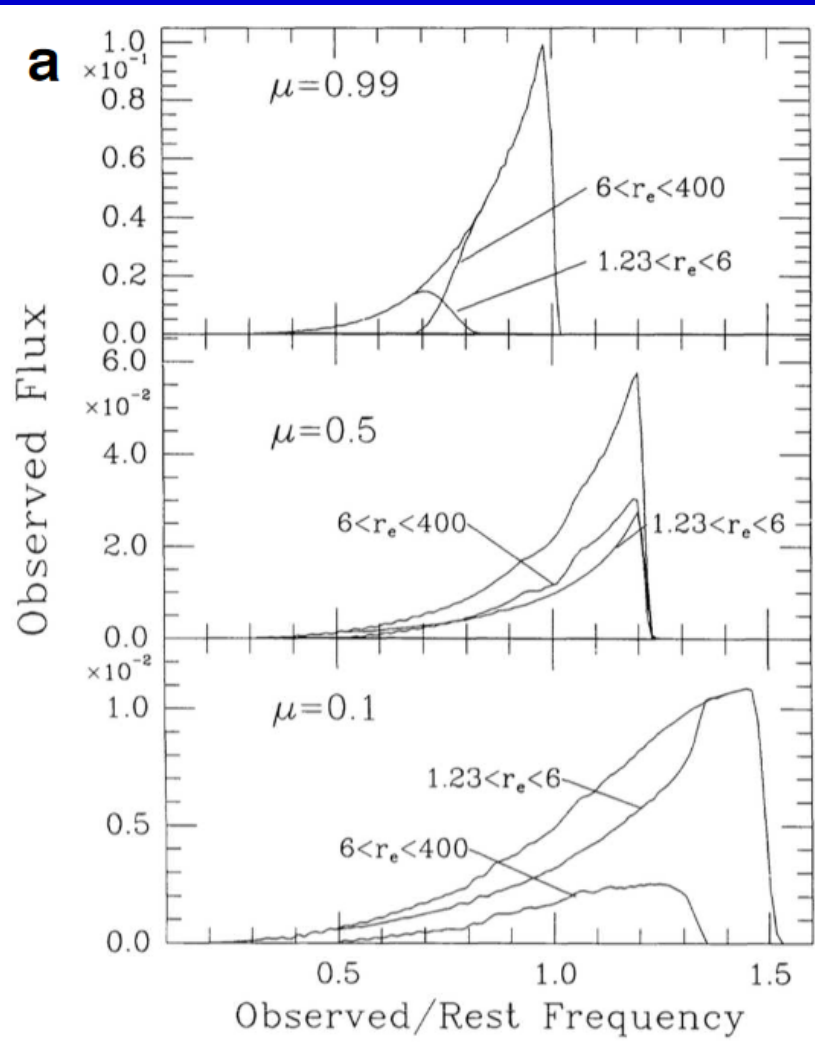
The inner edge

The place where the fluorescent line is formed is not necessarily the standard ISCO.

Especially for large accretion rates the situation is complicated.



Inclination is important



$\mu = \cos \theta$
 $\mu = 1$ – face-on

For inclined discs interplay between gravitational redshift and Doppler effect from inner and outer disc result in a profile with which it is difficult to put constraints on the inner boundary.

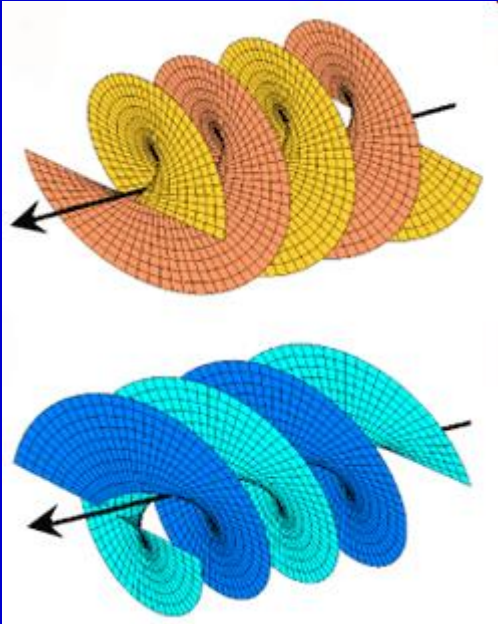
Measuring spins of stellar-mass BHs

Source	Spin a_*
GRS 1915+105	> 0.98
LMC X-1	$0.92^{+0.05}_{-0.07}$
M33 X-7	0.84 ± 0.05
4U 1543-47	0.80 ± 0.05
GRO J1655-40	0.70 ± 0.05
XTE J1550-564	$0.34^{+0.20}_{-0.28}$
LMC X-3	$< 0.3^b$
A0620-00	0.12 ± 0.18

Different methods used
1101.0811

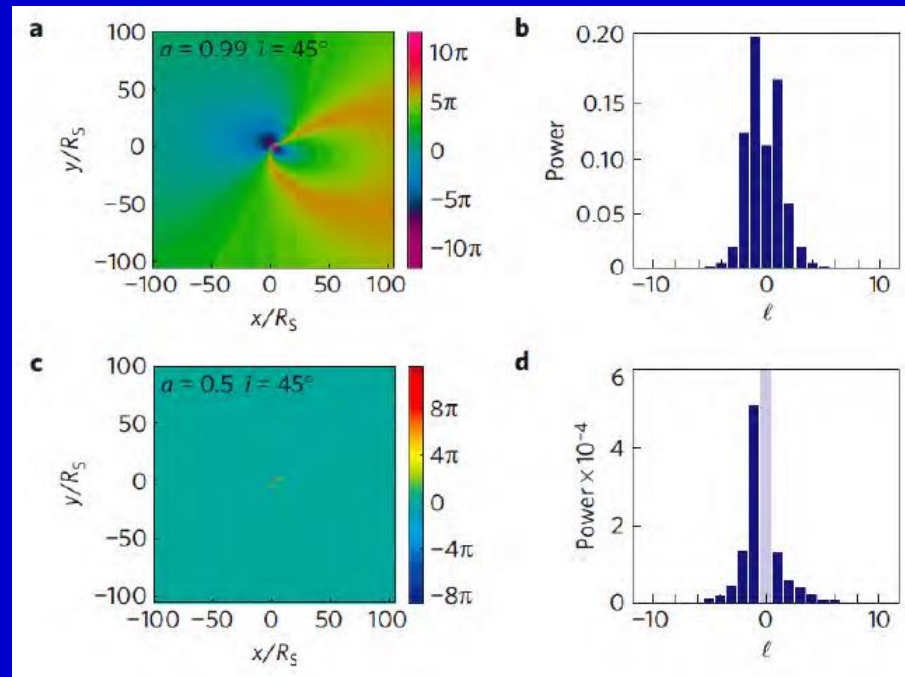
See a review on BH spin
(both XRB and AGN) in 1507.06153
and estimates of the spin parameter
with a model-depended method, but
for hundreds of sources in 1905.11319.

Twisted light



This effect can be used to learn about spin of accreting BHs.

If the source of the gravitational field also rotates, it drags space-time with it. Because of the rotation of the central mass, each photon of a light beam propagating along a null geodesic will experience a well-defined phase variation.



1104.3099

See <http://www.physics.gla.ac.uk/Optics/play/photonOAM/>
and astro-ph/0307430 about orbital angular momentum of photons